SWIRL, EXPANSION RATIO AND BLOCKAGE EFFECTS ON CONFINED TURBULENT FLOW

By

GREGORY LLOYD SCHARRER

Bachelor of Science in Engineering

Northern Arizona University

Flagstaff, Arizona

1982

Submitted to the Faculty of the Graduate College
of the Oklahoma State University
in partial fulfillment of the requirements
for the Degree of
MASTER OF SCIENCE
May, 1984

SWIRL, EXPANSION RATIO AND BLOCKAGE EFFECTS

ON CONFINED TURBULENT FLOW

Thesis Approved:

David G. Lilley
Thesis Adviser

A. J. Khajavi

R. L. Williams

Norman N. Durham
Dean of Graduate College

ACKNOWLEDGMENTS

The author wishes to express his sincere gratitude to his major adviser, Dr. David G. Lilley for his guidance and encouragement. Appreciation is also extended to the other committee members, Dr. Afshin J. Ghajar and Dr. Peter M. Moretti.

The author would like to extend a special thank you to Muftah T. Abujelala for his help and friendship, Mr. George Cooper and Mr. Preston Wilson for their assistance on the construction phase of the project, and Ms. Neisa Lock for her professional typing.

The author also wishes to gratefully acknowledge NASA Lewis Research Center and Air Force Wright Aeronautical Laboratories for financial support under Grant No. NAG 3-74.

TABLE OF CONTENTS

LIST OF TABLES

LIST OF FIGURES

NOMENCLATURE

C	velocity coefficient = $\rho V^2/[2(P_c - P_w)]$
CRZ	corner recirculation zone
CTRZ	central toroidal recirculation zone
D	test section diameter
d	inlet nozzle diameter
G	axial flux of momentum
L	downstream blockage location
p	time-mean pressure
Re	Reynolds number
S	swirl number
v = (u,v,w)	time-mean velocity (in x-, r-, θ-directions)
V	time-mean velocity vector magnitude
x,r,θ	axial, radial, azimuthal cylindrical polar coordinates
α	side-wall expansion angle
β	yaw angle of probe = $\tan^{-1}(w/u)$
δ	pitch angle of probe = $\tan^{-1}[v/(u^2 + w^2)^{1/2}]$
ρ	density
ϕ	swirl vane angle = $\tan^{-1}(w_{in}/u_{in})$, assuming perfect vanes

Subscripts

C	central pitot pressure port
d	relating to inlet nozzle diameter
in	inlet conditions

N,S,E,W	north, south, east, west pitot pressure ports
o	value of inlet to flowfield
h	swirl vane hub; expansion step height
p	relating to probe sensing tip diameter

Superscripts

'	alternate form, neglecting pressure variation
-	time-average quantity

CHAPTER I

INTRODUCTION

1.1. The Purpose of the Investigation

The state of the art in combustor design has been advanced significantly in recent years due to the need for greater fuel efficiency and fuel versatility (i.e., engines must be capable of burning cheaper fuels and/or several different types of fuels). Researchers have utilized many different means in order to study the phenomena of combustion: computer simulation (1-9); instantaneous and time-mean velocity measurements (2-20); flow visualization (7-9, 21-24); and heat transfer and temperature measurements (19, 23, 24).

The ultimate goal of research efforts is to develop cost-efficient computer programs that accurately describe the process for any combination of physical parameters. However, experimental data for the system to be modeled must be available in order to validate the models used in computer codes.

The present investigation is an experimental study utilizing flow visualization and time-mean velocity measurements to determine the effects of decreasing the expansion ratio (i.e., the test section diameter, D, divided by the inlet nozzle diameter, d) on isothermal flowfields having various degrees of swirl, side-wall expansion, and downstream blockage. Neutrally-buoyant helium-filled soap bubbles are

used to mark the flowfield for the flow visualization, and a five-hole pitot probe is used to measure the time-mean velocities.

1.2 Review of Previous Studies

Bradshaw and Wong (3) used three different geometric perturbations to study the reattachment of a turbulent shear layer. The study showed that a nonswirling flow reattaches 6 to 9 step heights downstream of separation. It was also observed that the flow just downstream of reattachment bears very little resemblance to a plane mixing layer or any other sort of thin shear, even if the residual influence of the boundary layer is small.

Macagno and Hung (5) used dye injection and still photographs to study a laminar oil flow past a 2:1 diameter expansion. Streamline and vorticity contours are presented. The contours show that the vorticity peak moves into the main flow when separation occurs, then moves back to the wall well downstream of the reattachment point.

Time-mean velocity measurements and several means of flow visualization were employed by Rhode (7) to study inert nonswirling and swirling flowfields. Photographs, streamline contours and velocity profiles of the flowfield are presented.

A five-hole pitot probe was used by Yoon (10) to measure velocities in a 30 cm diameter test section. Velocity profiles and streamline contours are presented to illustrate the effects of swirl and geometric parameters on the flowfield. The results of the present study will be compared to those obtained by Yoon to determine the effect of confinement on inert swirling and nonswirling flows.

A nonswirling flowfield, similar to that of Yoon (10) and Rhode (7), was studied by Chaturvedi (14) to determine the effect of inlet expansion angle on the flow. It was found that the reattachment point moved downstream from 6 to 9 step heights as the expansion angle was increased from 15 to 90 degrees. The author also suggested that varying the expansion ratio D/d would not affect the flow near the exit plane x/D = 0, because the primary effect of the change would be on the mixing process and diffusion after the maximum rate of turbulence production is obtained.

Syred and Dahman (16) studied the effect of confinement on an inert swirling flow. The effect of confinement was found to be complex due to two effects:

1. entrainment rates of swirling jets are very high, which can cause them to "stick" to the wall;
2. decay of swirl velocity is usually uneven across the enclosure.

The study used D/d ratio of 4 and 2; the present study uses D/d ratios of 1.5 and 1.

A Laser Doppler Anemometer located the reattachment point for a turbulent, nonswirling flow at 4.5 step heights downstream of the exit plane in a study performed by Yang and Yu (18). The authors theorized that the reattachment point was unusually far upstream as a result of a large back pressure caused by a short, rapidly contracting nozzle which followed by sudden enlargement. Most researchers (2, 3, 5, 6, 14, 21) found the reattachment point to be 6 to 9 step heights downstream of the exit plane.

The flowfield independence of Reynolds number for the facility used in this study was established by Rhode (7) and Yoon (10). Thus, the results contained herein are applicable to actual combustor hardware, which usually operate at slightly higher Reynolds numbers than those used in the present study.

1.3 Scope and Significance

This study implemented flow visualization and time-mean velocity measurements to document the flowfield changes which result from decreasing the expansion ratio D/d. Flow visualization was used to locate the most affected areas of the flow. Then, time-mean velocity measurements were taken to detail the flow in the affected regions. The raw data from the measurements were reduced using a FORTRAN computer program similar to that developed by Rhode (7) in which plotted output is obtained via a complot plotter.

The above procedure was performed for test sections having expansion ratio of 1.5 and 1.0. The results were then compared to previously obtained results for a test section having an expansion ratio equal to 2 (10).

The present work is significant for the following reasons:

1. The effect of the expansion ratio on the combustor flowfield is documented;
2. The results obtained complement the work of previous researchers (7, 10) and thus extend the available data base for combustion designers.

The present work is limited for the following reasons:

1. Measurements are taken only at multiples of the test section half-diameter;
2. The pitot probe is not sensitive to small velocities.

1.4 Outline of the Thesis

In the previous sections, a synopsis of relevant previous work is given. The synopsis is followed by a presentation of the scope and significance of this study.

Chapter II describes the facilities and instrumentation employed. The operation of the five-hole pitot probe is discussed, and the concept of swirl is defined and briefly discussed.

Chapter III details the measurement and data reduction procedures. The method of flow visualization is described along with an outline of the pitot probe calibration and measurement procedures. The data reduction process is also outlined.

The results of this study are discussed in Chapter IV with reference to appropriate photographs, tables, and figures in the appendices. The discussion includes a comparison of the present results to relevant previous work (7, 10, 14, 16).

This study is summarized in Chapter V, where recommendations for further work are also given.

CHAPTER II

FACILITIES AND EQUIPMENT

2.1 Confined Jet Test Facility

The confined jet test facility is described at length elsewhere (7-11). It has a variable speed axial flow fan that drives the flow through a settling chamber and into a contraction section designed by the method of Morel (25). The flow leaves the contraction section via a 15 cm diameter circular nozzle and enters the test section. The test section is a constant diameter (diameters of 15 and 22.5 cm are used) plexiglass tube with length greater than 5 tube diameters: This precludes the presence of end-effects in the measuring region $x/D \leq 2.0$. The test section and the typical combustion chamber it simulates are shown in Figure 1.

The side-wall angle α and the swirl vane angle ϕ are variable. No side-wall expansion is used for the smaller tube, while angles of α = 45 and 90 degrees are used for the larger tube. Swirl vane angles of 0, 45 and 70 degrees are used for both tubes.

Typical operating Reynolds numbers (based on average inlet velocity and inlet diameter) range from 50,000 to 150,000 depending upon fan speed and aerodynamic blockage by the swirl vanes. It has been shown that this is in the Reynolds number insensitive region for this facility (7) in terms of nondimensional flow characteristics further downstream.

The overall flow facility is shown schematically in Figure 2.

The effect of a downstream blockage on the upstream flow in the test section is important in combustion aerodynamics. Two blockages of area ratio 2 and 4 are used. The smaller blockage is illustrated in Figure 3. Its upstream face is contoured in a quarter circle, as found in practical ramjet combustors. The larger blockage is shown in Figure 4. Its upstream face has a 45 degree slope, more typical of gas turbine combustion chamber exits. These blockages, when used, are located 2 tube diameters downstream of the expansion plane x/D = 0.

2.2 Swirler

Swirling jets are commonly used to control the length and stability of the flame in a combustor. The effects of the degree of swirl on the flowfields and combustion have been extensively studied (7-11, 13, 15, 16, 20). These researchers all used either a vane swirler or tangential entry mixing chambers to impart swirl to the flow under study; a variable vane angle swirler is used in the present study.

Beer and Chigier (26) have proposed the following nondimensional criterion to characterize the amount of swirl imparted to the axial flow:

$$S = \frac{G_\theta}{G_x \, (d/2)} \tag{2.1}$$

where G_θ = axial flux of angular momentum

G_x = axial flux of axial momentum, including the pressure contribution

$d/2$ = swirler exit radius.

These quantities are defined mathematically as:

$$G_\theta = \int_0^{2\pi} \int_0^{d/2} [\rho uw + \overline{\rho u'w'}] r^2 dr d\theta \tag{2.2}$$

$$G_x = \int_0^{2\pi} \int_0^{d/2} [\rho u^2 + \overline{\rho u'^2} + (p - p_\infty)] r dr d\theta. \tag{2.3}$$

The pressure term is often omitted from G_x, thus yielding the dynamic axial momentum flux G_x':

$$G_x' = \int_0^{2\pi} \int_0^{d/2} [\rho u^2 + \overline{\rho u'^2}] r dr d\theta. \tag{2.4}$$

This leads to the alternate definition of the swirl number:

$$S' = \frac{G_\theta}{G_x' (d/2)} . \tag{2.5}$$

If the turbulent stress terms are neglected, the time-mean u and w velocity components across the swirler are sufficient to calculate S or S'. Sander (20) cataloged both S and S' for five commonly used idealized swirler exit velocity profiles.

The swirler used in this study was constructed at Oklahoma State University according to a preliminary design plan from NASA. The physical features of the swirler are diagrammed in detail in (28); the performance of the swirler is detailed in (20, 29); and the swirler is shown in Figure 5. The ten variable angle flat blades of pitch-to-chord ratio 0.68 give good turning efficiency; but Sander (20) has shown that the idealized ϕ vs. S relationships are not correct.

2.3 Flow Visualization Equipment

Flow visualization was used in the study for the following reasons: 1) to examine the overall flowfield; 2) to locate regions of interest in which pitot-probe measurements might be taken; 3) as a means to compare the flowfields of this study to those studied by Rhode (7). Neutrally-buoyant helium bubbles were selected to mark the flow because this method yielded acceptable results in previous studies (7,8), and the equipment was readily accessible.

The flow visualization equipment consisted of: a bubble generator; a light source; and a camera and tripod. Figure 6 shows how the flow visualization equipment is set up for use in the confined jet facility.

The bubble generator is a Sage Action Inc. model 3. It consists of an injector (shown in Figure 7) in which the bubbles are formed, and a console that supplies the helium, compressed air and soap solution to the injector. The injector is located far upstream of the test section inlet to avoid disturbance of the flow pattern to be studied. The injector is 1.6 cm diameter, 11.5 cm long, and has a 1 cm diameter stem normal to the main body. The bubbles are 0.5 to 1.0 mm diameter, and they are supplied at a fairly even rate (7).

A sheet of light 4 cm wide is used to illuminate the rx plane. The light source is an American Optical Co. slide projector. An opaque cardboard slide with a 4 cm wide slit controls light passage to the flowfield.

Kodak film rated ASA 400 is used in the camera. The film is over-developed to compensate for underexposure; this makes the film equivalent

to an ASA 1000 rating.

The camera is a NIKKORMAT FT-3 by NIKON. The lens used is a 50 mm, 1:1.4 by NIKKOR. Shutter speeds ranging from 0.5 to 0.125 seconds are used with f stops of 1.4 and 2.

2.4 Five-Hole Pitot Probe Instrumentation

A five-hole pitot probe was chosen as the measuring instrument for this study because the probe is reliable, accurate, and it is capable of measuring both the magnitude and the direction of the flow velocity. The pitot probe used in this study is a model DC-125-12-CD manufactured by United Sensor and Control Corporation. The accuracy of this particular probe is well-documented (7, 10, 11).

The probe, as shown in Figure 8, is a long, straight shaft with a hook-shaped sensing head: This allows the probe shaft to be rotated without altering the probe tip location. As the name implies, there are five holes in the tip of the probe: one in the center of the tip, and one each to the north, south, east and west of the center of the tip.

There are several possible ways to measure the flowfield using a five-hole pitot probe. The method employed here is to align the probe yaw angle with the flow yaw angle while deducing the pitch angle and the total velocity coefficient from calibrations. This method was chosen because it requires relatively simple data reduction procedures and it utilizes readily available orientation equipment.

In addition to the pitot probe, the instrumentation consists of a manual traverse mechanism, two five-way ball valves, a differential pressure transducer, a power supply, and an integrating digital voltmeter.

The differential pressure transducer is a model 590D from Datametrics Inc.; it has a pressure range from 0 to 1.3×10^3 Pa, and its deviation from linearity over this pressure range is shown in Figure 9. The integrating voltmeter is a TSI model 1076. The power supply is a Hewlett-Packard model 721A.

The auxillary equipment consisted of a General Radio Inc. model 631-B Strobotac and a pitot static probe. The strobotac was used to set the wind tunnel fan speed. The pitot static probe was used in conjunction with the previously described transducer and voltmeter to measure the dynamic pressure in the nozzle throat just upstream of the exit plane. The ambient temperature and pressure were measured by a Cenco Corp. barometer/thermometer unit.

CHAPTER III

DATA AQUISITION AND REDUCTION PROCEDURES

3.1 Flow Visualization Procedure

The flow visualization procedure began with the alignment of the test section axis with the wind tunnel axis. This is accomplished using a laser and a centering disk: The laser beam is positioned in line with the wind tunnel axis; the centering disk is fitted onto the downstream end of the tube; and the tube is positioned so the laser beam passes through the hole in the center of the disk.

The camera is mounted on the tripod and located normal to the tube to include the region $0 \leq x/D \leq 2$ in its field of view. The bubble injector is located in the wind tunnel as shown in Figure 6; and the wind tunnel speed is set as prescribed in Table I.

For the 22.5 cm diameter tube, photographs are taken for ϕ = 0, 45 and 70 degrees, with and without the small blockage in place. No photographs could be obtained with the large blockage in place due to the lack of adequate light penetration into the flow domain.

For the 15 cm diameter tube, photographs are taken for ϕ = 0 degrees, with and without the small blockage in place. No photographs could be obtained for ϕ = 45 or 70 degrees because the soap bubbles splash against the inside of the tube and obscure the view into the flowfield. Again, no photographs could be taken with the large blockage in place because of lighting problems.

3.2 Pitot Probe Measurement Procedures

The first step in the pitot probe measurements is to align the test section axis with the wind tunnel axis; this is accomplished as described in Section 3.1. Then, the five-hole pitot probe is positioned so the measurement coordinate axes coincide with the text section coordinate axes. This is accomplished in the following manner: The radial traverse location is set to zero; the angular vernier is set to zero; and the probe is locked into the traverse mechanism so that its base only is in the laser path, and no light is reflected off the sides of the probe base. The centering disk is then removed.

Before the wind tunnel is turned on, the pressure transducer must be set to zero. There is a "zero adjust screw" in the transducer for this purpose: the screw is turned until the voltmeter reads a constant zero value. At this time, the local pressure and temperature are recorded.

The wind tunnel is turned on and the fan speed is set as prescribed in Table I, using a strobotac. A static pitot probe is inserted in the nozzle throat of the wind tunnel and the inlet dynamic pressure is measured using the pressure transducer and the atmosphere ports on the five-way ball valves. If the inlet dynamic pressure corresponding to a particular fan speed is known, the fan speed can be set to obtain the known inlet dynamic pressure since the strobotac is not always available. Once the inlet dynamic pressure is measured, the static probe is removed to avoid interference of the flowfield to be measured.

The preliminaries are now complete and the traverse procedure begins. First, the probe is rotated to align the tip with the local flow direction: this is done by turning the ball valves so that the transducer senses $(p_W - p_E)$. When this value settles in the region $-.002 \text{ mV} \leq (p_W - p_E) \leq .002 \text{ mV}$, the probe is aerodynamically nulled, and the yaw angle β is read from the angular vernier and recorded. Second, the ball values are turned so the transducer senses $(p_N - p_S)$. When this value becomes reasonably constant, it is recorded: the integrating voltmeter gives a reasonably constant value after 3 or 4 time-constants when its 100 second time-constant is used; usually only 3 or 4 time-constants with the 10 second time-constant are required. Third, the ball values are moved to expose the transducer to the $(p_C - p_W)$ pressure difference. Again, this value is recorded when it becomes reasonably constant. Fourth, the transducer is exposed to $(p_C - p_{atm})$, and this value is recorded as the others are. Finally, the probe is moved radially upwards by 7.5 mm and the four steps are repeated. The traverse stops at the farthest radial point the probe can measure - 10.6 cm for the 22.5 cm diameter tube and 5.3 cm for the 15 cm diameter tube.

3.3 Pitot Probe Calibration

A five-hole pitot probe must be calibrated in order to translate the measured quantities β, $(p_N - p_S)$, and $(p_C - p_W)$ into a velocity magnitude and a direction. The calibration characteristics (see Figure 11 which is described later) yield a velocity coefficient C and a pitch angle δ for the given values of $(p_N - p_S)$ and $(p_C - p_W)$, where C

is defined as

$$C = V^2/[2(p_C - p_W)] \tag{3.1}$$

The velocity magnitude V is given by

$$V = [\frac{2}{\rho}(p_C - p_W) \cdot C]^{1/2} \tag{3.2}$$

and, since the velocity direction is known from the angles β and δ, the three components of time-mean velocity are readily deducible.

The five-hole pitot probe is calibrated using a contoured nozzle free jet having a 3.5 cm diameter throat. The probe is mounted horizontally on a Troyke Manufacturing Co. model BH-9 rotary table, as shown in Figure 10. Compressed air is used to calibrate the jet, its mass flow rate is controlled by a small pressure regulator and it is measured by a Fischer and Porter model 10A1735A rotameter.

All calibrations are performed at a rotameter setting of 10. This corresponds to a velocity of 9.6 m/s and a probe Reynolds number $Re_p = 1900$. A previous study (7) showed that the calibration characteristics are independent of Reynolds number for $Re_p \geq 1090$.

Once the instruments are zeroed, as in Section 3.2, the calibration begins by nulling out the probe [i.e., $(p_W - p_E) = 0$] for a pitch angle $\delta = 0$. The probe is then rotated to $\beta = -55$ degrees. At this point, the pressures $(p_N - p_S)$ and $(p_C - p_W)$ are recorded. This procedure is repeated over the range -55 degrees $\leq \beta \leq$ 55 degrees in 5 degree increments. Then, the five-hole probe is removed, the pitch angle is returned to zero, and the static pitot probe is mounted in

place of the five-hole probe to measure the dynamic pressure of the jet. The results of the calibration are shown in Figure 11.

3.4 Data Reduction

A FORTRAN code similar to that developed by Rhode (7) is used to reduce the data. The code uses the traverse data and the pitch angle calibration characteristic (see Figure 11(a)) in conjunction with a cubic spline interpolation technique to obtain the pitch angle δ . Then, the velocity coefficient C is determined using δ and the velocity coefficient calibration characteristic (Figure 11(b)). The absolute velocity is determined from Equation (3.2), the velocity components are determined from V, β , δ and simple geometry.

It should be noted that the effect of the fluctuating turbulent component of velocity has been ignored in relating sensed pressures to time-mean velocities. The additional terms cannot be measured by the instruments in use here, and although the effect on pressure probes is still unknown, the error incurred is likely to be less than five percent except in very high turbulence regions.

It should also be noted that the five-hole pitot probe is of questionable accuracy in high shear regions. However, these regions are encountered infrequently in this study. Therefore, the general trends found herein are certainly valid.

CHAPTER IV

RESULTS

Nonswirling and swirling inert flows are investigated in axisymmetric test sections with expansion ratio of 1.0 or 1.5, which may be equipped with a downstream blockage of area ratio 2 or 4. Flow visualization and time-mean velocity measurements are performed as described in Chapter III. The effect of the following geometric parameters on the extent of the flowfield recirculation zones is analyzed: expansion ratio D/d = 1.5 and 1, sidewall expansion angle α = 45 and 90 degrees, swirl vane angle ϕ = 0, 45 and 70 degrees, and downstream blockage of area ratio 2 and 4. The nozzle inlet Reynolds numbers employed in this study are high enough to ensure that the flowfields being investigated are independent of the Reynolds number; the Reynolds number corresponding to each flow case is listed in Table I. Flow characteristics are tabulated in terms of yaw angle β , pitch angle δ and normalized u, v, and w velocity components in Appendix A. Axial and swirl velocity profiles for all flows studied are shown in Appendix B.

Each section in this chapter consists of an analysis of the results obtained-both photographic and velocity measurements - and an attempt to correlate the present results to results obtained by other researchers using different expansion ratios.

4.1 Effect of Swirl on Open-Ended Flows

A variable-angle vane swirler is used in the present study to impart a tangential velocity component to the inlet flow. Swirl vane angles of 0 (swirler removed), 45 and 70 degrees are used. These angles correspond to idealized swirl numbers S of 0, 0.67 and 1.83 under the definition of swirl number introduced in Section 2.2, and the assumption of perfect efficiency of the blades in turning the flow. This is in fact not the case in practice (20). Figure 12 parts a through c shows the flow visualization photographs and Figure 13 parts a through c shows the axial and swirl velocity profiles for ϕ = 0, 45 and 70 degrees, respectively, for the test section with expansion ratio D/d = 1.5. Figures 14 and 15, parts a through c, show the corresponding results for the test section with D/d = 1.

The swirler is removed to obtain results for the nonswirling case. Figure 12(a) shows the corner recirculation zone (CRZ) extending to approximately x/D = 1.25; this translates to 7.5 step heights from the exit plane x/D = 0. Inspection of Figure 13(a) verifies that the reattachment point is between x/D = 1.0 and 1.5, but the reattachment location cannot be specified based on this figure. Moon and Rudinger (12) used a similar expansion ratio (D/d = 1.43) and found the reattchment point at x/D = 1.25 (approximately 8 step heights downstream of the exit plane). This is in good agreement with the present study.

Figure 12(b) shows that a small CRZ exits for the moderate (ϕ = 45 degrees) swirl case. The reattachment point is located at about x/D = 0.25. No CRZ is apparent for the strong swirl flow (ϕ = 70 degrees) in Figure 12(c): centrifugal forces dominate this flow. The

centrifugal forces in the flow result in the formation of a central torodial recirculation zone (CTRZ) and a precessing vortex core, as shown in these two photographs.

The precessing vortex core is a region of high swirl, low axial velocity flow along the axis, and relatively constant small diameter. It extends from the end of the CTRZ to the test section exit. The CTRZ is a wide reverse flow region encountered near the inlet. Figure 12(b) shows the CTRZ ending at x/D = 1.5 for the moderate swirl case, and Figure 12(c) shows the same region ending at x/D = 0.75 for the strong swirl case.

The swirl velocity profiles are nearly uniform in the near-wall region but decrease in an almost linear slope to a zero value at the centerline. The radial location of the maximum swirl velocity moves outward for the strong swirl case due to centrifugal effects. The swirl nonuniformity at x/D = 0.5 is due to the insensitivity of the five-hole pitot probe to small velocities, this same result was obtained in similar problems also being encountered in (7, 10).

The velocity profiles in Figure 15 parts a, b and c show how the flowfield of Figure 13 changes when the expansion ratio is reduced to 1.0. The axial velocity in Figure 15(a) is the plug flow that is expected after viewing the photograph in Figure 14 (there are no photos for the swirling flows with D/d = 1.0 because of experimental difficulties - the soap bubbles became attached to the tube wall). Centrifugal effects dominate both the axial and swirl profiles of parts b and c of Figure 15: the highest velocities are located farthest from the centerline. The profiles change very little as they move downstream. In addition, there is no CTRZ for the moderate swirl case and only a small

CTRZ extending to x/D = 0.5 for the strong swirl case.

For D/d > 1.0, the nonswirling flowfield does not change with expansion ratio: at D/d = 1.0 there is no CRZ. After comparing the present data for D/d = 1.5 with the data of Yoon (10), Moon and Rudinger (12), and data tabulated by Sandir and Hashra (31), it can be seen that the reattachment point for a suddenly expanding nonswirling flow is found between 6 to 9 step heights downstream of the inlet regardless of the expansion ratio. The tabulation of the data from (31) is added to the present data and that of (10), to show the consistancy of reattachment point location for D/d > 1, in Table XXIII.

Table XXIV and Figure 16 show the variation of CTRZ length with expansion ratio, the present data is added to that of (10) in the table and the figure. They show no clear trend for moderate swirl: the CTRZ length decreases from 1.5 to 1.5 to 0 diameters as the expansion ratio decreases from 2 to 1.5 to 1. However, there is a steady decrease in CTRZ length for strong swirl: it goes from 1.2 to 0.75 to 0.5 diameters as the expansion ratio goes from 2 to 1.5 to 1. In general, the length of the CTRZ decreases as the expansion ratio decreases, and this effect becomes more pronounced as the swirl strength increases.

4.2 Effect of Gradual Expansion on Open-Ended Flows

Gradual expansion flows with α = 45 degrees were photographed and measured at x/D = 0.5 and 1.0 for ϕ = 0, 45 and 70 degrees. This was for the case D/d = 1.5 only. The flow visualization photographs are shown in Figure 17 parts a through c, and the velocity profiles are shown in parts a, b and c of Figure 18.

Previous researchers (7, 9, 10) have shown, and the pictures in Figure 17 confirm, that a gradual expansion inlet has no effect on the flowfield more than one diameter from the test section inlet. Figures 18 and 19 show that gradual expansion has only a small effect on the flow near the inlet. The nonswirling flow measurements plotted in Figure 18(a) appear to be identical to the corresponding sudden expansion flow data in Figure 13(a). The photographs of Figure 12(a) and Figure 17(a) are also comparable: they both identify the reattachment point at $x/D = 1.25$. The swirling flow photographs (Figure 18 parts b and c) show no change in CTRZ length with gradual expansion; and the velocity profiles of Figure 18 parts b and c differ from parts b and c of Figure 13 only in the increased near-wall swirl velocity for gradual expansion in the upstream region only (i.e., approximately $x/D < 1.0$).

Yoon (10) concluded that the major effect of gradual expansion is to encourage the air to flow along the wall and accelerate axial velocities close to the wall. That effect is diminished when the expansion ratio decreases.

Since a gradual expansion does not appreciably alter a flowfield, it would be redundant to investigate a gradual expansion flow with downstream blockage. Hence blockage effects investigated in Section 4.3 are for the sudden expansion and no expansions cases only.

4.3 Effect of Blockages on Flows

To better illustrate the effects of downstream blockages, the data obtained with each blockage in place are compared to the data obtained for open-ended flows. Measurements were taken at the same locations (when necessary) as for the open-ended flows of Section 4.1;

and flow visualization photographs are shown with the small blockage (area ratio 2) in place. The flow visualization photographs and the velocity profiles for the flows with the small blockage are shown in Figures 19 through 22. The velocity profiles for flows with the large blockage (area ratio 4) are shown in Figure 23 and 24. The blockages are placed 2 diameters downstream of the exit plane in each case.

Figure 19(a) shows the small blockage in a nonswirling flow with expansion ratio 1.5. When compared to Figure 12(a) it is seen that the CRZ is shortened somewhat, with reattachment at x/D = 1.2, but the pathlines are altered only at the blockage; therefore Figure 20(a) shows the velocity profiles at x/D = 2.0 only. The axial velocity is essentially zero near the wall and the centerline region is accelerated, as expected. In addition, a small swirl velocity is induced in the near-wall region.

The moderate swirl flow shown pictorially in Figure 19(b) and profiled in Figure 20(b) has a shorter CTRZ (it extends to x/D = 1.25) and higher axial velocities near the centerline than the corresponding open-ended flow shown in part b of Figures 12 and 13. The corner recirculation zone appears to be unaffected by the blockage; but only a large change could be detected on a CRZ of this length (0.25 diameters). Also, the swirl velocity and the swirl velocity gradient in the radial direction increases slightly with the small blockage in place.

When the swirl vane angle is increased to 70 degrees, the CTRZ length decreases to x/D = 0.4 and the precessing vortex core becomes noticeably wider, as seen in Figure 19(c). Figure 20(c) shows axial velocities that are diminished in the near-wall region and accelerated near the centerline, and swirl velocities that are increased near the centerline

in comparison to the velocities shown in Figure 13(c). The only change from the moderate swirl case is the wider vortex core.

Decreasing the expansion ratio to 1 does not change the relation between the small blocked flows and the open-ended flows that is documented above. Figures 21 and 22 show: axial velocities that are diminished near the wall and increased near the centerline; swirl velocities that are increased near the centerline and diminished near the wall for the swirling flows; and a small induced swirl velocity near the wall for the nonswirling flow. The only change is for the strong swirl flow of Figure 22(c): the centerline axial velocities at $x/D = 0.5$ and 1 are large and negative, indicating that the CTRZ is longer for the small blocked flow than for the open-ended flow. This phenomenon does not occur in strong swirl flows for other expansion ratios; it is most likely a result of continuity: the near-centerline velocities are increased and the near-wall velocities are not yet appreciably diminished, thus the centerline flow is reversed to balance the mass flow.

When the data of Figures 19 through 22 are compared to the analogous data of (10), it is clear that placing a small blockage 2 diameters downstream of the exit plane produces the same changes from the open-ended case regardless of the expansion ratio: the axial and swirl velocities decrease near the wall and increase near the centerline for swirling and nonswirling flows, with the exception of the small induced swirl in the nonswirling flow.

The effect of a stronger blockage (area ratio 4) is also investigated for swirl vane angles $\phi = 0$, 45 and 70 degrees on flowfields with expansion ratios of 1.5 or 1. The axial and swirl velocity profiles are

shown in Figures 23 and 24 for D/d = 1.5 and 1, respectively.

The nonswirling flow of Figure 23(a) shows a CRZ extending to about x/D = 1.2, larger centerline velocities than for the unblocked flow and a slight induced swirl in the near-wall region at x/D = 2. This flowfield is very similar to that of Figue 20(a) - the small blocked flow.

The axial velocity profiles of Figure 23(b) detail the significant effect of the large blockage on the moderately swirling flow. The near-wall velocities are blunted all the way upstream to x/D = 0.5, and the accompanying centerline acceleration results in the absence of a CTRZ. The swirl velocities shown in the same figure are noticeably greater than those of part b of Figures 13 and 20. It is likely that the CRZ is also eliminated but, no pictures are available to substantiate that claim.

Figure 23(c) shows that there is a negative axial velocity region at x/D = 0.5 but, it is small; therefore, it is probable that the CTRZ ends near x/D = 0.5. Again, the centerline axial and swirl velocities are increased and the near-wall axial and swirl velocities are decreased from their unblocked counterparts due to the presence of the blockage.

It should be noted that the centerline axial velocities for the strong swirl flow do not increase nearly as much as for the moderate swirl flow; this is probably due to the lower axial momentum of the strong swirl flow.

Reducing the expansion ratio to 1 results in the flowfield alterations shown in Figure 24 parts a, b, and c. The nonswirling flow of part a exhibits the familiar change: induced swirl near the blockage and centerline acceleration. For the moderate swirl of part b, the

velocity profiles are nearly identical to Figure 23(b) for expansion ratio 1.5: large increase in centerline axial and swirl velocities and diminished near-wall velocities. Again, the strong swirl flow of part c is essentially an exaggerated version of Figure 22(c): the centerline axial velocities at x/D = 0.5 and 1.0 are negative; the off-centerline axial and swirl velocities are very large; and the axial and swirl velocities diminish near the wall.

Correlating the present data to that of (10) for D/d = 2, it is clear that the effect of a blockage is to: accelerate the axial and swirl velocities near the centerline; diminish those velocities near the wall; and decrease the length of the CTRZ. The effect is greater when the degree of blockage is greater. For strong swirl flows, a blockage increases the length of CTRZ when the expansion ratio is 1. Otherwise (i.e., D/d 1), a blockage shortens the CTRZ.

Artistic impressions of the data presented are shown in Figures 25 through 31. The corresponding figures of (10) are repeated in Figures 32 through 35 for comparative purposes.

CHAPTER V

CLOSURE

5.1 Summary

This study uses flow visualization and time-mean velocity measurements to analyze the effects of swirl, downstream blockage, inlet expansion and expansion ratio on confined, inert flows. The flow yaw and pitch angles, the three normalized velocity components and the flow visualization photographs are presented for swirl vane angles ϕ = 0, 45 and 70 degrees, blockages of area ratio 2 and 4 located 2 diameters from the test section inlet, expansion angles α = 45 and 90 degrees, and expansion ratios of 1.5 and 1.

The CRZ is prominent in nonswirling expanding flows, but it decreases when swirl is introduced and disappears when centrifugal forces predominate. The presence of swirl results in the formation of a CTRZ. Initially, increases in ϕ result in an increase in CTRZ length. However, increasing ϕ to very high swirl strengths results in a shortening of the CTRZ.

Placing a blockage in the flowfield creates an adverse pressure gradient near the wall and a favorable pressure gradient near the centerline. This results in increased axial and swirl velocities near the centerline and decreased velocities near the wall. The blockage also decreases the CTRZ length, except for strong swirl flows with no expansion (i.e., D/d = 1). The degree of the effect increases as the degree of blockage increases.

Reduction of the expansion ratio results in a reduction of the CTRZ, as is apparent when the present data are compared to that of Yoon (10). There is no CTRZ for moderate swirl in a nonexpanding flow. Also, placing a blockage in a nonexpanding, strongly swirling flow increases the CTRZ length; an opposite effect is observed for expanding (i.e. $D/d > 1$) flows. The CRZ length (measured in step heights) does not change with expansion ratio for $D/d > 1$.

Changing the inlet from sudden to gradual expansion has a minimal effect on the flow.

5.2 Recommendations for Further Work

This study is one in a series of studies on confined, inert swirling flows. Major flow features and turbulence data are now available. The characteristics of different inlet swirl vanes are needed: work should be done with curved vanes, and different size and number of vanes in the present swirl-vane pack. This will provide a comprehensive data base of inlet and flowfield measurements which is needed for associated flowfield prediction studies.

REFERENCES

1. Abujelala, M. T. and D. G. Lilley. "Confined Swirling Flow Predictions," Paper AIAA-83-0316, Reno, Nevada, January 10-13, 1983.

2. Ha Minh, H. and P. Chaissaing. "Perturbations of Turbulent Pipe Flow," Proceedings, Symposium on Turbulent Shear Flows, Pennsylvania State University, April 1977, pp. 13.9-13.17.

3. Bradshaw, P. and F. Y. F. Wong. "Reattachment of a Confined Turbulent Diffusion Flame Burner," Journal of Fluid Mechanics, Volume 52, Pt. 1, 1972, pp. 113-135.

4. Hutchinson, P., E. E. Khalil, and J. H. Whitelaw. "Measurement and Calculation of Furnace-Flow Properties," Journal of Energy, Volume 1, July-August 1977, pp. 211-219.

5. Macagno, E. D., and Tin-Kan Hung. "Computational and Experimental Study of a Captive Annular Eddy," Journal of Fluid Mechanics, Vol. 28, Pt. 1, 1967, pp. 43-64.

6. Nozaki, T., and Keiji Hatta. "Reattachment Flow Issuing From a Finite Width Nozzle (Report 3: Effects of Inclinations of Reattachment Wall)," Bulletin of the JSME, Volume 25, No. 200, February 1982.

7. Rhode, D. L. "Predictions and Measurements of Isothermal Flowfields in Axisymmetric Combustor Geometries," Ph.D. Thesis, Oklahoma State University, Stillwater, Oklahoma, December 1981.

8. Rhode, D. L., D. G. Lilley, and D. K. McLaughlin. "On the Prediction of Swirling Flowfields Found in Axisymmetric Combustor Geometries," ASME Journal of Fluids Engng., Vol. 104, 1982, pp. 378-384.

9. Rhode, D. L., D. G. Lilley, and D. K. McLaughlin. "Mean Flowfields in Axisymmetric Combustor Geometries with Swirl," Paper AIAA-82-0177, Orlando, Florida, Jan. 11-14, 1982.

10. Yoon, H. K. "Five-Hole Pitot Probe Time-Mean Velocity Measurements in Confined Swirling Flows," M.S. Thesis, Oklahoma State University, Stillwater, Oklahoma, July 1982.

11. Yoon, H. K., and D. G. Lilley. "Five-Hole Pitot Probe Time-Mean Velocity Measurements in Confined Swirling Flows," Paper AIAA-85-0315, Reno, Nevada, Jan. 1983.

12. Moon, L. F., and G. Rudinger. "Velocity Distribution in an Abruptly Expanding Circular Duct," Journal of Fluids Engineering, March 1977, pp. 226-230.

13. Janjua, S. I. "Turbulence Measurements in a Complex Flowfield Using a Six-Orientation Hot-Wire Probe Technique," M.S. Thesis, Oklahoma State University, Stillwater, Oklahoma, December 1981.

14. Chaturvedi, M. C. "Flow Characteristics of Axisymmetric Expansions," Proceeding, Journal of the Hydraulics Division, ASCE, Vol. 89, No. HY3, 1963, pp. 61-92.

15. Mathur, M. L., and N. R. L. MacCallum. "Swirling Air Jets Issuing from Vane Swirlers. Part 1: Free Jets; Part 2: Enclosed Jets," Journal of the Institute of Fuel, Vol. 40, May, 1967, pp. 238-245.

16. Syred, N., and K. R. Dahman. "Effect of High Levels of Confinement Upon the Aerodynamics of Swirl Burners," Journal of Energy, Vol. 2, No. 1, Jan.-Feb. 1978; pp. 8-15.

17. Afrosimova, V. N. "Study of the Aerodynamics of a Furnace Space," Thermal Engineering, Vol. 14, Part 1, 1967, pp. 10-15.

18. Yang, B. T., and M. H. Yu. "The Flowfield in a Suddenly Enlarged Combustion Chamber," AIAA Journal, Vol. 21, No. 1, Jan. 1983, pp. 92-97.

19. Owen, F. K. "Laser Velocimeter Measurements of a Confined Turbulent Diffusion Flame Burner," Paper AIAA-76-33, Washington, D. C., Jan. 26-28, 1976.

20. Sander, G. F. "Axial Vane-Type Swirler Performance Characteristics," M.S. Thesis, Oklahoma State University, Stillwater, Oklahoma, July, 1983.

21. Abbott, D. E., and S. J. Kline. "Experimental Investigation of Subsonic Turbulent Flow Over Single and Double Backward Facing Steps," Journal of Basic Engineering, Sept. 1962, pp. 317-325.

22. Bird, J. D. "Visualization of a Flowfield by Tuft Grid Technique," Journal of Aeronautical Science, Vol. 19, 1952, pp. 481-485.

23. Back, L. H. and E. J. Roschke. "Shear Layer Flow Regimes and Wave Instabilities and Reattachment Lengths Downstream of an Abrupt Circular Channel Expansion," Journal of Applied Mechanics, Transactions ASME, Vol. 94E, Sept. 1972, pp. 677-81.

24. Runchal, A. K. "Mass Transfer Investigation in Turbulent Flow Downstream of Sudden Enlargement of a Circular Pipe for Very High Schmidt Numbers," Journal of Heat Transfer, Transactions of ASME, Vol. 88C, Feb. 1966, pp. 131-136.

25. Morel, T. "Comprehensive Design of Axisymmetric Wind Tunnel Contractions," Paper ASME 75-FE-17, Minneapolis, Minnesota, May 5-7, 1975.

26. Beer, J. M., and N. A. Chigier. Combusion Aerodynamics, London: Applied Science; New York: Halsted-Wiley, 1972.

27. Hinze, J. O. Turbulence: An Introduction to its Mechanism and Theory, New York: McGraw-Hill, 1959.

28. McKillop, B. E., and D. G. Lilley. "A Variable Vane Angle Swirler," Report on Work in Progress, Oklahoma State University, Stillwater, Oklahoma, July, 1982.

29. Sander, G. F. "The Performance of an Annular Vane Swirler," Paper AIAA 83-1326, Seattle, Washington, June 27-29, 1983.

30. Lefebvre, A. H. Gas Turbine Combustion, New York: McGraw-Hill, 1983.

31. Sindir, M. M., and P. T. Harsha. Assessment of Turbulence Models for Scramjet Flowfields, NASA CR 3643, 1982.

APPENDIX A

TABLES

TABLE I

WIND TUNNEL FAN SPEEDS AND INLET NOZZLE REYNOLDS NUMBERS

ϕ	Fan Speed (rpm)	Re_d(D/d = 1.5)	Re_d(D/d = 1.0)
0	1950	125,000	86,400
45	2600	66,600	64,400
70	2600	28,700	28,000

TABLE II

VELOCITY DATA FOR ϕ = 0, α = 90, D/d = 1.5, OPEN ENDED

R/D	X/D 0.5	1.0	1.5	2.0
0.467	0.000	0.000	0.000	0.000
0.433	0.000	0.000	0.000	0.000
0.400	0.000	0.000	0.000	0.000
0.367	0.000	0.000	0.000	0.000
0.333	0.000	0.000	0.000	0.000
0.300	0.000	0.000	0.000	0.000
0.267	360.000	359.800	358.200	358.000
0.233	0.000	0.000	0.000	0.000
0.200	0.000	0.000	0.000	0.000
0.167	0.000	0.000	0.000	0.000
0.133	0.000	0.000	0.000	0.000
0.100	0.000	0.000	0.000	0.000
0.067	0.000	0.000	0.000	0.000
0.033	0.000	0.000	0.000	0.000
0.000	360.000	360.000	358.600	358.000

a) yaw angle

TABLE II (Continued)

R/D	X/D 0.5	1.0	1.5	2.0
0.467	0.000	0.000	0.000	0.000
0.433	0.000	0.000	0.000	0.000
0.400	0.000	0.000	0.000	0.000
0.367	0.000	0.000	0.000	0.000
0.333	0.000	0.000	0.000	0.000
0.300	0.000	0.000	0.000	0.000
0.267	-2.371	-0.911	-0.908	-3.382
0.233	0.000	0.000	0.000	0.000
0.200	0.000	0.000	0.000	0.000
0.167	0.000	0.000	0.000	0.000
0.133	0.000	0.000	0.000	0.000
0.100	0.000	0.000	0.000	0.000
0.067	0.000	0.000	0.000	0.000
0.033	0.000	0.000	0.000	0.000
0.000	-3.257	-1.505	-0.131	-2.173

b) pitch angle

TABLE II (Continued)

R/D	X/D 0.5	1.0	1.5	2.0
0.467	-0.142	-0.033	0.126	0.146
0.433	-0.127	-0.004	0.204	0.280
0.400	0.138	0.175	0.264	0.322
0.367	0.324	0.327	0.353	0.375
0.333	0.586	0.483	0.447	0.427
0.300	0.843	0.645	0.541	0.482
0.267	0.964	0.779	0.616	0.538
0.233	0.986	0.855	0.689	0.587
0.200	0.988	0.895	0.740	0.631
0.167	0.974	0.905	0.776	0.665
0.133	0.982	0.911	0.792	0.698
0.100	0.969	0.902	0.809	0.708
0.067	0.957	0.910	0.811	0.721
0.033	0.972	0.909	0.812	0.728
0.000	0.968	0.906	0.808	0.729

c) u/u_0

TABLE II (Continued)

R/D	X/D 0.5	1.0	1.5	2.0
0.467	-0.102	0.000	0.000	-0.048
0.433	-0.167	0.058	-0.011	-0.003
0.400	-0.014	-0.069	-0.037	-0.011
0.367	-0.036	-0.068	-0.048	-0.020
0.333	-0.033	-0.067	-0.043	-0.025
0.300	-0.013	-0.057	-0.040	-0.018
0.267	-0.027	-0.024	-0.030	-0.018
0.233	-0.064	-0.007	-0.015	-0.009
0.200	-0.070	-0.016	-0.003	-0.001
0.167	-0.077	-0.024	-0.010	-0.005
0.133	-0.082	-0.037	-0.021	-0.011
0.100	-0.074	-0.045	-0.026	-0.019
0.067	-0.087	-0.055	-0.035	-0.027
0.033	-0.097	-0.062	-0.041	-0.030
0.000	-0.103	-0.067	-0.048	-0.042

d) v/u_o

TABLE II (Continued)

R/D	X/D 0.5	1.0	1.5	2.0
0.467	0.007	-0.006	-0.015	-0.005
0.433	-0.004	0.074	-0.025	-0.010
0.400	0.004	-0.012	-0.025	-0.011
0.367	0.009	-0.022	-0.033	-0.013
0.333	0.016	-0.019	-0.030	-0.015
0.300	-0.000	-0.018	-0.026	-0.017
0.267	-0.010	-0.008	-0.030	-0.017
0.233	-0.010	-0.006	-0.019	-0.018
0.200	-0.010	-0.003	-0.010	-0.015
0.167	-0.014	-0.003	-0.011	-0.012
0.133	-0.007	-0.003	-0.003	-0.002
0.100	-0.027	-0.016	0.006	-0.000
0.067	-0.003	-0.003	0.006	-0.000
0.033	-0.003	-0.003	0.006	-0.000
0.000	-0.000	-0.000	-0.000	-0.000

e) w/u_0

TABLE III

VELOCITY DATA FOR ϕ = 45, α = 90, D/d = 1.5, OPEN ENDED

R/D	X/D 0.5	1.0	1.5	2.0
0.467	1.246	0.831	0.458	0.513
0.433	1.111	0.704	0.484	0.525
0.400	0.807	0.545	0.493	0.532
0.367	0.456	0.398	0.484	0.524
0.333	0.142	0.287	0.465	0.512
0.300	-0.082	0.199	0.444	0.489
0.267	-0.243	0.128	0.409	0.445
0.233	-0.316	0.079	0.371	0.391
0 200	-0.317	0.027	0.314	0.318
0.167	-0.291	0.002	0.248	0.241
0.133	-0.227	-0.023	0.180	0.167
0.100	-0.171	-0.040	0.120	0.106
0.067	-0.111	-0.052	0.064	0.060
0.033	-0.068	-0.079	0.021	0.033
0.000	-0.108	-0.072	0.004	0.035

a) yaw angle

TABLE III (Continued)

R/D	X/D 0.5	1.0	1.5	2.0
0.467	0.000	0.000	0.000	0.000
0.433	0.000	0.000	0.000	0.000
0.400	0.000	0.000	0.000	0.000
0.367	0.000	0.000	0.000	0.000
0.333	0.000	0.000	0.000	0.000
0.300	0.000	0.000	0.000	0.000
0.267	-13.001	-5.477	-2.057	-0.949
0.233	0.000	0.000	0.000	0.000
0.200	0.000	0.000	0.000	0.000
0.167	0.000	0.000	0.000	0.000
0.133	0.000	0.000	0.000	0.000
0.100	0.000	0.000	0.000	0.000
0.067	0.000	0.000	0.000	0.000
0 033	0.000	0.000	0.000	0.000
0.000	0.000	-7.094	-3.013	-1.290

b) pitch angle

TABLE III (Continued)

R/D	X/D 0.5	1.0	1.5	2.0
0.467	1.246	0.831	0.458	0.513
0.433	1.111	0.704	0.484	0.525
0.400	0.807	0.545	0.493	0.532
0.367	0.456	0.398	0.484	0.524
0.333	0.142	0.287	0.465	0.512
0.300	-0.082	0.199	0.444	0.489
0.267	-0.243	0.128	0.409	0.445
0.233	-0.316	0.079	0.371	0.391
0.200	-0.317	0.027	0.314	0.318
0.167	-0.291	0.002	0.248	0.241
0.133	-0.227	-0.023	0.180	0.167
0.100	-0.171	-0.040	0.120	0.106
0.067	-0.111	-0.052	0.064	0.060
0.033	-0.068	-0.079	0.021	0.033
0.000	-0.108	-0.072	0.004	0.035

c) u/u_0

TABLE III (Continued)

R/D	X/D 0.5	1.0	1.5	2.0
0.467	-0.032	-0.006	0.055	0.066
0.433	-0.157	-0.095	-0.043	-0.004
0.400	-0.210	-0.112	-0.036	-0.001
0.367	-0.264	-0.133	-0.046	-0.008
0.333	-0.231	-0.129	-0.045	-0.016
0.300	-0.090	-0.123	-0.041	-0.021
0.267	-0.026	-0.152	-0.036	-0.027
0.233	-0.001	-0.142	-0.031	-0.032
0.200	0.006	-0.183	-0.031	-0.044
0.167	0.000	-0.078	-0.035	-0.050
0.133	-0.004	-0.072	-0.040	-0.064
0.100	-0.023	-0.069	-0.045	-0.069
0.067	-0.028	-0.061	-0.049	-0.063
0.033	-0.046	-0.048	-0.056	-0.052
0.000	-0.033	-0.033	-0.047	0.000

d) v/u_0

TABLE III (Continued)

R/D	X/D 0.5	1.0	1.5	2.0
0.467	0.586	0.693	0.722	0.767
0.433	0.566	0.714	0.740	0.767
0.400	0.493	0.697	0.754	0.777
0.367	0.391	0.689	0.781	0.783
0.333	0.326	0.683	0.806	0.800
0.300	0.394	0.693	0.828	0.815
0.267	0.456	0.684	0.839	0.816
0.233	0.476	0.701	0.834	0.808
0.200	0.478	0.703	0.817	0.779
0.167	0.438	0.705	0.763	0.726
0.133	0.364	0.660	0.690	0.649
0.100	0.273	0.577	0.566	0.543
0.067	0.178	0.439	0.422	0.394
0.033	0.095	0.287	0.240	0.221
0.000	0.017	0.108	0.069	-0.000

e) w/u_0

TABLE IV

VELOCITY DATA FOR ϕ = 70, α = 90, D/d = 1.5, OPEN ENDED

R/D	X/D 0.5	1.0	1.5	2.0
0.467	0.000	0.000	0.000	0.000
0.433	0.000	0.000	0.000	0.000
0.400	0.000	0.000	0.000	0.000
0.367	0.000	0.000	0.000	0.000
0.333	0.000	0.000	0.000	0.000
0.300	0.000	0.000	0.000	0.000
0.267	95.600	93.000	83.000	71.000
0.233	0.000	0.000	0.000	0.000
0.200	0.000	0.000	0.000	0.000
0.167	0.000	0.000	0.000	0.000
0.133	0.000	0.000	0.000	0.000
0.100	0.000	0.000	0.000	0.000
0.067	0.000	0.000	0.000	0.000
0.033	0.000	0.000	0.000	0.000
0.000	103.000	93.800	86.800	75.200

a) yaw angle

TABLE IV (Continued)

R/D	X/D 0.5	1.0	1.5	2.0
0.467	0.000	0.000	0.000	0.000
0.433	0.000	0.000	0.000	0.000
0.400	0.000	0.000	0.000	0.000
0.367	0.000	0.000	0.000	0.000
0.333	0.000	0.000	0.000	0.000
0.300	0.000	0.000	0.000	0.000
0.267	-40.376	-17.137	-11.658	-8.626
0.233	0.000	0.000	0.000	0.000
0.200	0.000	0.000	0.000	0.000
0.167	0.000	0.000	0.000	0.000
0.133	0.000	0.000	0.000	0.000
0.100	0.000	0.000	0.000	0.000
0.067	0.000	0.000	0.000	0.000
0.033	0.000	0.000	0.000	0.000
0.000	0.000	-20.867	-12.953	-9.446

b) pitch angle

TABLE IV (Continued)

R/D	X/D 0.5	1.0	1.5	2.0
0.467	1.350	0.669	0.870	0.738
0.433	0.999	0.690	0.841	0.775
0.400	0.618	0.653	0.786	0.759
0.367	0.300	0.579	0.697	0.709
0.333	0.102	0.490	0.588	0.606
0.300	-0.054	0.377	0.471	0.470
0.267	-0.152	0.244	0.321	0.346
0.233	-0.212	0.096	0.177	0.209
0.200	-0.249	-0.058	0.017	0.090
0.167	-0.284	-0.180	-0.161	-0.015
0.133	-0.230	-0.245	-0.145	-0.068
0.100	-0.127	-0.192	-0.116	-0.070
0.067	-0.057	-0.085	-0.094	-0.079
0.033	0.062	-0.024	-0.017	-0.049
0.000	0.112	0.055	0.028	-0.056

c) u/u_0

TABLE IV (Continued)

R/D	X/D 0.5	1.0	1.5	2.0
0.467	0.000	-0.148	-0.113	-0.032
0.433	-0.288	-0.119	-0.089	-0.192
0.400	-0.356	-0.187	-0.138	-0.249
0.367	-0.369	-0.217	-0.166	-0.257
0.333	-0.387	-0.234	-0.197	-0.283
0.300	-0.379	-0.281	-0.208	-0.306
0.267	-0.376	-0.314	-0.224	-0.336
0.233	-0.390	-0.336	-0.242	-0.354
0.200	-0.398	-0.374	-0.253	-0.372
0.167	-0.390	-0.404	-0.262	-0.388
0.133	-0.403	-0.416	-0.252	-0.401
0.100	-0.434	-0.448	-0.311	-0.401
0.067	-0.358	-0.430	-0.278	-0.420
0.033	-0.327	-0.411	-0.305	-0.425
0.000	-0.276	0.000	0.000	0.000

d) v/u_0

TABLE IV (Continued)

R/D	X/D 0.5	1.0	1.5	2.0
0.467	1.728	1.799	1.722	1.582
0.433	1.624	1.854	1.755	1.661
0.400	1.546	1.897	1.799	1.705
0.367	1.603	1.966	1.816	1.755
0.333	1.629	1.965	1.832	1.761
0.300	1.734	1.975	1.836	1.778
0.267	1.742	1.929	1.822	1.750
0.233	1.729	1.837	1.742	1.705
0.200	1.610	1.674	1.648	1.614
0.167	1.386	1.462	1.439	1.478
0.133	1.119	1.213	1.257	1.298
0.100	0.837	0.952	1.004	1.051
0.067	0.540	0.652	0.810	0.808
0.033	0.272	0.362	0.489	0.497
0.000	0.183	0.167	0.083	0.242

TABLE V

VELOCITY DATA FOR $\bar{\phi}$ = 0, D/d = 1.0, OPEN ENDED

R/D	X/D 0.5	1.0	1.5	2.0
0.350	0.000	0.000	0.000	0.000
0.300	0.000	0.000	0.000	0.000
0.250	0.000	0.000	0.000	0.000
0.200	0.000	0.000	0.000	0.000
0.150	0.000	0.000	0.000	0.000
0.100	0.000	0.000	0.000	0.000
0.050	0.000	0.000	0.000	0.000
0.000	360.000	360.000	0.400	0.000

a) yaw angle

R/D	X/D 0.5	1.0	1.5	2.0
0.350	0.000	0.000	0.000	0.000
0.300	0.000	0.000	0.000	0.000
0.250	0.000	0.000	0.000	0.000
0.200	0.000	0.000	0.000	0.000
0.150	0.000	0.000	0.000	0.000
0.100	0.000	0.000	0.000	0.000
0.050	0.000	0.000	0.000	0.000
0.000	-2.559	-2.766	-2.464	0.000

b) pitch angle

TABLE V (Continued)

R/D	X/D 0.5	1.0	1.5	2.0
0.350	0.957	1.021	1.074	1.079
0.300	0.963	1.034	1.074	1.081
0.250	0.964	1.020	1.076	1.084
0.200	0.949	1.012	1.078	1.086
0.150	0.947	1.011	1.078	1.083
0.100	0.934	1.003	1.076	1.086
0.050	0.930	1.004	1.079	1.086
0.000	0.915	0.976	1.077	1.088

c) u/u_0

R/D	X/D 0.5	1.0	1.5	2.0
0.350	-0.078	-0.037	-0.023	-0.039
0.300	-0.090	-0.043	-0.042	-0.047
0.250	-0.071	-0.067	-0.045	-0.051
0.200	-0.095	-0.059	-0.049	-0.053
0.150	-0.086	-0.063	-0.049	-0.052
0.100	-0.095	-0.073	-0.047	-0.051
0.050	-0.103	-0.055	-0.047	-0.050
0.000	-0.104	-0.068	-0.044	-0.049

d) v/u_0

TABLE V (Continued)

R/D	X/D 0.5	1.0	1.5	2.0
0.350	-0.010	-0.021	0.015	0.008
0.300	-0.010	-0.007	-0.000	0.008
0.250	-0.003	0.014	-0.000	-0.000
0.200	-0.000	0.004	-0.000	-0.000
0.150	-0.003	-0.004	-0.000	-0.000
0.100	0.003	-0.021	-0.000	-0.000
0.050	0.006	0.011	-0.000	-0.000
0.000	-0.000	-0.000	-0.000	-0.000

e) w/u_o

TABLE VI

VELOCITY DATA FOR ϕ = 45, D/d = 1.0, OPEN-ENDED

R/D	X/D 0.5	1.0	1.5	2.0
0.350	0.000	0.000	0.000	0.000
0.300	0.000	0.000	0.000	0.000
0.250	0.000	0.000	0.000	0.000
0.200	0.000	0.000	0.000	0.000
0.150	0.000	0.000	0.000	0.000
0.100	0.000	0.000	0.000	0.000
0.050	0.000	0.000	0.000	0.000
0.000	360.000	52.600	49.400	0.000

a) yaw angle

R/D	X/D 0.5	1.0	1.5	2.0
0.350	0.000	0.000	0.000	0.000
0.300	0.000	0.000	0.000	0.000
0.250	0.000	0.000	0.000	0.000
0.200	0.000	0.000	0.000	0.000
0.150	0.000	0.000	0.000	0.000
0.100	0.000	0.000	0.000	0.000
0.050	0.000	0.000	0.000	0.000
0.000	-17.541	-4.311	-0.650	0.000

b) pitch angle

TABLE VI (Continued)

R/D	X/D 0.5	1.0	1.5	2.0
0.350	1.173	1.146	1.205	1.236
0.300	1.108	1.172	1.182	1.222
0.250	0.893	1.084	1.081	1.130
0.200	0.648	0.840	0.867	0.932
0.150	0.600	0.637	0.732	0.759
0.100	0.696	0.607	0.687	0.652
0.050	0.725	0.565	0.620	0.564
0.000	0.496	0.341	0.367	0.426

c) u/u_0

R/D	X/D 0.5	1.0	1.5	2.0
0.350	0.051	-0.090	-0.067	0.038
0.300	-0.086	-0.138	-0.133	-0.021
0.250	-0.171	-0.169	-0.207	-0.040
0.200	-0.184	-0.195	-0.253	-0.071
0.150	-0.188	-0.174	-0.214	-0.094
0.100	-0.184	-0.113	-0.185	-0.141
0.050	-0.338	-0.095	-0.211	-0.169
0.000	-0.248	0.143	-0.153	-0.135

d) v/u_0

TABLE VI (Continued)

R/D	X/D 0.5	1.0	1.5	2.0
0.350	1.398	1.356	1.284	1.271
0.300	1.571	1.500	1.439	1.426
0.250	1.599	1.632	1.533	1.533
0.200	1.340	1.528	1.315	1.381
0.150	1.023	1.094	0.892	0.992
0.100	0.807	0.794	0.650	0.680
0.050	0.745	0.659	0.520	0.441
0.000	0.057	0.013	0.105	-0.000

e) w/u_0

TABLE VII

VELOCITY DATA FOR ϕ = 70, D/d = 1.0, OPEN-ENDED

R/D	X/D 0.5	1.0	1.5	2.0
0.350	0.000	0.000	0.000	0.000
0.300	0.000	0.000	0.000	0.000
0.250	0.000	0.000	0.000	0.000
0.200	0.000	0.000	0.000	0.000
0.150	0.000	0.000	0.000	0.000
0.100	0.000	0.000	0.000	0.000
0.050	0.000	0.000	0.000	0.000
0.000	63.800	77.000	74.400	0.000

a) yaw angle

R/D	X/D 0.5	1.0	1.5	2.0
0.350	0.000	0.000	0.000	0.000
0.300	0.000	0.000	0.000	0.000
0.250	0.000	0.000	0.000	0.000
0.200	0.000	0.000	0.000	0.000
0.150	0.000	0.000	0.000	0.000
0.100	0.000	0.000	0.000	0.000
0.050	0.000	0.000	0.000	0.000
0.000	57.534	-19.987	-10.871	0.000

b) pitch angle

TABLE VII (Continued)

R/D	X/D 0.5	1.0	1.5	2.0
0.350	1.143	1.430	1.187	1.192
0.300	0.865	1.027	0.883	0.842
0.250	0.602	0.596	0.526	0.532
0.200	0.406	0.506	0.413	0.446
0.150	0.418	0.483	0.457	0.480
0.100	0.388	0.527	0.559	0.533
0.050	0.285	0.397	0.510	0.437
0.000	-0.090	0.474	0.762	0.208

c) u/u_0

R/D	X/D 0.5	1.0	1.5	2.0
0.350	-0.746	-0.460	-0.748	-0.392
0.300	-0.874	-0.792	-0.887	-0.602
0.250	-0.920	-0.840	-0.962	-0.683
0.200	-1.001	-0.860	-1.012	-0.745
0.150	-1.098	-0.878	-1.009	-0.775
0.100	-0.893	-0.622	-0.922	-0.785
0.050	-0.861	-0.732	-0.989	-0.887
0.000	0.000	-0.310	-0.346	0.741

d) v/u_0

TABLE VII (Continued)

R/D	X/D 0.5	1.0	1.5	2.0
0.350	3.517	3.504	3.409	3.205
0.300	3.183	3.319	3.204	3.017
0.250	2.830	2.956	2.922	2.736
0.200	2.564	2.604	2.610	2.481
0.150	2.071	2.224	2.224	2.077
0.100	1.681	1.681	1.660	1.497
0.050	0.932	1.166	1.027	0.937
0.000	-0.008	-0.000	0.148	0.423

e) w/u_0

TABLE VIII

VELOCITY DATA FOR ϕ = 0, α = 45, D/d = 1.5

R/D	X/D 0.5	X/D 1.0
0.467	0.000	0.000
0.433	0.000	0.000
0.400	0.000	0.000
0.367	0.000	0.000
0.333	0.000	0.000
0.300	0.000	0.000
0.267	360.000	359.600
0.233	0.000	0.000
0.200	0.000	0.000
0.167	0.000	0.000
0.133	0.000	0.000
0.100	0.000	0.000
0.067	0.000	0.000
0.033	0.000	0.000
0.000	360.000	359.800

a) yaw angle

R/D	X/D 0.5	X/D 1.0
0.467	0.000	0.000
0.433	0.000	0.000
0.400	0.000	0.000
0.367	0.000	0.000
0.333	0.000	0.000
0.300	0.000	0.000
0.267	-3.798	-3.156
0.233	0.000	0.000
0.200	0.000	0.000
0.167	0.000	0.000
0.133	0.000	0.000
0.100	0.000	0.000
0.067	0.000	0.000
0.033	0.000	0.000
0.000	-4.742	-3.515

b) pitch angle

TABLE VIII (Contiued)

R/D	X/D 0.5	1.0
0.467	-0.110	-0.067
0.433	-0.105	-0.066
0.400	-0.104	0.139
0.367	0.134	0.297
0.333	0.433	0.483
0.300	0.775	0.644
0.267	0.980	0.797
0.233	1.014	0.882
0.200	1.010	0.931
0.167	1.009	0.940
0.133	1.012	0.945
0.100	1.010	0.949
0.067	1.006	0.945
0.033	1.007	0.951
0.000	1.011	0.944

c) u/u_0

R/D	X/D 0.5	1.0
0.467	-0.103	-0.072
0.433	-0.125	-0.070
0.400	-0.076	-0.131
0.367	-0.088	-0.101
0.333	-0.055	-0.089
0.300	-0.026	-0.061
0.267	-0.022	-0.032
0.233	-0.067	-0.003
0.200	-0.076	-0.023
0.167	-0.087	-0.049
0.133	-0.077	-0.052
0.100	-0.088	-0.058
0.067	-0.097	-0.073
0.033	-0.094	-0.063
0.000	-0.097	-0.078

d) v/u_0

TABLE VIII (Continued)

R/D	X/D 0.5	1.0
0.467	0.010	0.009
0.433	0.026	0.017
0.400	0.049	-0.016
0.367	0.005	-0.015
0.333	0.017	-0.003
0.300	-0.005	-0.000
0.267	-0.007	-0.000
0.233	-0.004	-0.000
0.200	-0.004	-0.003
0.167	-0.004	-0.007
0.133	-0.000	-0.007
0.100	-0.007	-0.003
0.067	-0.007	-0.003
0.033	-0.007	-0.000
0.000	-0.000	-0.000

e) w/u_0

TABLE IX

VELOCITY DATA FOR ϕ = 45, α =45, D/d = 1.5

R/D	X/D 0.5	X/D 1.0
0.467	0.000	0.000
0.433	0.000	0.000
0.400	0.000	0.000
0.367	0.000	0.000
0.333	0.000	0.000
0.300	0.000	0.000
0.267	79.200	83.800
0.233	0.000	0.000
0.200	0.000	0.000
0.167	0.000	0.000
0.133	0.000	0.000
0.100	0.000	0.000
0.067	0.000	0.000
0.033	0.000	0.000
0.000	36.600	83.800

a) yaw angle

R/D	X/D 0.5	X/D 1.0
0.467	0.000	0.000
0.433	0.000	0.000
0.400	0.000	0.000
0.367	0.000	0.000
0.333	0.000	0.000
0.300	0.000	0.000
0.267	0.000	-26.610
0.233	0.000	0.000
0.200	0.000	0.000
0.167	0.000	0.000
0.133	0.000	0.000
0.100	0.000	0.000
0.067	0.000	0.000
0.033	0.000	0.000
0.000	34.792	-34.709

b) pitch angle

TABLE IX

VELOCITY DATA FOR ϕ = 70, α = 45, D/d = 1.5

R/D	X/D 0.5	X/D 1.0
0.467	1.067	0.823
0.433	0.947	0.699
0.400	0.667	0.546
0.367	0.397	0.417
0.333	0.205	0.313
0.300	0.061	0.234
0.267	-0.065	0.173
0.233	-0.130	0.137
0.200	-0.188	0.108
0.167	-0.186	0.091
0.133	-0.189	0.061
0.100	-0.131	0.049
0.067	-0.079	0.025
0.033	-0.032	0.025
0.000	-0.080	0.189

c) u/u_0

R/D	X/D 0.5	X/D 1.0
0.467	-0.106	-0.038
0.433	-0.232	-0.159
0.400	-0.278	-0.229
0.367	-0.346	-0.253
0.333	-0.340	-0.266
0.300	-0.315	-0.250
0.267	-0.283	-0.264
0.233	-0.249	-0.261
0.200	-0.155	-0.259
0.167	-0.137	-0.272
0.133	-0.142	-0.285
0.100	-0.117	-0.313
0.067	-0.154	-0.333
0.033	0.100	0.000
0.000	0.051	0.163

d) v/u_0

TABLE IX (Continued)

R/D	X/D 0.5	1.0
0.467	0.915	0.643
0.433	0.611	0.666
0.400	0.544	0.651
0.367	0.474	0.627
0.333	0.469	0.614
0.300	0.496	0.623
0.267	0.514	0.613
0.233	0.521	0.624
0.200	0.545	0.639
0.167	0.516	0.615
0.133	0.467	0.565
0.100	0.360	0.450
0.067	0.219	0.306
0.033	0.075	0.131
0.000	0.109	0.140

e) w/u_o

TABLE X

VELOCITY DATA FOR ϕ = 70, α = 45, D/d = 1.5

R/D	X/D 0.5	X/D 1.0
0.467	0.000	0.000
0.433	0.000	0.000
0.400	0.000	0.000
0.367	0.000	0.000
0.333	0.000	0.000
0.300	0.000	0.000
0.267	72.000	95.800
0.233	0.000	0.000
0.200	0.000	0.000
0.167	0.000	0.000
0.133	0.000	0.000
0.100	0.000	0.000
0.067	0.000	0.000
0.033	0.000	0.000
0.000	4.000	95.400

a) yaw angle

R/D	X/D 0.5	X/D 1.0
0.467	0.000	0.000
0.433	0.000	0.000
0.400	0.000	0.000
0.367	0.000	0.000
0.333	0.000	0.000
0.300	0.000	0.000
0.267	0.000	-13.619
0.233	0.000	0.000
0.200	0.000	0.000
0.167	0.000	0.000
0.133	0.000	0.000
0.100	0.000	0.000
0.067	0.000	0.000
0.033	0.000	0.000
0.000	15.601	-16.532

b) pitch angle

TABLE X (Continued)

R/D	X/D 0.5	1.0
0.467	1.267	0.718
0.433	0.861	0.746
0.400	0.584	0.687
0.367	0.383	0.638
0.333	0.245	0.533
0.300	0.130	0.435
0.267	0.068	0.314
0.233	0.000	0.159
0.200	-0.103	0.006
0.167	-0.183	-0.106
0.133	-0.148	-0.117
0.100	-0.061	-0.088
0.067	0.040	0.013
0.033	0.076	0.065
0.000	0.355	0.388

c) u/u_0

R/D	X/D 0.5	1.0
0.467	-0.016	-0.089
0.433	-0.261	-0.168
0.400	-0.347	-0.267
0.367	-0.389	-0.310
0.333	-0.434	-0.328
0.300	-0.440	-0.361
0.267	-0.444	-0.398
0.233	-0.478	-0.423
0.200	-0.308	-0.279
0.167	-0.327	-0.289
0.133	-0.328	-0.280
0.100	-0.328	-0.276
0.067	-0.355	-0.317
0.033	0.157	0.000
0.000	0.037	0.109

d) v/u_0

TABLE X (Continued)

R/D	X/D 0.5	1.0
0.467	1.783	1.778
0.433	1.750	1.793
0.400	1.736	1.809
0.367	1.742	1.813
0.333	1.743	1.833
0.300	1.772	1.798
0.267	1.767	1.778
0.233	1.716	1.680
0.200	1.639	1.576
0.167	1.412	1.373
0.133	1.141	1.151
0.100	0.764	0.926
0.067	0.343	0.543
0.033	0.121	0.201
0.000	-0.000	0.027

e) w/u_o

TABLE XI

VELOCITY DATA FOR ϕ = 0, α = 90, D/d = 1.5, SMALL BLOCKAGE AT L/D = 2

R/D	X/D 2.0
0.467	0.000
0.433	0.000
0.400	0.000
0.367	0.000
0.333	0.000
0.300	0.000
0.267	359.000
0.233	0.000
0.200	0.000
0.167	0.000
0.133	0.000
0.100	0.000
0.067	0.000
0.033	0.000
0.000	359.000

a) yaw angle

R/D	X/D 2.0
0.467	0.000
0.433	0.000
0.400	0.000
0.367	0.000
0.333	0.000
0.300	0.000
0.267	-2.697
0.233	0.000
0.200	0.000
0.167	0.000
0.133	0.000
0.100	0.000
0.067	0.000
0.033	0.000
0.000	-2.383

b) pitch angle

TABLE XI (Continued)

R/D	X/D 2.0
0.467	0.118
0.433	0.144
0.400	0.235
0.367	0.347
0.333	0.472
0.300	0.555
0.267	0.640
0.233	0.694
0.200	0.732
0.167	0.766
0.133	0.800
0.100	0.821
0.067	0.846
0.033	0.854
0.000	0.866

c) u/u_0

R/D	X/D 2.0
0.467	-0.017
0.433	-0.044
0.400	-0.183
0.367	-0.220
0.333	-0.179
0.300	-0.138
0.267	-0.107
0.233	-0.086
0.200	-0.073
0.167	-0.064
0.133	-0.055
0.100	-0.054
0.067	-0.048
0.033	-0.040
0.000	-0.036

d) v/u_0

TABLE XI (Continued)

R/D	X/D 2.0
0.467	-0.172
0.433	-0.134
0.400	-0.137
0.367	-0.126
0.333	-0.120
0.300	-0.098
0.267	-0.085
0.233	-0.068
0.200	-0.046
0.167	-0.032
0.133	-0.028
0.100	-0.014
0.067	-0.015
0.033	-0.015
0.000	-0.015

e) w/u_0

TABLE XII

VELOCITY DATA FOR ϕ = 45, α = 90, D/d = 1.5, SMALL BLOCKAGE AT L/D = 2

R/D	X/D 0.5	1.0	1.5	2.0
0.467	0.000	0.000	0.000	0.000
0.433	0.000	0.000	0.000	0.000
0.400	0.000	0.000	0.000	0.000
0.367	0.000	0.000	0.000	0.000
0.333	0.000	0.000	0.000	0.000
0.300	0.000	0.000	0.000	0.000
0.267	26.600	56.000	59.800	61.400
0.233	0.000	0.000	0.000	0.000
0.200	0.000	0.000	0.000	0.000
0.167	0.000	0.000	0.000	0.000
0.133	0.000	0.000	0.000	0.000
0.100	0.000	0.000	0.000	0.000
0.067	0.000	0.000	0.000	0.000
0.033	0.000	0.000	0.000	0.000
0.000	352.400	50.400	59.800	60.000

a) yaw angle

TABLE XII (Continued)

R/D	X/D 0.5	1.0	1.5	2.0
0.467	0.000	0.000	0.000	0.000
0.433	0.000	0.000	0.000	0.000
0.400	0.000	0.000	0.000	0.000
0.367	0.000	0.000	0.000	0.000
0.333	0.000	0.000	0.000	0.000
0.300	0.000	0.000	0.000	0.000
0.267	-7.425	-4.668	-13.330	-19.638
0.233	0.000	0.000	0.000	0.000
0.200	0.000	0.000	0.000	0.000
0.167	0.000	0.000	0.000	0.000
0.133	0.000	0.000	0.000	0.000
0.100	0.000	0.000	0.000	0.000
0.067	0.000	0.000	0.000	0.000
0.033	0.000	0.000	0.000	0.000
0.000	-53.174	-4.419	-6.962	-17.338

b) pitch angle

TABLE XII (Continued)

R/D	X/D 0.5	1.0	1.5	2.0
0.467	0.912	0.646	0.381	0.174
0.433	0.967	0.606	0.405	0.226
0.400	0.839	0.452	0.415	0.320
0.367	0.563	0.424	0.421	0.420
0.333	0.223	0.345	0.409	0.498
0.300	0.038	0.291	0.405	0.557
0.267	-0.127	0.252	0.397	0.597
0.233	-0.207	0.242	0.383	0.628
0.200	-0.224	0.241	0.387	0.677
0.167	-0.174	0.260	0.416	0.730
0.133	-0.078	0.298	0.498	0.780
0.100	0.077	0.424	0.622	0.760
0.067	0.241	0.628	0.754	0.601
0.033	0.345	0.833	0.799	0.418
0.000	0.422	0.865	0.717	0.229

c) u/u_0

TABLE XII (Continued)

R/D	X/D 0.5	1.0	1.5	2.0
0.467	-0.138	-0.005	-0.076	-0.006
0.433	-0.017	-0.093	-0.066	-0.207
0.400	-0.128	-0.153	-0.123	-0.330
0.367	-0.228	-0.175	-0.147	-0.385
0.333	-0.333	-0.194	-0.169	-0.371
0.300	-0.293	-0.210	-0.195	-0.348
0.267	-0.227	-0.226	-0.232	-0.316
0.233	-0.223	-0.248	-0.262	-0.296
0.200	-0.249	-0.275	-0.199	-0.164
0.167	-0.281	-0.324	-0.237	-0.130
0.133	-0.340	-0.407	-0.278	-0.114
0.100	-0.381	-0.513	-0.275	-0.092
0.067	-0.395	-0.511	-0.239	-0.043
0.033	-0.316	-0.350	-0.060	-0.061
0.000	-0.215	-0.167	-0.187	-0.309

d) v/u_0

TABLE XII (Continued)

R/D	X/D 0.5	1.0	1.5	2.0
0.467	0.697	0.738	0.863	0.849
0.433	0.667	0.765	0.853	0.845
0.400	0.646	0.771	0.851	0.851
0.367	0.543	0.740	0.864	0.885
0.333	0.405	0.754	0.893	0.913
0.300	0.434	0.774	0.919	0.964
0.267	0.551	0.805	0.945	1.017
0.233	0.621	0.867	1.019	1.079
0.200	0.673	0.951	1.100	1.163
0.167	0.718	1.028	1.144	1.215
0.133	0.698	1.080	1.141	1.157
0.100	0.610	0.989	1.036	0.918
0.067	0.449	0.781	0.728	0.534
0.033	0.243	0.403	0.291	0.210
0.000	0.043	-0.033	-0.127	-0.031

e) w/u_0

TABLE XIII

VELOCITY DATA FOR ϕ = 70, α = 90, D/d = 1.5, SMALL BLOCKAGE AT L/D = 2

R/D	X/D 0.5	1.0	1.5	2.0
0.467	0.000	0.000	0.000	0.000
0.433	0.000	0.000	0.000	0.000
0.400	0.000	0.000	0.000	0.000
0.367	0.000	0.000	0.000	0.000
0.333	0.000	0.000	0.000	0.000
0.300	0.000	0.000	0.000	0.000
0.267	124.000	74.400	70.000	72.800
0.233	0.000	0.000	0.000	0.000
0.200	0.000	0.000	0.000	0.000
0.167	0.000	0.000	0.000	0.000
0.133	0.000	0.000	0.000	0.000
0.100	0.000	0.000	0.000	0.000
0.067	0.000	0.000	0.000	0.000
0.033	0.000	0.000	0.000	0.000
0.000	142.000	89.400	70.000	72.200

a) yaw angle

TABLE XIII (Continued)

R/D	X/D 0.5	1.0	1.5	2.0
0.467	0.000	0.000	0.000	0.000
0.433	0.000	0.000	0.000	0.000
0.400	0.000	0.000	0.000	0.000
0.367	0.000	0.000	0.000	0.000
0.333	0.000	0.000	0.000	0.000
0.300	0.000	0.000	0.000	0.000
0.267	-36.207	-15.581	-14.725	-16.845
0.233	0.000	0.000	0.000	0.000
0.200	0.000	0.000	0.000	0.000
0.167	0.000	0.000	0.000	0.000
0.133	0.000	0.000	0.000	0.000
0.100	0.000	0.000	0.000	0.000
0.067	0.000	0.000	0.000	0.000
0.033	0.000	0.000	0.000	0.000
0.000	43.607	-22.500	-10.495	-15.147

b) pitch angle

TABLE XIII (Continued)

R/D	X/D 0.5	1.0	1.5	2.0
0.467	0.769	0.720	0.518	0.278
0.433	0.722	0.673	0.586	0.362
0.400	0.621	0.499	0.556	0.463
0.367	0.437	0.388	0.516	0.568
0.333	0.226	0.339	0.480	0.638
0.300	0.026	0.270	0.439	0.709
0.267	-0.061	0.235	0.373	0.820
0.233	-0.064	0.218	0.306	0.795
0.200	0.000	0.187	0.303	0.743
0.167	0.053	0.171	0.360	0.609
0.133	0.068	0.124	0.342	0.327
0.100	0.104	0.116	0.232	0.007
0.067	0.147	0.110	0.059	-0.165
0.033	0.233	0.157	0.010	-0.227
0.000	0.403	0.460	0.406	-0.150

c) u/u_0

TABLE XIII (Continued)

R/D	X/D 0.5	1.0	1.5	2.0
0.467	-0.300	-0.132	-0.048	-0.028
0.433	-0.004	-0.138	-0.202	-0.389
0.400	-0.154	-0.231	-0.303	-0.574
0.367	-0.242	-0.270	-0.363	-0.627
0.333	-0.332	-0.306	-0.401	-0.653
0.300	-0.401	-0.349	-0.450	-0.627
0.267	-0.460	-0.400	-0.365	-0.627
0.233	-0.512	-0.456	-0.403	-0.611
0.200	-0.584	-0.524	-0.433	-0.402
0.167	-0.630	-0.586	-0.475	-0.369
0.133	-0.688	-0.648	-0.468	-0.339
0.100	-0.670	-0.698	-0.465	-0.285
0.067	-0.659	-0.761	0.000	-0.286
0.033	0.403	0.000	0.069	-0.297
0.000	0.266	0.257	0.091	0.182

d) v/u_0

TABLE XIII (Continued)

R/D	X/D 0.5	1.0	1.5	2.0
0.467	1.867	1.801	1.881	1.610
0.433	1.899	1.849	1.871	1.701
0.400	1.913	1.887	1.866	1.804
0.367	1.891	1.923	1.927	1.931
0.333	1.843	1.960	1.985	2.061
0.300	1.888	2.027	2.029	2.207
0.267	1.947	2.093	2.114	2.254
0.233	2.037	2.149	2.175	2.184
0.200	2.052	2.134	2.154	2.041
0.167	1.897	1.949	1.959	1.729
0.133	1.500	1.545	1.531	1.170
0.100	0.992	1.072	0.944	0.688
0.067	0.454	0.574	0.309	0.491
0.033	0.179	0.274	0.428	0.337
0.000	-0.145	-0.168	0.501	0.118

e) w/u_o

TABLE XIV

VELOCITY DATA FOR ϕ = 0, D/d = 1.0, SMALL BLOCKAGE AT L/D = 2

R/D	X/D 2.0
0.350	0.000
0.300	0.000
0.250	0.000
0.200	0.000
0.150	0.000
0.100	0.000
0.050	0.000
0.000	359.600

a) yaw angle

R/D	X/D 2.0
0.350	0.000
0.300	0.000
0.250	0.000
0.200	0.000
0.150	0.000
0.100	0.000
0.050	0.000
0.000	-1.671

b) pitch angle

R/D	X/D 2.0
0.350	1.150
0.300	1.294
0.250	1.365
0.200	1.405
0.150	1.436
0.100	1.444
0.050	1.462
0.000	1.470

c) u/u_0

R/D	X/D 2.0
0.350	-0.388
0.300	-0.419
0.250	-0.330
0.200	-0.250
0.150	-0.176
0.100	-0.125
0.050	-0.090
0.000	-0.043

d) v/u_0

TABLE XIV (Continued)

R/D	X/D 2.0
0.350	-0.036
0.300	-0.036
0.250	-0.029
0.200	-0.025
0.150	-0.010
0.100	-0.010
0.050	-0.010
0.000	-0.010

e) w/u_o

TABLE XV

VELOCITY DATA FOR ϕ = 45, D/d = 1.0, SMALL BLOCKAGE AT L/D = 2

R/D	X/D 0.5	1.0	1.5	2.0
0.350	0.000	0.000	0.000	0.000
0.300	0.000	0.000	0.000	0.000
0.250	0.000	0.000	0.000	0.000
0.200	0.000	0.000	0.000	0.000
0.150	0.000	0.000	0.000	0.000
0.100	0.000	0.000	0.000	0.000
0.050	0.000	0.000	0.000	0.000
0.000	33.000	68.400	54.400	0.000

a) yaw angle

R/D	X/D 0.5	1.0	1.5	2.0
0.350	0.000	0.000	0.000	0.000
0.300	0.000	0.000	0.000	0.000
0.250	0.000	0.000	0.000	0.000
0.200	0.000	0.000	0.000	0.000
0.150	0.000	0.000	0.000	0.000
0.100	0.000	0.000	0.000	0.000
0.050	0.000	0.000	0.000	0.000
0.000	-25.293	-26.901	-30.316	0.000

b) pitch angle

TABLE XV (Continued)

R/D	X/D 0.5	1.0	1.5	2.0
0.350	1.001	1.024	0.737	0.585
0.300	1.053	1.057	0.727	0.704
0.250	1.003	0.972	0.711	0.732
0.200	0.862	0.860	0.661	0.721
0.150	0.832	0.891	0.662	0.680
0.100	1.185	1.190	1.012	0.918
0.050	1.410	1.313	1.242	1.399
0.000	1.221	1.237	1.247	1.366

c) u/u_0

R/D	X/D 0.5	1.0	1.5	2.0
0.350	-0.062	-0.054	-0.119	-0.540
0.300	-0.210	-0.223	-0.319	-0.707
0.250	-0.335	-0.371	-0.456	-0.692
0.200	-0.510	-0.577	-0.647	-0.750
0.150	-0.662	-0.799	-0.855	-0.937
0.100	-0.669	-0.798	-0.856	-1.164
0.050	-0.779	-0.819	-0.842	-0.998
0.000	-0.665	-0.477	-0.728	-0.770

d) v/u_0

TABLE XV (Continued)

R/D	X/D 0.5	1.0	1.5	2.0
0.350	1.377	1.349	0.943	0.806
0.300	1.538	1.476	1.086	0.983
0.250	1.737	1.657	1.282	1.163
0.200	1.956	1.879	1.485	1.379
0.150	1.923	1.843	1.655	1.717
0.100	1.364	1.389	1.466	1.934
0.050	0.994	0.997	1.126	1.587
0.000	0.211	0.263	0.614	0.887

e) w/u_0

TABLE XVI

VELOCITY DATA FOR ϕ = 70, D/d = 1.0, SMALL BLOCKAGE AT L/D = 2

R/D	X/D 0.5	1.0	1.5	2.0
0.350	0.000	0.000	0.000	0.000
0.300	0.000	0.000	0.000	0.000
0.250	0.000	0.000	0.000	0.000
0.200	0.000	0.000	0.000	0.000
0.150	0.000	0.000	0.000	0.000
0.100	0.000	0.000	0.000	0.000
0.050	0.000	0.000	0.000	0.000
0.000	40.400	63.400	69.200	0.000

a) yaw angle

R/D	X/D 0.5	1.0	1.5	2.0
0.350	0.000	0.000	0.000	0.000
0.300	0.000	0.000	0.000	0.000
0.250	0.000	0.000	0.000	0.000
0.200	0.000	0.000	0.000	0.000
0.150	0.000	0.000	0.000	0.000
0.100	0.000	0.000	0.000	0.000
0.050	0.000	0.000	0.000	0.000
0.000	-0.797	-19.640	-14.346	0.000

b) pitch angle

TABLE XVI (Continued)

R/D	X/D 0.5	1.0	1.5	2.0
0.350	1.100	1.110	1.090	1.353
0.300	0.926	0.879	0.958	1.404
0.250	0.825	0.584	0.704	1.446
0.200	0.803	0.639	0.835	1.559
0.150	0.853	0.682	0.968	1.294
0.100	0.783	0.686	0.969	0.513
0.050	0.526	0.378	0.582	-0.003
0.000	-0.607	-0.654	0.125	0.654

c) u/u_0

R/D	X/D 0.5	1.0	1.5	2.0
0.350	-0.218	-0.350	-0.311	-0.777
0.300	-0.623	-0.710	-0.615	-1.011
0.250	-0.769	-0.881	-0.795	-1.030
0.200	-1.014	-1.021	-0.896	-1.004
0.150	-1.265	-1.226	-0.944	-1.032
0.100	-1.337	-1.346	-0.974	-1.096
0.050	-1.541	-1.614	-1.083	0.000
0.000	0.000	0.000	0.000	-0.012

d) v/u_0

TABLE XVI (Continued)

R/D	X/D 0.5	1.0	1.5	2.0
0.350	3.426	3.297	3.477	3.316
0.300	3.229	3.326	3.627	3.697
0.250	3.077	3.123	3.489	3.930
0.200	2.997	3.059	3.298	3.502
0.150	2.535	2.819	2.980	2.585
0.100	1.899	2.111	2.327	1.324
0.050	1.446	1.354	1.634	0.393
0.000	0.683	0.493	0.737	0.557

e) w/u_o

TABLE XVII

VELOCITY DATA FOR ϕ = 0, D/d = 1.5, α = 90, LARGE BLOCKAGE AT L/D = 2

R/D	X/D 0.5	1.0	1.5	2.0
0.467	0.000	0.000	0.000	0.000
0.433	0.000	0.000	0.000	0.000
0.400	0.000	0.000	0.000	0.000
0.367	0.000	0.000	0.000	0.000
0.333	0.000	0.000	0.000	0.000
0.300	0.000	0.000	0.000	0.000
0.267	360.000	359.000	356.800	348.800
0.233	0.000	0.000	0.000	0.000
0.200	0.000	0.000	0.000	0.000
0.167	0.000	0.000	0.000	0.000
0.133	0.000	0.000	0.000	0.000
0.100	0.000	0.000	0.000	0.000
0.067	0.000	0.000	0.000	0.000
0.033	0.000	0.000	0.000	0.000
0.000	360.000	360.000	358.000	352.400

a) yaw angle

TABLE XVII (Continued)

R/D	X/D 0.5	1.0	1.5	2.0
0.467	0.000	0.000	0.000	0.000
0.433	0.000	0.000	0.000	0.000
0.400	0.000	0.000	0.000	0.000
0.367	0.000	0.000	0.000	0.000
0.333	0.000	0.000	0.000	0.000
0.300	0.000	0.000	0.000	0.000
0.267	0.347	-3.277	-5.591	-9.147
0.233	0.000	0.000	0.000	0.000
0.200	0.000	0.000	0.000	0.000
0.167	0.000	0.000	0.000	0.000
0.133	0.000	0.000	0.000	0.000
0.100	0.000	0.000	0.000	0.000
0.067	0.000	0.000	0.000	0.000
0.033	0.000	0.000	0.000	0.000
0.000	2.550	-2.000	-5.103	-8.492

b) pitch angle

TABLE XVII (Continued)

R/D	X/D 0.5	1.0	1.5	2.0
0.467	0.041	0.000	0.067	0.078
0.433	0.000	0.058	0.124	0.161
0.400	0.063	0.126	0.230	0.230
0.367	0.269	0.276	0.305	0.314
0.333	0.516	0.445	0.411	0.397
0.300	0.810	0.621	0.519	0.495
0.267	0.930	0.753	0.596	0.580
0.233	0.943	0.829	0.683	0.659
0.200	0.940	0.869	0.719	0.730
0.167	0.938	0.877	0.750	0.792
0.133	0.939	0.880	0.768	0.830
0.100	0.940	0.879	0.780	0.863
0.067	0.938	0.878	0.780	0.882
0.033	0.940	0.876	0.783	0.897
0.000	0.941	0.878	0.782	0.866

c) u/u_0

TABLE XVII (Continued)

R/D	X/D 0.5	1.0	1.5	2.0
0.467	0.000	0.000	0.000	0.162
0.433	0.000	-0.099	0.124	0.071
0.400	0.092	0.000	0.115	-0.008
0.367	0.096	0.148	0.105	-0.053
0.333	0.092	0.119	0.092	-0.065
0.300	0.081	0.102	0.083	-0.075
0.267	0.059	0.092	0.076	-0.061
0.233	0.039	0.074	0.069	-0.065
0.200	0.028	0.056	0.057	-0.065
0.167	0.021	0.046	0.046	-0.055
0.133	0.015	0.035	0.038	-0.048
0.100	0.014	0.028	0.030	-0.030
0.067	0.010	0.019	0.022	-0.004
0.033	0.009	0.014	0.017	0.005
0.000	0.004	0.011	0.014	0.039

d) v/u_o

TABLE XVII (Continued)

R/D	X/D 0.5	1.0	1.5	2.0
0.467	-0.000	0.000	-0.050	-0.082
0.433	0.000	-0.061	-0.042	-0.075
0.400	-0.000	-0.040	-0.045	-0.079
0.367	-0.001	-0.030	-0.059	-0.076
0.333	-0.002	-0.023	-0.048	-0.079
0.300	-0.003	-0.020	-0.044	-0.066
0.267	-0.016	-0.011	-0.031	-0.053
0.233	-0.003	-0.006	-0.017	-0.037
0.200	-0.003	-0.003	-0.018	-0.025
0.167	-0.003	-0.000	-0.010	-0.014
0.133	-0.003	-0.000	-0.011	-0.014
0.100	-0.003	-0.000	-0.000	-0.000
0.067	-0.000	-0.000	-0.000	-0.000
0.033	-0.000	-0.000	-0.000	-0.000
0.000	-0.000	-0.000	-0.000	-0.000

e) w/u_0

TABLE XVIII

VELOCITY DATA FOR ϕ = 45, D/d = 1.5, α = 90, LARGE BLOCKAGE AT L/D = 2

R/D	X/D 0.5	1.0	1.5	2.0
0.467	0.000	0.000	0.000	0.000
0.433	0.000	0.000	0.000	0.000
0.400	0.000	0.000	0.000	0.000
0.367	0.000	0.000	0.000	0.000
0.333	0.000	0.000	0.000	0.000
0.300	0.000	0.000	0.000	0.000
0.267	44.000	64.400	61.800	75.600
0.233	0.000	0.000	0.000	0.000
0.200	0.000	0.000	0.000	0.000
0.167	0.000	0.000	0.000	0.000
0.133	0.000	0.000	0.000	0.000
0.100	0.000	0.000	0.000	0.000
0.067	0.000	0.000	0.000	0.000
0.033	0.000	0.000	0.000	0.000
0.000	16.600	61.000	68.600	75.000

a) yaw angle

TABLE XVIII (Continued)

R/D	X/D 0.5	1.0	1.5	2.0
0.467	0.000	0.000	0.000	0.000
0.433	0.000	0.000	0.000	0.000
0.400	0.000	0.000	0.000	0.000
0.367	0.000	0.000	0.000	0.000
0.333	0.000	0.000	0.000	0.000
0.300	0.000	0.000	0.000	0.000
0.267	-0.867	-4.769	-7.922	-9.874
0.233	0.000	0.000	0.000	0.000
0.200	0.000	0.000	0.000	0.000
0.167	0.000	0.000	0.000	0.000
0.133	0.000	0.000	0.000	0.000
0.100	0.000	0.000	0.000	0.000
0.067	0.000	0.000	0.000	0.000
0.033	0.000	0.000	0.000	0.000
0.000	3.875	-3.856	-6.638	-8.923

b) pitch angle

TABLE XVIII (Continued)

R/D	X/D 0.5	1.0	1.5	2.0
0.467	0.014	0.642	0.516	0.063
0.433	0.121	0.544	0.464	0.134
0.400	0.292	0.467	0.427	0.166
0.367	0.473	0.408	0.368	0.211
0.333	0.676	0.353	0.312	0.250
0.300	0.807	0.290	0.279	0.281
0.267	0.835	0.239	0.256	0.338
0.233	0.753	0.231	0.254	0.591
0.200	0.567	0.179	0.292	0.497
0.167	0.352	0.181	0.368	0.614
0.133	0.220	0.240	0.469	0.757
0.100	0.188	0.390	0.669	0.992
0.067	0.324	0.686	0.999	1.434
0.033	0.494	1.021	1.148	1.921
0.000	0.645	1.160	1.072	2.341

c) u/u_0

TABLE XVIII (Continued)

R/D	X/D 0.5	1.0	1.5	2.0
0.467	0.205	0.088	0.132	0.114
0.433	0.114	0.069	-0.001	0.019
0.400	0.170	0.016	-0.039	-0.123
0.367	0.218	0.008	-0.051	-0.163
0.333	0.203	-0.013	-0.063	-0.175
0.300	0.172	-0.029	-0.059	-0.170
0.267	0.075	-0.039	-0.058	-0.178
0.233	0.026	-0.045	-0.050	-0.174
0.200	-0.061	-0.064	-0.044	-0.159
0.167	-0.078	-0.087	-0.022	-0.161
0.133	-0.092	-0.109	0.004	-0.146
0.100	-0.114	-0.132	0.046	-0.138
0.067	-0.158	-0.148	0.092	-0.135
0.033	-0.152	-0.114	0.203	-0.040
0.000	-0.118	-0.012	0.386	0.165

d) v/u_o

TABLE XVIII (Continued)

R/D	X/D 0.5	1.0	1.5	2.0
0.467	0.822	0.793	0.737	0.755
0.433	0.765	0.788	0.773	0.809
0.400	0.724	0.777	0.796	0.870
0.367	0.782	0.774	0.818	0.916
0.333	0.859	0.794	0.831	0.975
0.300	0.941	0.806	0.878	1.048
0.267	0.995	0.834	0.904	1.105
0.233	1.007	0.862	0.949	1.103
0.200	0.944	0.919	1.031	1.269
0.167	0.879	1.029	1.145	1.406
0.133	0.898	1.146	1.260	1.581
0.100	0.918	1.309	1.396	1.789
0.067	0.818	1.280	1.325	1.931
0.033	0.541	0.798	0.890	1.855
0.000	0.121	0.110	0.075	0.698

e) w/u_0

TABLE XIX

VELOCITY DATA FOR ϕ = 70, D/d = 1.5, α = 90, LARGE BLOCKAGE AT L/D = 2

R/D	X/D 0.5	1.0	1.5	2.0
0.467	0.000	0.000	0.000	0.000
0.433	0.000	0.000	0.000	0.000
0.400	0.000	0.000	0.000	0.000
0.367	0.000	0.000	0.000	0.000
0.333	0.000	0.000	0.000	0.000
0.300	0.000	0.000	0.000	0.000
0.267	72.200	72.400	79.800	82.200
0.233	0.000	0.000	0.000	0.000
0.200	0.000	0.000	0.000	0.000
0.167	0.000	0.000	0.000	0.000
0.133	0.000	0.000	0.000	0.000
0.100	0.000	0.000	0.000	0.000
0.067	0.000	0.000	0.000	0.000
0.033	0.000	0.000	0.000	0.000
0.000	39.800	70.000	78.000	82.200

a) yaw angle

TABLE XIX (Continued)

R/D	X/D 0.5	1.0	1.5	2.0
0.467	0.000	0.000	0.000	0.000
0.433	0.000	0.000	0.000	0.000
0.400	0.000	0.000	0.000	0.000
0.367	0.000	0.000	0.000	0.000
0.333	0.000	0.000	0.000	0.000
0.300	0.000	0.000	0.000	0.000
0.267	-50.980	-23.297	-15.894	-14.235
0.233	0.000	0.000	0.000	0.000
0.200	0.000	0.000	0.000	0.000
0.167	0.000	0.000	0.000	0.000
0.133	0.000	0.000	0.000	0.000
0.100	0.000	0.000	0.000	0.000
0.067	0.000	0.000	0.000	0.000
0.033	0.000	0.000	0.000	0.000
0.000	32.130	-20.836	-17.144	-14.680

b) pitch angle

TABLE XIX (Continued)

R/D	X/D 0.5	1.0	1.5	2.0
0.467	0.573	0.517	0.361	0.384
0.433	0.440	0.509	0.384	0.458
0.400	0.363	0.394	0.393	0.403
0.367	0.155	0.289	0.346	0.364
0.333	0.014	0.225	0.284	0.307
0.300	-0.101	0.173	0.241	0.328
0.267	-0.131	0.165	0.276	0.383
0.233	-0.092	0.185	0.278	0.502
0.200	0.064	0.272	0.400	0.627
0.167	0.251	0.438	0.579	0,782
0.133	0.498	0.632	0.706	0.855
0.100	0.713	0.693	0.927	0.834
0.067	0.685	0.640	0.771	0.635
0.033	0.488	0.427	0.501	0.253
0.000	0.200	0.260	0.705	0.573

c) u/u_0

TABLE XIX (Continued)

R/D	X/D 0.5	1.0	1.5	2.0
0.467	-0.339	-0.251	-0.068	-0.022
0.433	-0.005	-0.053	-0.123	-0.270
0.400	-0.083	-0.154	-0.262	-0.454
0.367	-0.149	-0.194	-0.320	-0.521
0.333	-0.204	-0.230	-0.369	-0.574
0.300	-0.260	-0.287	-0.451	-0.633
0.267	-0.310	-0.355	-0.536	-0.709
0.233	-0.383	-0.444	-0.629	-0.807
0.200	-0.482	-0.529	-0.703	-0.930
0.167	-0.620	-0.630	-0.858	-1.042
0.133	-0.740	-0.749	-0.915	-1.218
0.100	-0.832	-0.810	-0.997	-0.928
0.067	-0.993	-0.921	-1.063	-0.988
0.033	-1.234	-1.217	-1.325	-1.023
0.000	0.000	0.000	0.799	0.468

d) v/u_0

TABLE XIX (Continued)

R/D	X/D 0.5	1.0	1.5	2.0
0.467	1.851	1.826	1.929	1.804
0.433	1.904	1.926	2.014	1.891
0.400	1.901	1.992	2.058	1.963
0.367	1.927	2.058	2.092	2.067
0.333	1.971	2.141	2.188	2.242
0.300	2.073	2.242	2.292	2.394
0.267	2.207	2.363	2.462	2.594
0.233	2.399	2.518	2.649	2.790
0.200	2.599	2.676	2.844	2.948
0.167	2.756	2.828	2.977	2.918
0.133	2.711	2.738	3.010	2.697
0.100	2.277	2.212	2.415	2.292
0.067	1.713	1.632	1.733	1.587
0.033	1.298	1.186	1.085	0.790
0.000	0.304	0.340	0.347	0.477

e) w/u_0

TABLE XX

VELOCITY DATA FOR ϕ = 0, D/d = 1.0, LARGE BLOCKAGE AT L/D = 2

R/D	X/D 1.5	2.0
0.350	0.000	0.000
0.300	0.000	0.000
0.250	0.000	0.000
0.200	0.000	0.000
0.150	0.000	0.000
0.100	0.000	0.000
0.050	0.000	0.000
0.000	360.000	359.200

a) yaw angle

R/D	X/D 1.5	2.0
0.350	0.000	0.000
0.300	0.000	0.000
0.250	0.000	0.000
0.200	0.000	0.000
0.150	0.000	0.000
0.100	0.000	0.000
0.050	0.000	0.000
0.000	-1.630	-14.620

b) pitch angle

R/D	X/D 1.5	2.0
0.350	1.231	1.276
0.300	1.239	1.376
0.250	1.247	1.500
0.200	1.253	1.624
0.150	1.253	1.720
0.100	1.257	1.797
0.050	1.265	1.838
0.000	1.261	1.864

c) u/u_o

R/D	X/D 1.5	2.0
0.350	-0.056	-0.490
0.300	-0.071	-0.573
0.250	-0.086	-0.590
0.200	-0.086	-0.538
0.150	-0.086	-0.449
0.100	-0.082	-0.318
0.050	-0.074	-0.185
0.000	-0.074	-0.053

d) v/u_o

TABLE XX (Continued)

R/D	X/D 1.5	2.0
0.350	0.017	0.009
0.300	0.009	0.010
0.250	-0.000	-0.021
0.200	-0.000	-0.023
0.150	-0.000	-0.024
0.100	-0.000	-0.025
0.050	-0.000	-0.013
0.000	-0.000	-0.000

e) w/u_o

TABLE XXI

VELOCITY DATA FOR ϕ = 45, D/d = 1.0, LARGE BLOCKAGE AT L/D = 2

R/D	X/D 0.5	1.0	1.5	2.0
0.350	0.000	0.000	0.000	0.000
0.300	0.000	0.000	0.000	0.000
0.250	0.000	0.000	0.000	0.000
0.200	0.000	0.000	0.000	0.000
0.150	0.000	0.000	0.000	0.000
0.100	0.000	0.000	0.000	0.000
0.050	0.000	0.000	0.000	0.000
0.000	5.400	56.000	52.600	0.000

a) yaw angle

R/D	X/D 0.5	1.0	1.5	2.0
0.350	0.000	0.000	0.000	0.000
0.300	0.000	0.000	0.000	0.000
0.250	0.000	0.000	0.000	0.000
0.200	0.000	0.000	0.000	0.000
0.150	0.000	0.000	0.000	0.000
0.100	0.000	0.000	0.000	0.000
0.050	0.000	0.000	0.000	0.000
0.000	0.000	-18.480	-20.588	0.000

b) pitch angle

TABLE XXI (Continued)

R/D	X/D 0.5	1.0	1.5	2.0
0.350	1.070	1.071	0.978	0.928
0.300	1.152	1.089	0.970	1.073
0.250	1.072	0.995	0.962	1.261
0.200	0.879	0.879	0.933	1.405
0.150	0.896	0.934	0.966	1.548
0.100	1.302	1.231	1.370	2.496
0.050	1.512	1.306	1.704	3.081
0.000	1.366	1.290	1.514	3.685

c) u/u_0

R/D	X/D 0.5	1.0	1.5	2.0
0.350	0.068	0.025	-0.132	-0.501
0.300	-0.054	-0.106	-0.262	-0.664
0.250	-0.204	-0.252	-0.366	-0.732
0.200	-0.388	-0.438	-0.513	-0.803
0.150	-0.533	-0.598	-0.714	-0.925
0.100	-0.428	-0.598	-0.741	-1.142
0.050	-0.498	-0.731	-0.557	-0.818
0.000	-0.381	-0.207	-0.462	0.000

d) v/u_0

TABLE XXI (Continued)

R/D	X/D 0.5	1.0	1.5	2.0
0.350	1.440	1.463	1.336	1.268
0.300	1.609	1.614	1.438	1.404
0.250	1.827	1.752	1.614	1.603
0.200	2.011	1.956	1.831	1.891
0.150	1.887	1.833	2.034	2.296
0.100	1.284	1.339	1.753	2.140
0.050	0.982	0.949	1.081	1.851
0.000	0.226	0.023	0.316	0.348

e) w/u_o

TABLE XXII

VELOCITY DATA FOR ϕ = 70, D/d = 1.0, LARGE BLOCKAGE AT L/D = 2

R/D	X/D 0.5	1.0	1.5	2.0
0.350	0.000	0.000	0.000	0.000
0.300	0.000	0.000	0.000	0.000
0.250	0.000	0.000	0.000	0.000
0.200	0.000	0.000	0.000	0.000
0.150	0.000	0.000	0.000	0.000
0.100	0.000	0.000	0.000	0.000
0.050	0.000	0.000	0.000	0.000
0.000	58.800	72.400	77.200	0.000

a) yaw angle

R/D	X/D 0.5	1.0	1.5	2.0
0.350	0.000	0.000	0.000	0.000
0.300	0.000	0.000	0.000	0.000
0.250	0.000	0.000	0.000	0.000
0.200	0.000	0.000	0.000	0.000
0.150	0.000	0.000	0.000	0.000
0.100	0.000	0.000	0.000	0.000
0.050	0.000	0.000	0.000	0.000
0.000	0.000	-17.593	-15.792	0.000

b) pitch angle

TABLE XXII (Continued)

R/D	X/D 0.5	1.0	1.5	2.0
0.350	0.825	0.832	0.880	0.797
0.300	0.501	0.570	0.649	0.798
0.250	0.246	0.334	0.489	0.879
0.200	0.366	0.419	0.679	1.056
0.150	1.021	0.992	1.264	1.739
0.100	2.261	2.094	2.583	3.155
0.050	3.149	3.334	3.549	2.965
0.000	-0.777	-1.215	1.372	1.302

c) u/u_0

R/D	X/D 0.5	1.0	1.5	2.0
0.350	0.020	0.032	-0.431	-0.740
0.300	-0.403	-0.355	-0.828	-1.018
0.250	-0.717	-0.659	-1.163	-1.181
0.200	-1.122	-1.115	-1.603	-1.413
0.150	-1.682	-1.676	-2.087	-1.824
0.100	-2.553	-2.611	-2.939	-2.301
0.050	-3.692	-3.567	-4.284	-3.097
0.000	0.000	0.000	0.000	0.000

d) v/u_0

TABLE XXII (Continued)

R/D	X/D 0.5	1.0	1.5	2.0
0.350	3.463	3.289	3.237	3.197
0.300	3.658	3.519	3.470	3.511
0.250	3.911	3.817	3.869	4.000
0.200	4.354	4.277	4.384	4.723
0.150	4.805	4.749	4.995	5.482
0.100	5.079	5.131	5.249	5.600
0.050	4.599	4.727	3.833	4.395
0.000	0.524	0.258	0.953	2.151

e) w/u_o

TABLE XXIII

CORNER RECIRCULATION LENGTHS FOR NONSWIRLING FLOWS

Expansion Ratio (D/d)	CRZ Length in Step Heights(h)
1.43	8
1.5	7.5
1.73	8
2	8
3	6.25

TABLE XXIV

CENTRAL RECIRCULATION LENGTHS FOR SWIRLING FLOW

D/d	ϕ = 45	ϕ = 70
1.0	0	0.5
1.5	1.5	0.75
2.0	1.6	1.2

APPENDIX B

FIGURES

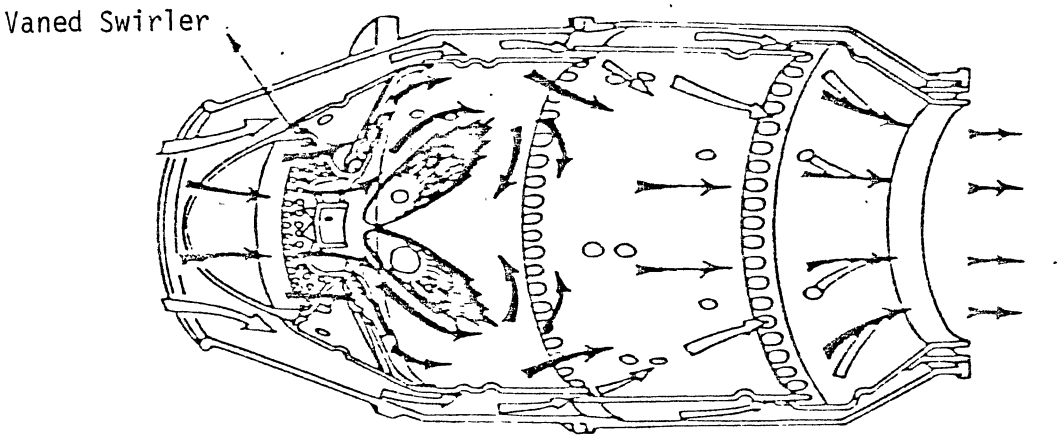

(a) Typical Axisymmetric Combustion Chamber of a Gas Turbine Engine.

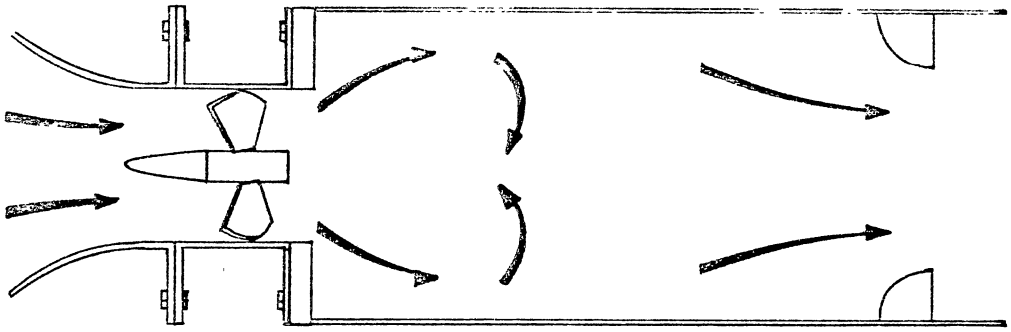

(b) Simplified Test Section

Figure 1. Typical Axisymmetric Gas Turbine Combustion Chamber

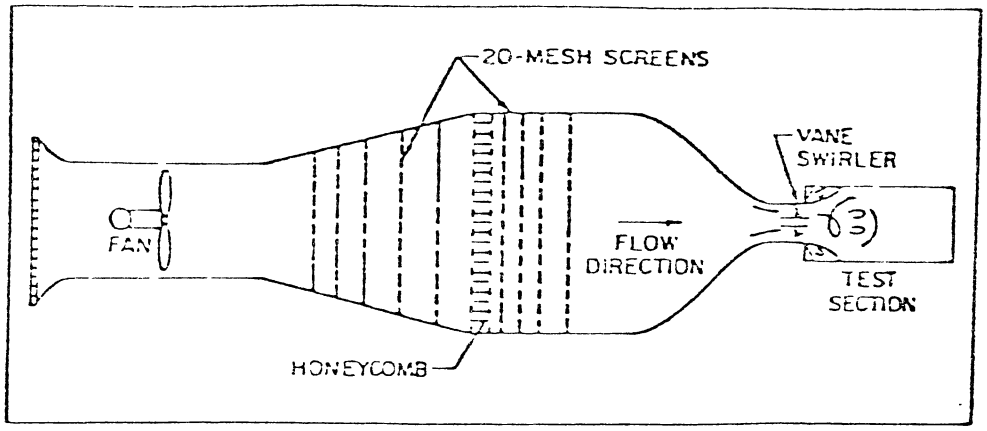

Figure 2. Schematic of Overall Flow Facility

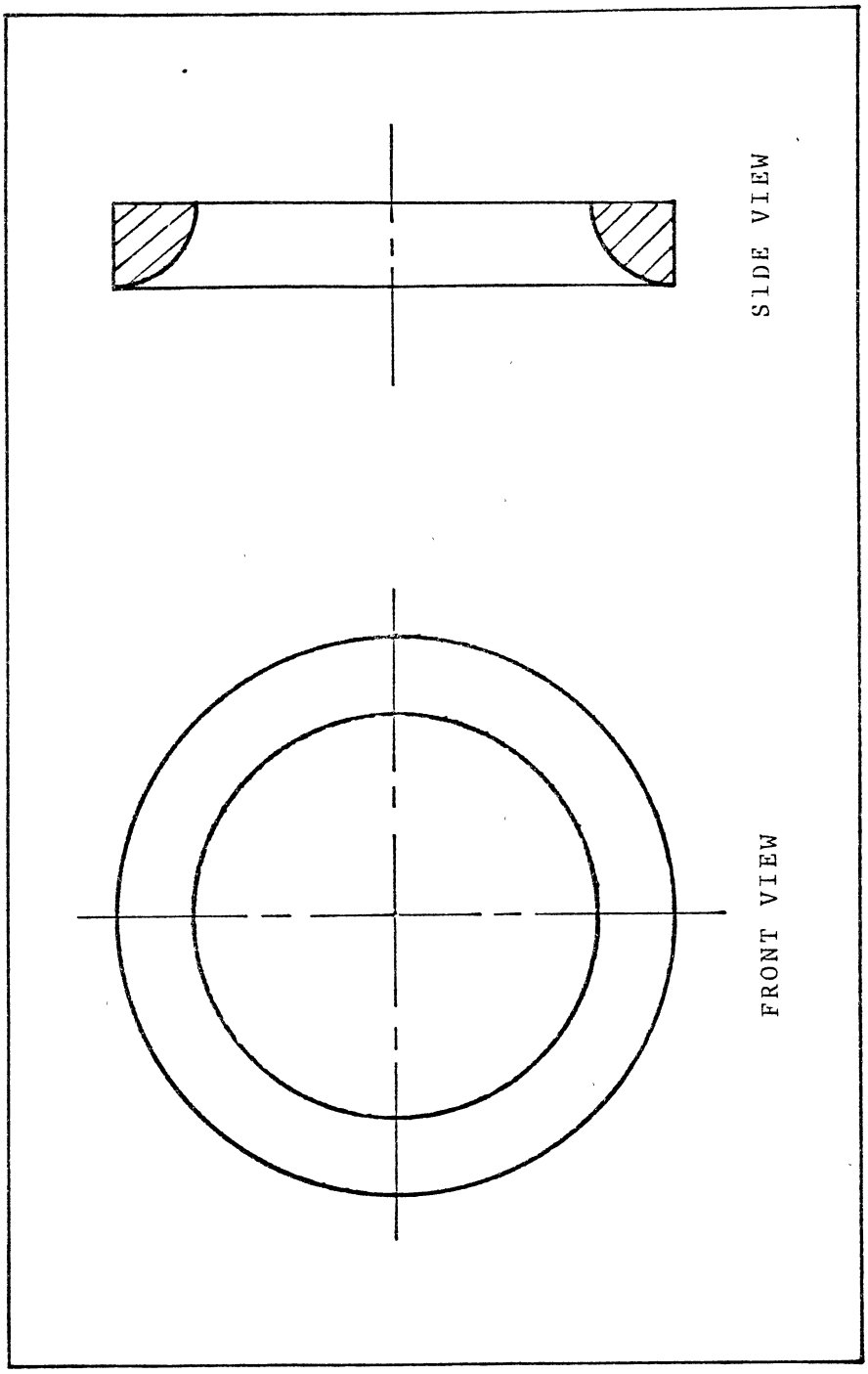

Figure 3. Small Blockage

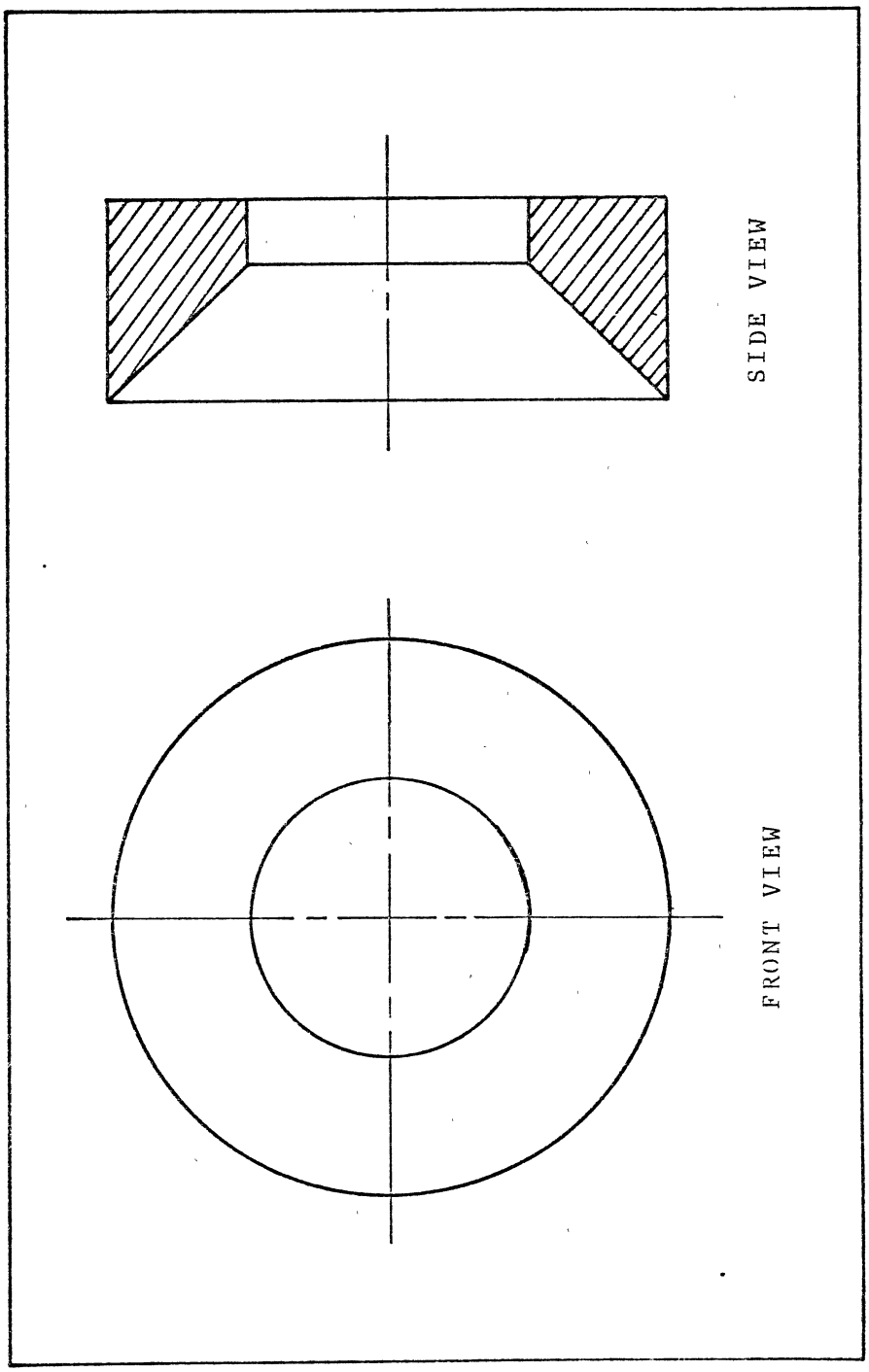

Figure 4. Large Blockage

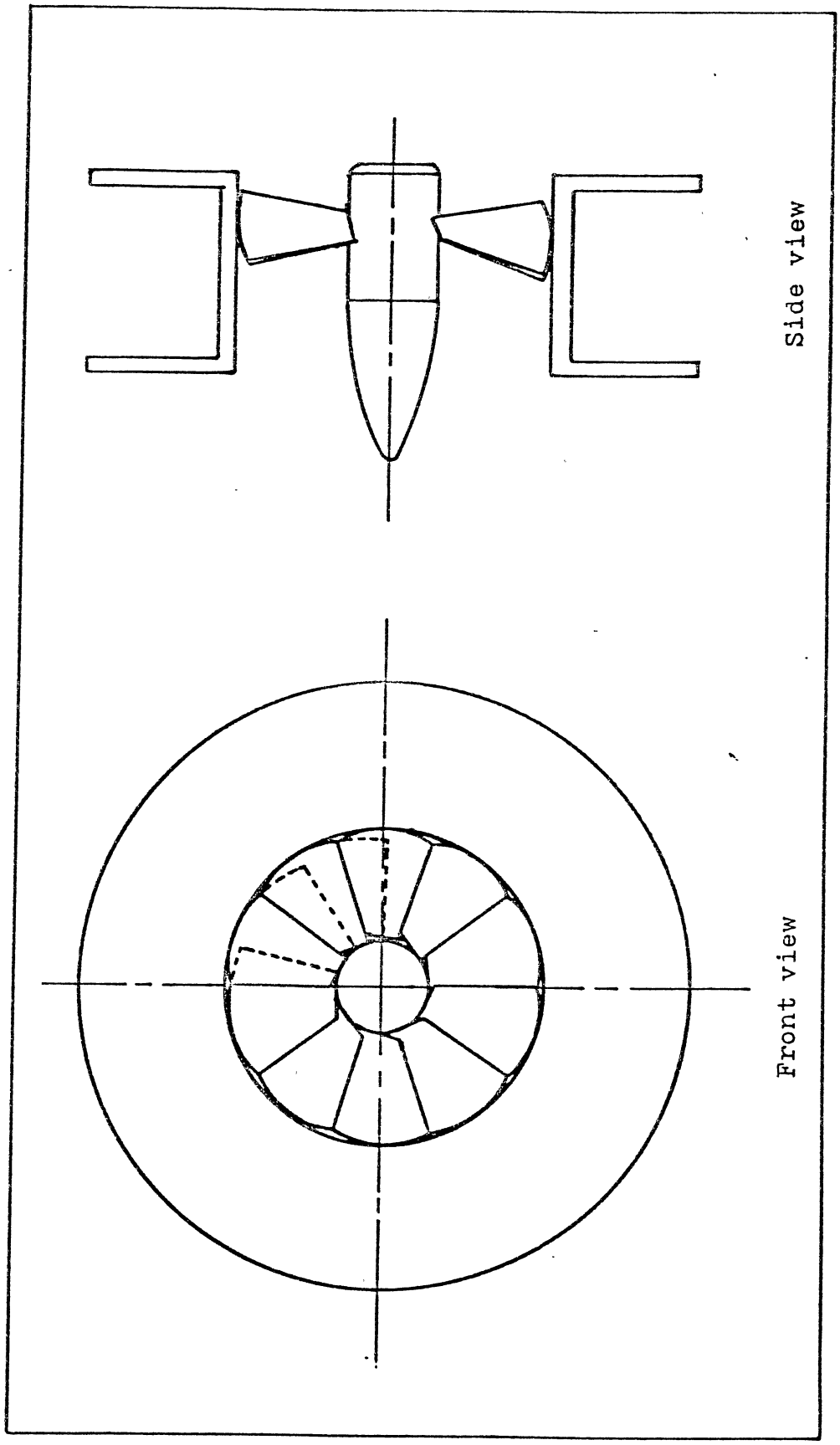

Figure 5. Swirler

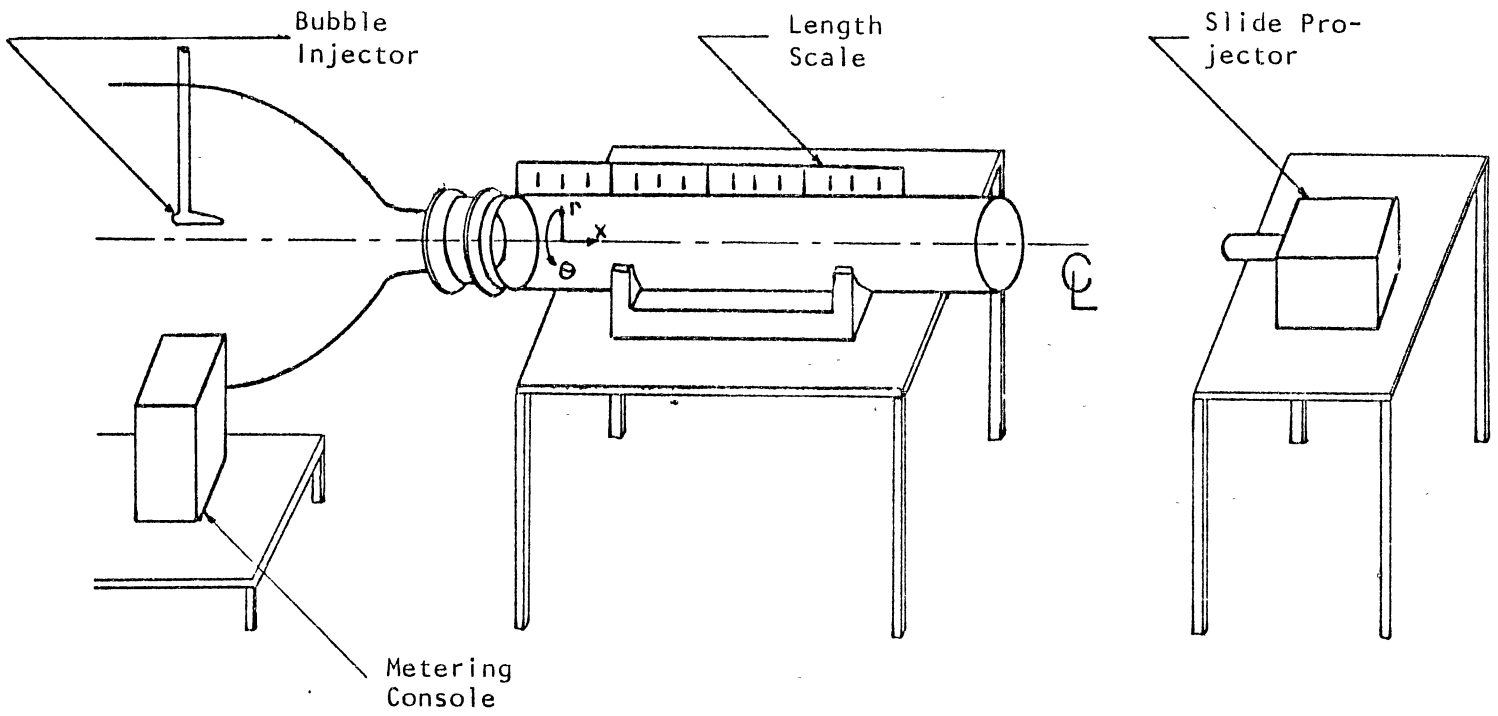

Figure 6. Apparatus for Neutrally-Buoyant Bubble Flow Visualization Experiment

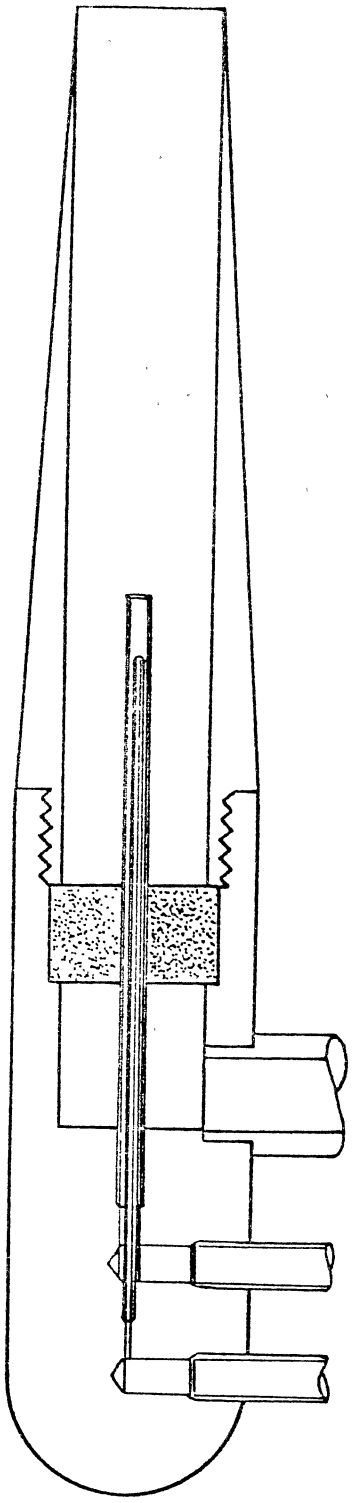

Figure 7. Neutrally-Buoyant Bubble Injector

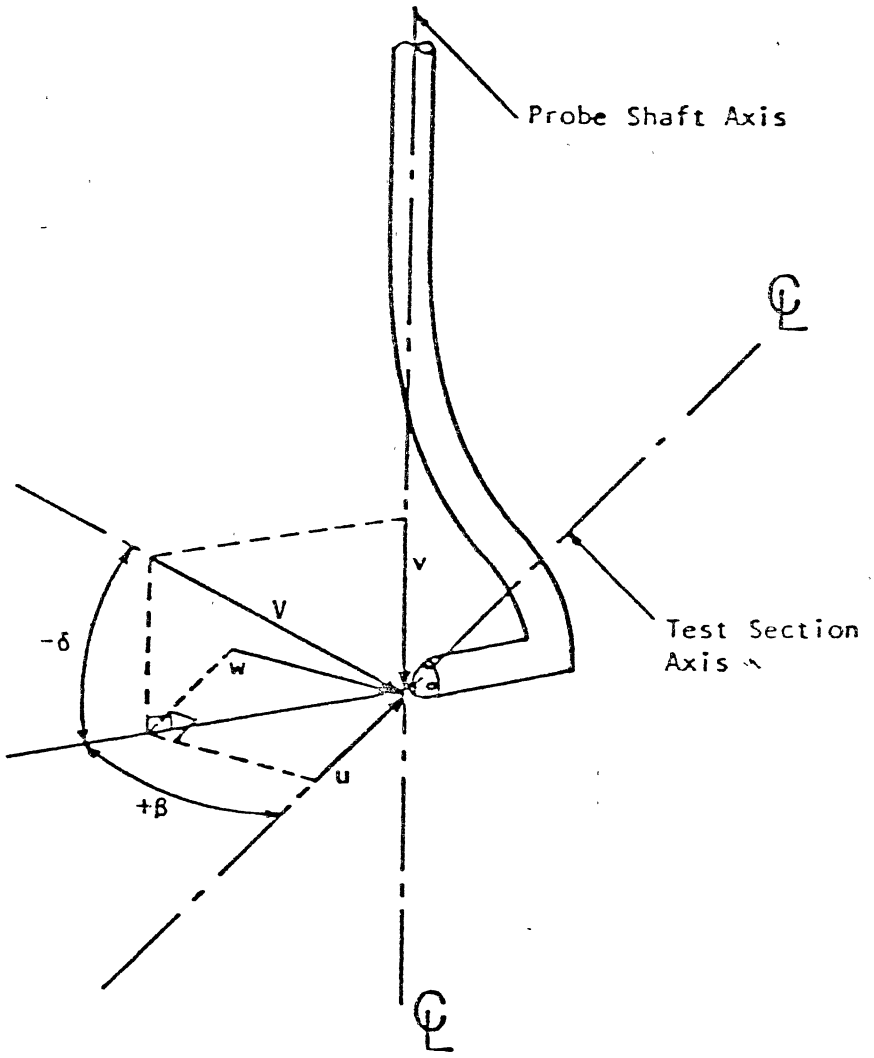

Figure 8. Velocity Components and Flow Direction Angles Associated with Five-Hole Pitot Measurements

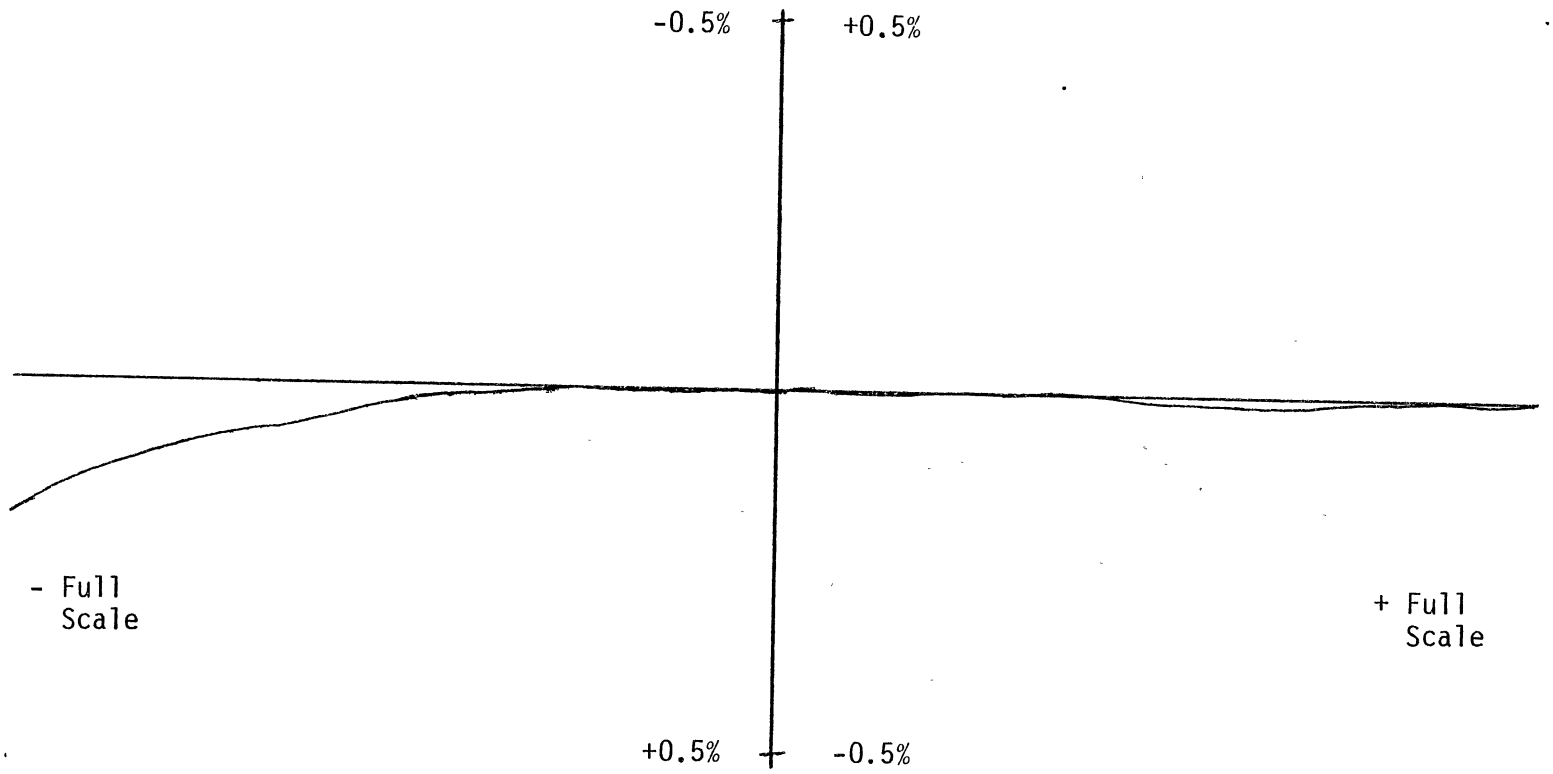

Figure 9. Linearity Deviation vs. Pressure for the Datametrics Pressure Transducer

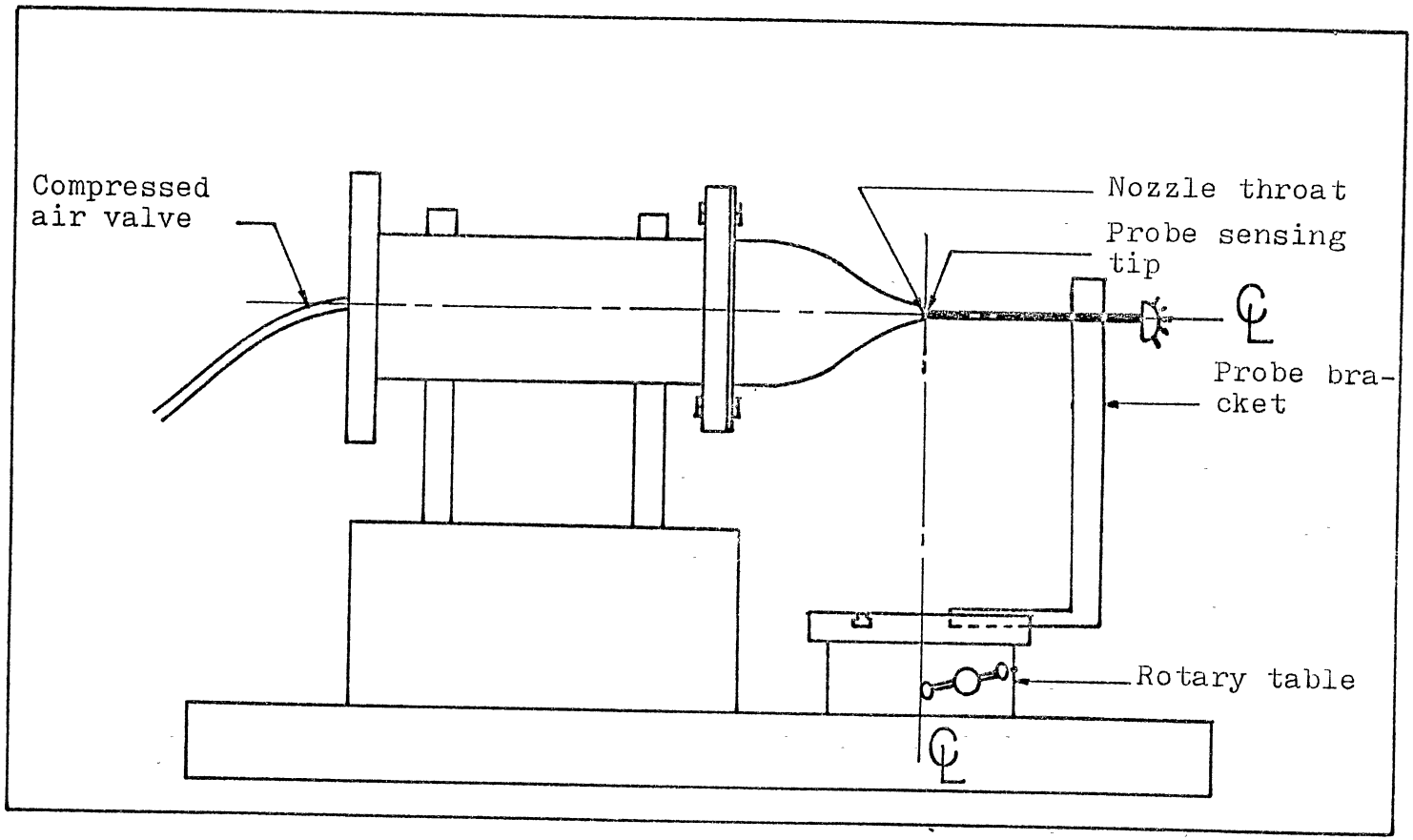

Figure 10. Calibration Apparatus.

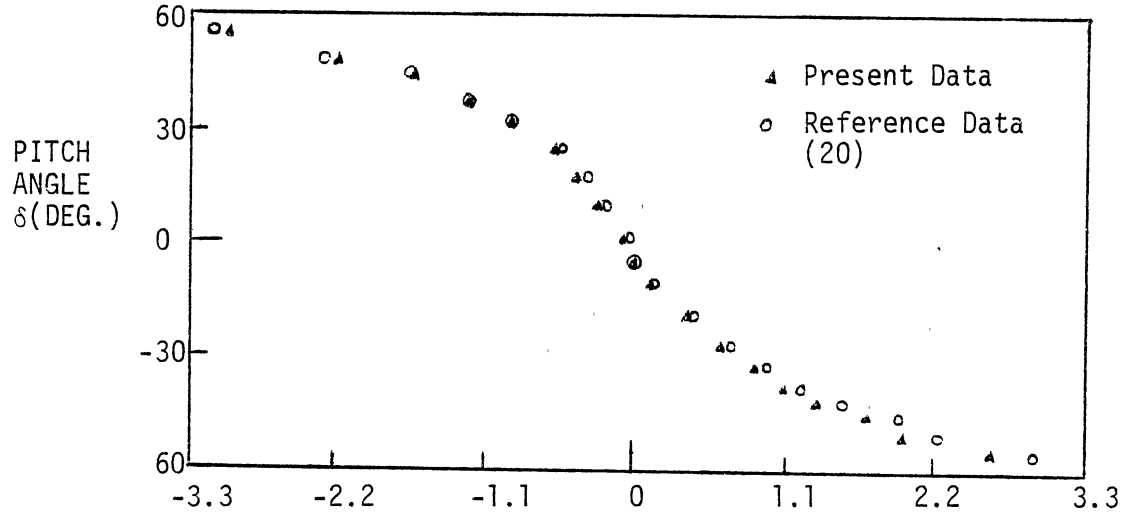

(a) Pitch Angle Calibration Characteristic

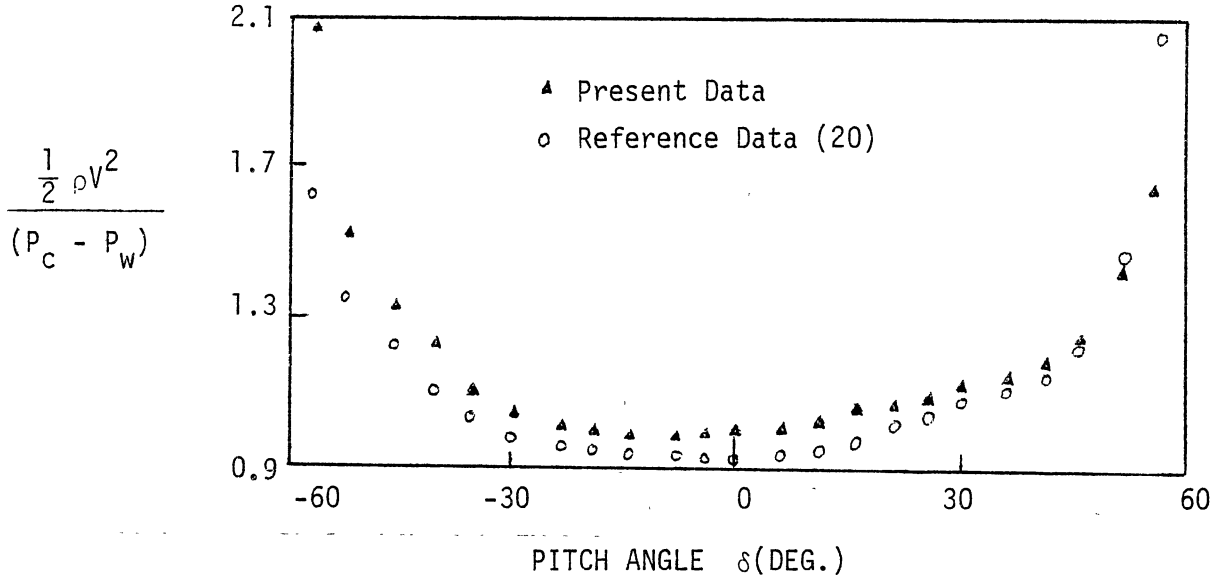

(b) Velocity Coefficient Calibration Characteristic

Figure 11. Calibration Characteristics for the Five-Hole Pitot

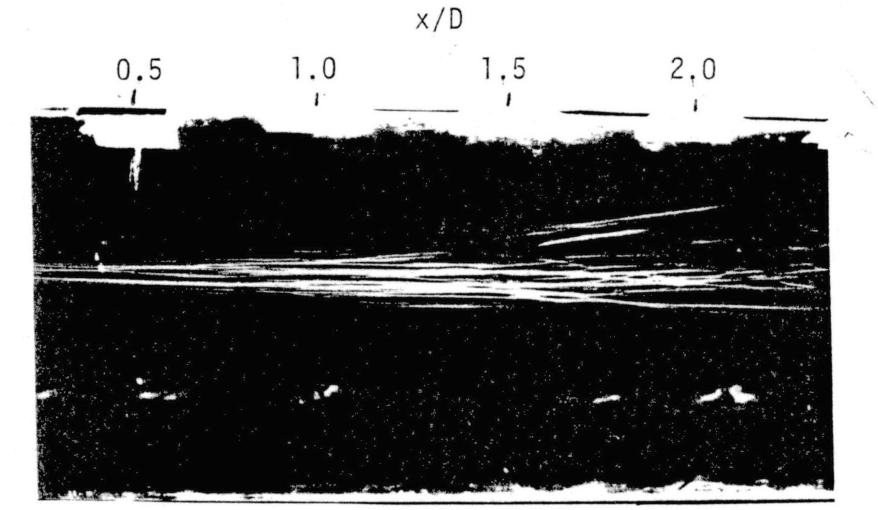

(a) $\phi = 0°$

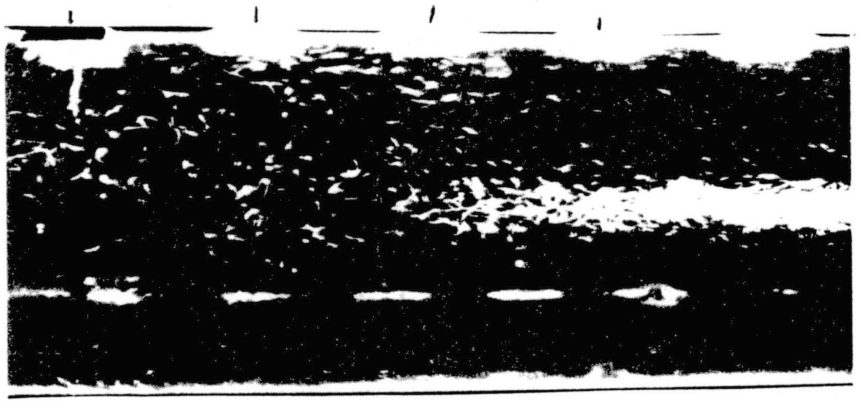

(b) $\phi = 45°$

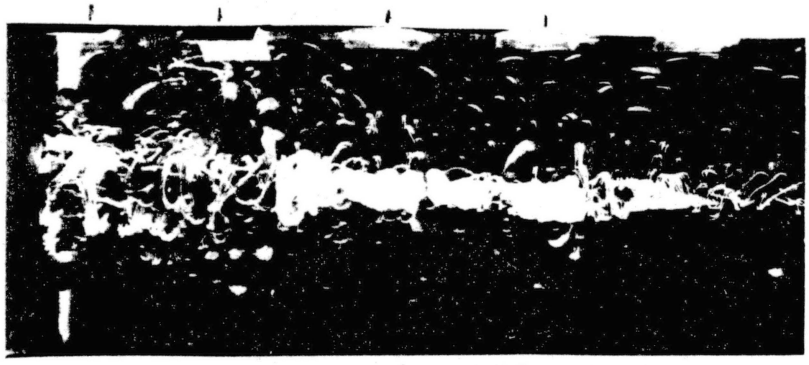

(c) $\phi = 70°$

Figure 12. Flow Visualization Photographs for Open-Ended Flows with Expansion Ratio D/d = 1.5 and Expansion Angle $\alpha = 90°$

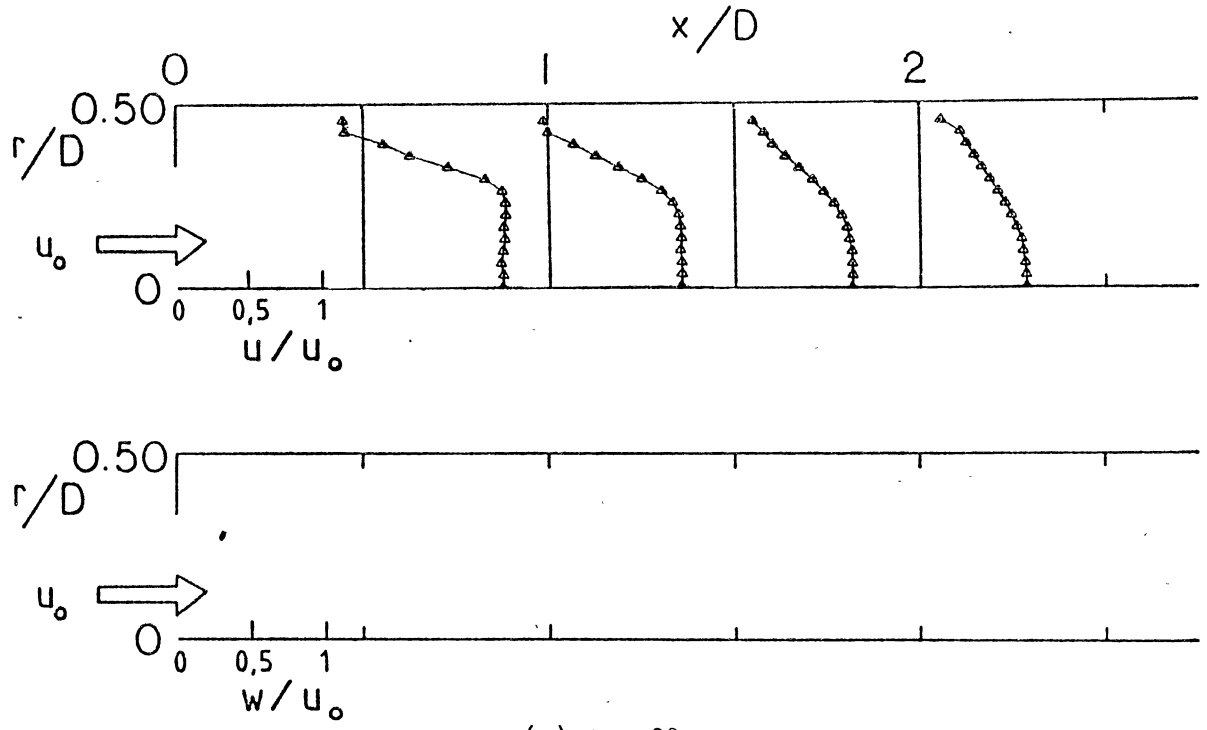

(a) $\phi = 0°$

Figure 13. Velocity Profiles for Open-Ended Flows with Expansion Ratio D/d = 1.5 and Expansion Angle $\alpha = 90°$.

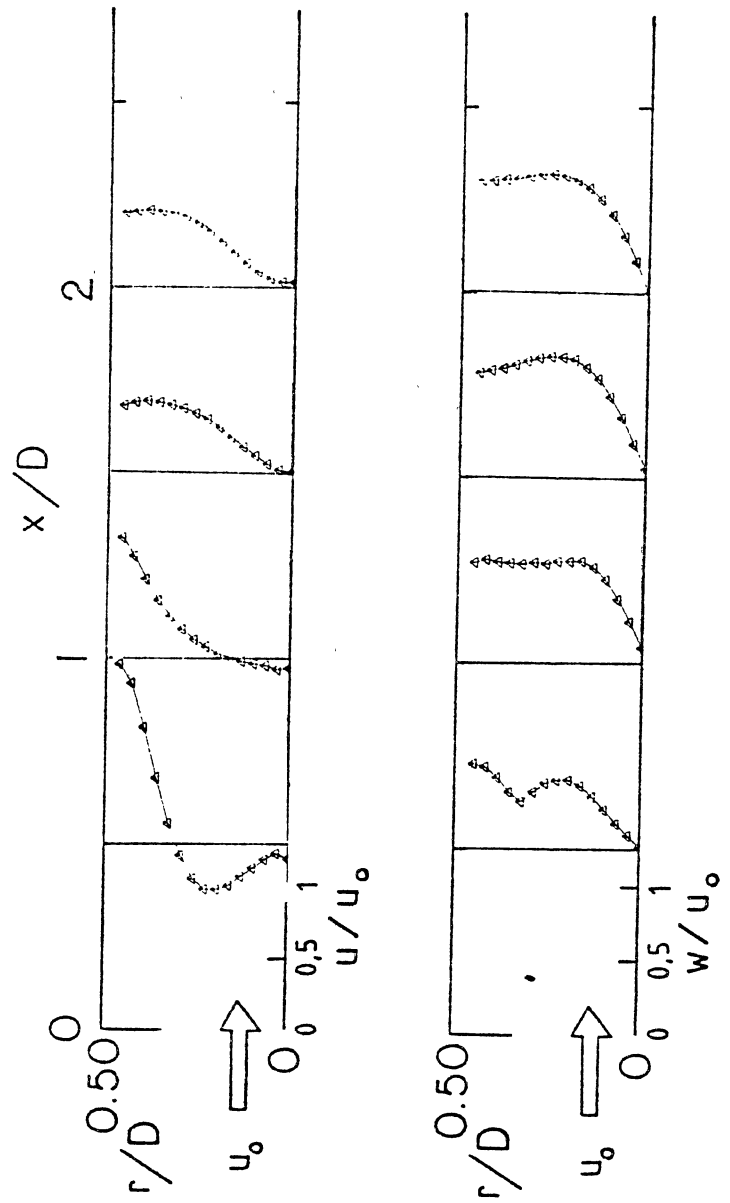

(b) $\phi = 45°$

Figure 13. (Continued)

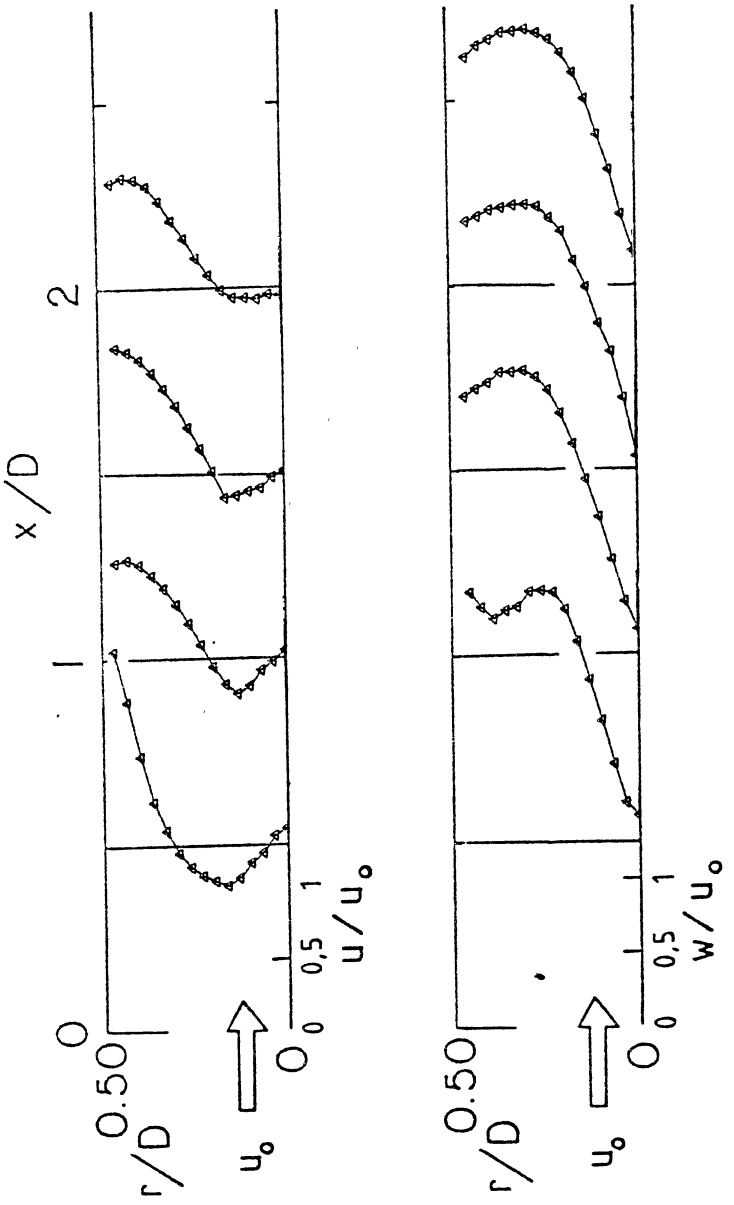

(c) ϕ = 70°

Figure 13. (Continued)

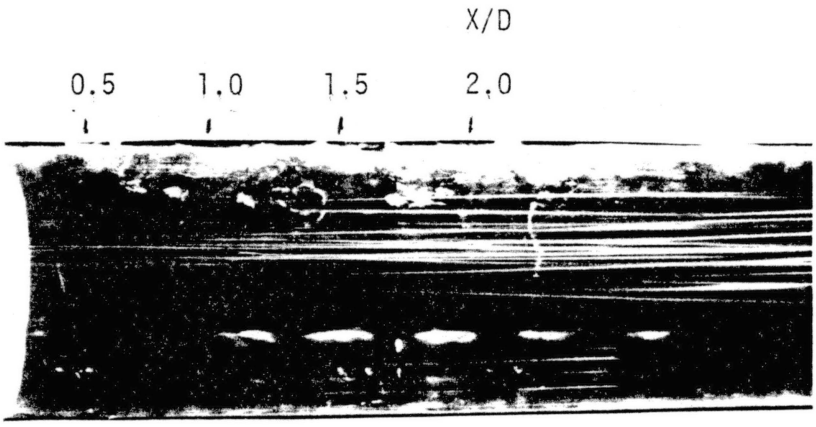

Figure 14. Flow Visualization Photograph for Open-Ended Nonswirling Flow with Expansion Ratio D/d = 1.0

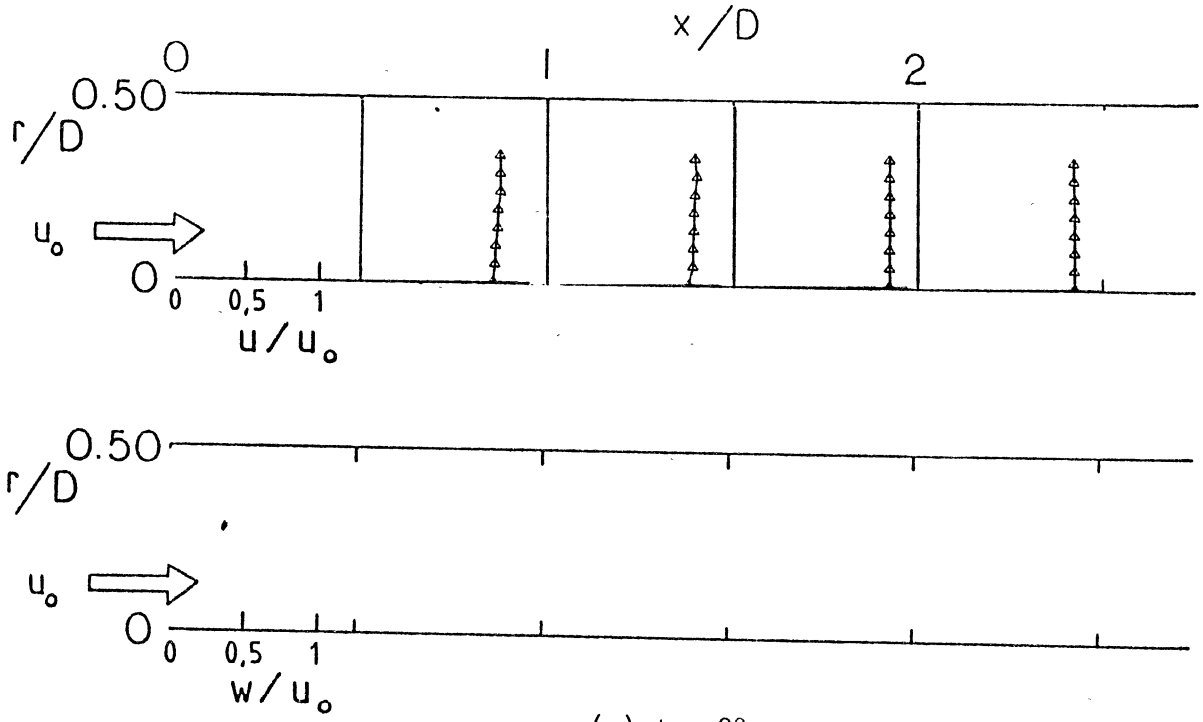

(a) $\phi = 0°$

Figure 15. Velocity Profiles for Open-Ended Flows with Expansion Ratio D/d = 1.0

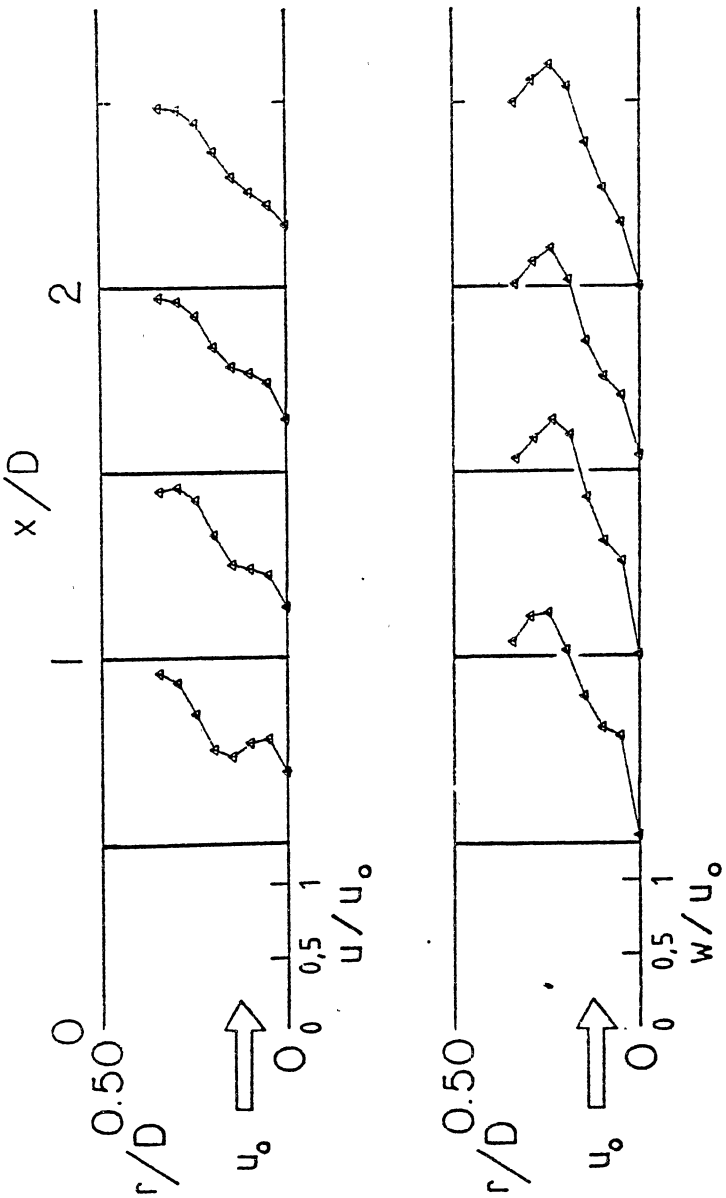

(b) ϕ = 45°

Figure 15. (Continued)

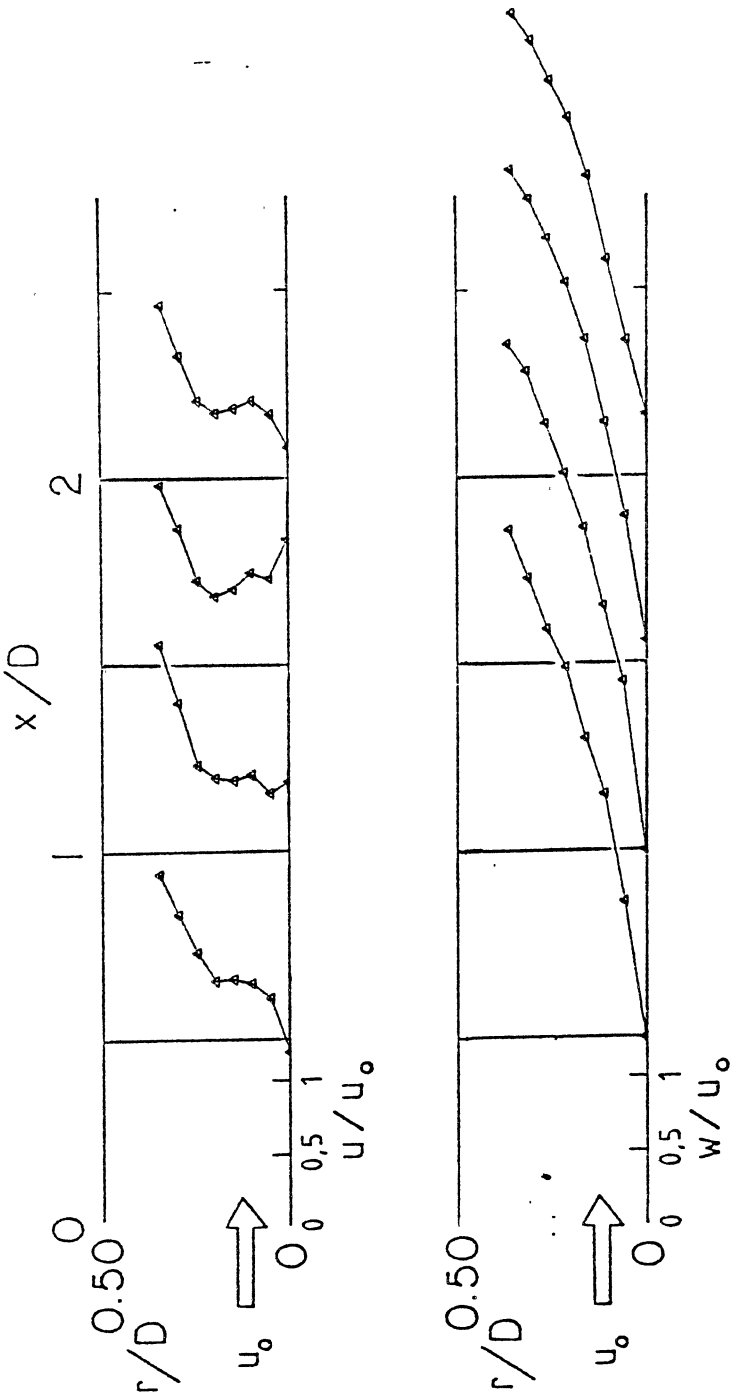

(c) ϕ = 70°

Figure 15. (Continued)

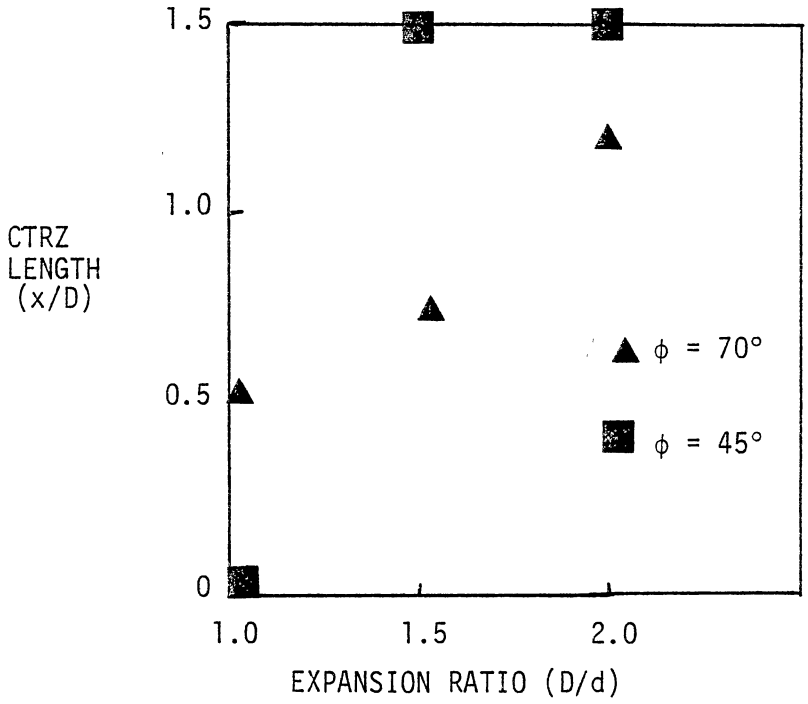

Figure 16. Central Recirculation Zone Lengths vs. Expansion Ratio for Swirling Flow

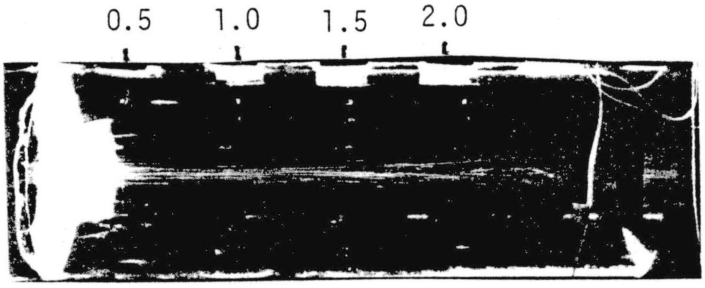

(a) $\phi = 0°$

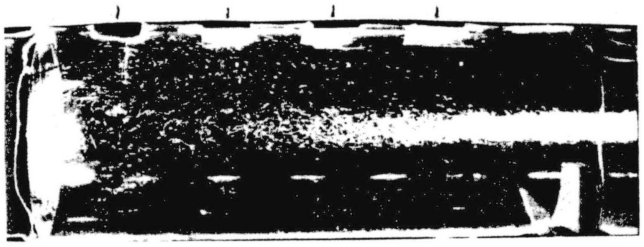

(b) $\phi = 45°$

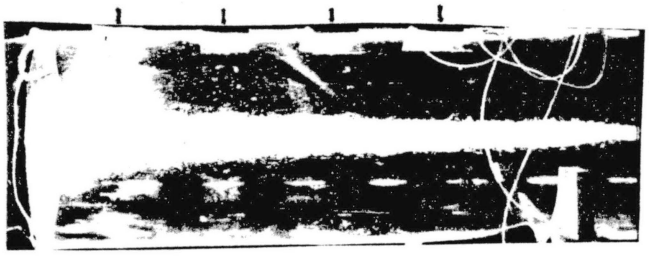

(c) $\phi = 70°$

Figure 17. Flow Visualization Photographs for Open-Ended Flows with Expansion Ratio D/d = 1.5 and Expansion Angle $\alpha = 45°$

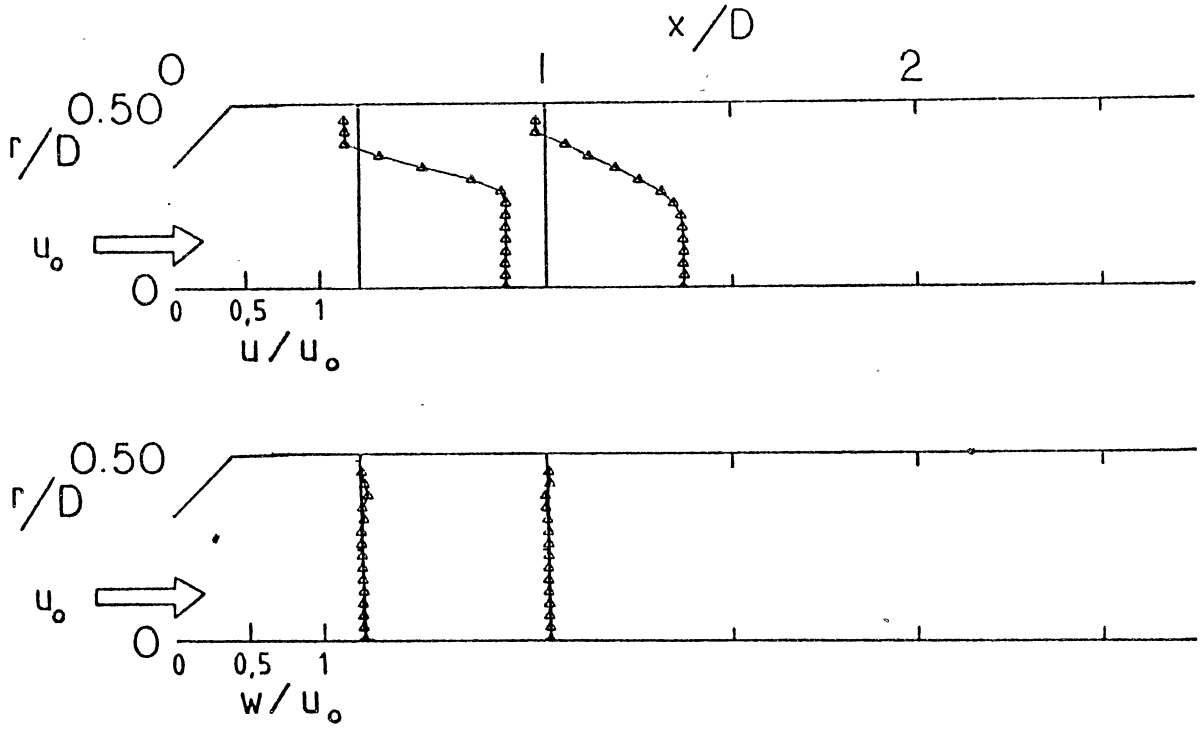

(a) = 0°

Figure 18. Velocity Profiles for Open-Ended Flows with Expansion Ratio D/d = 1.5 and Expansion Angle α = 45°

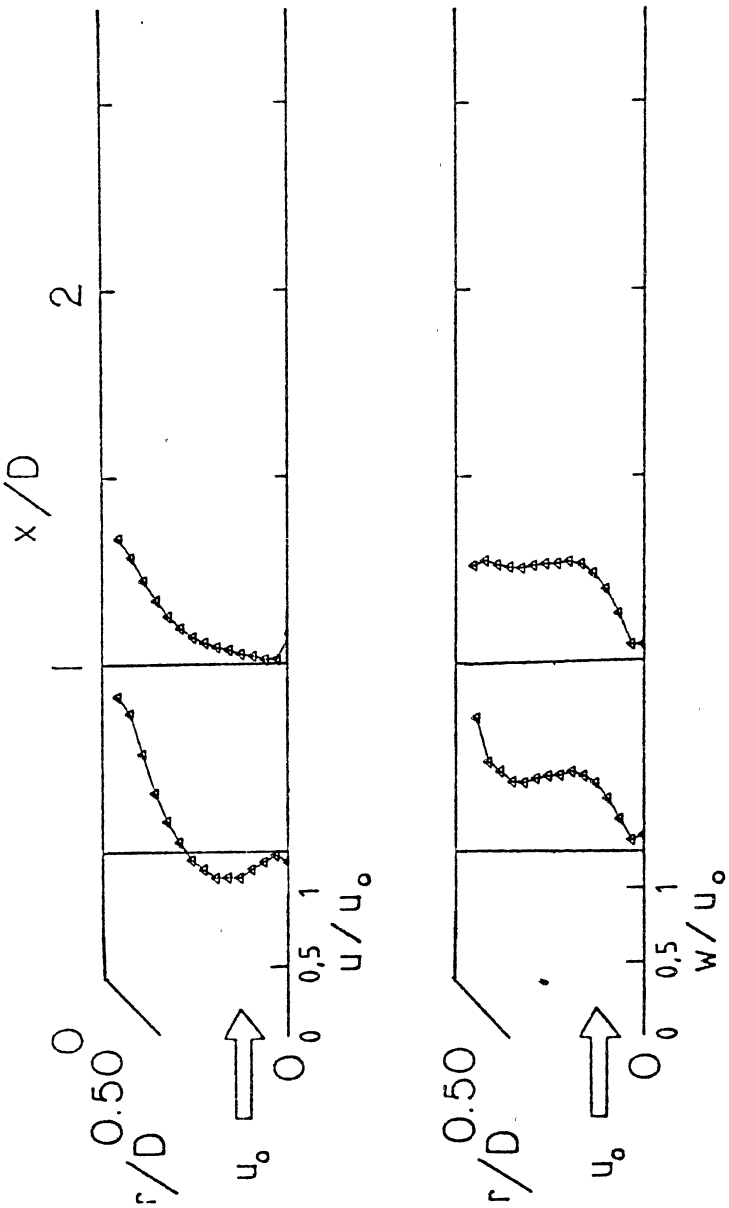

(b) $\phi = 45°$

Figure 18. (Continued)

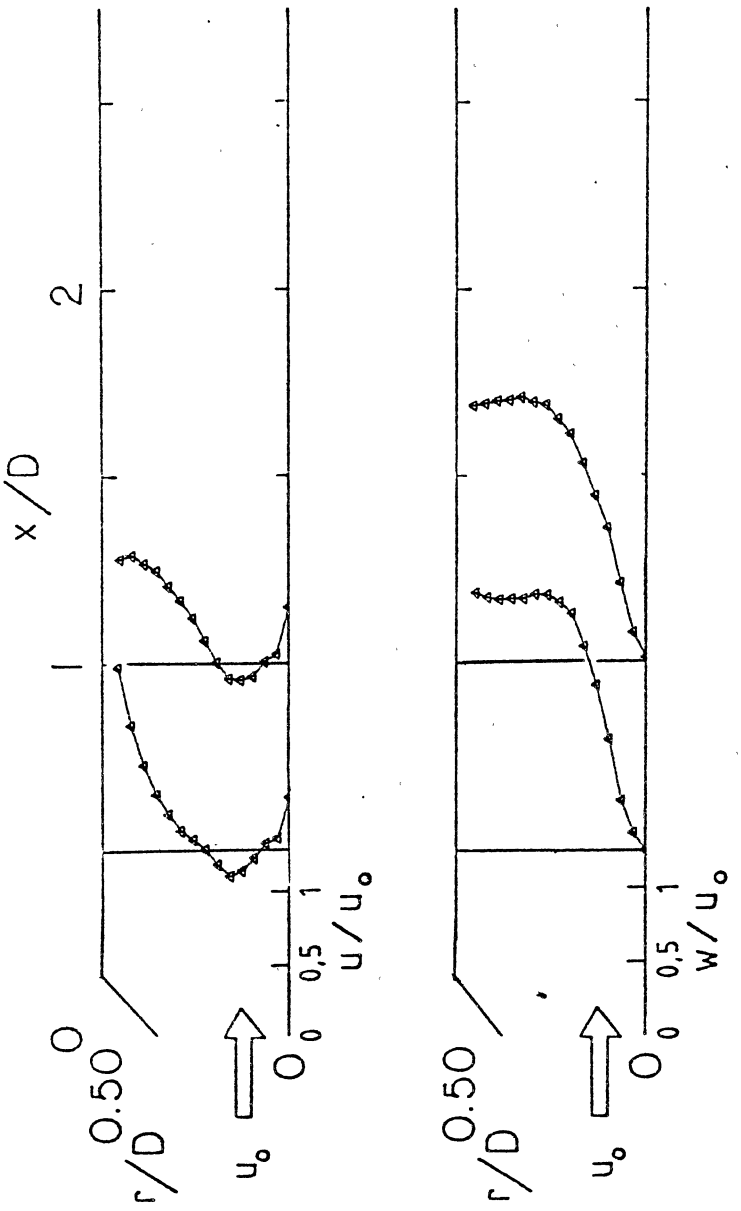

(c) ϕ = 70°

Figure 18. (Continued)

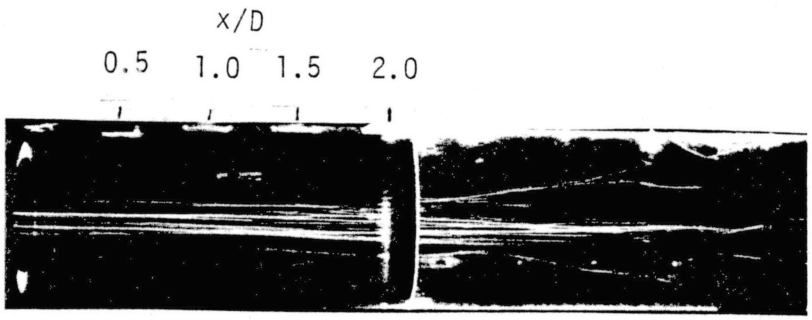

(a) $\phi = 0°$

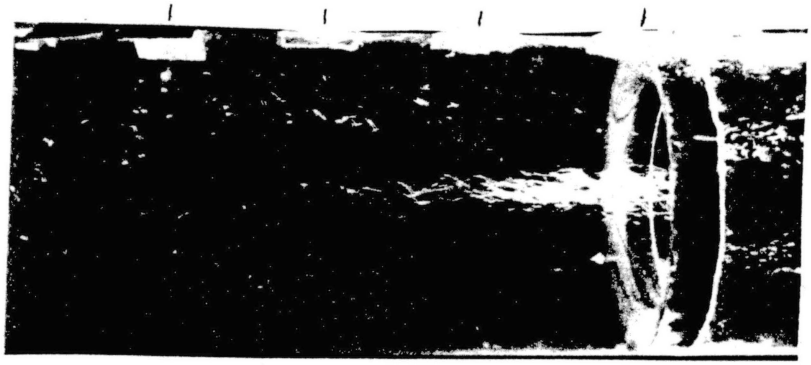

(b) $\phi = 45°$

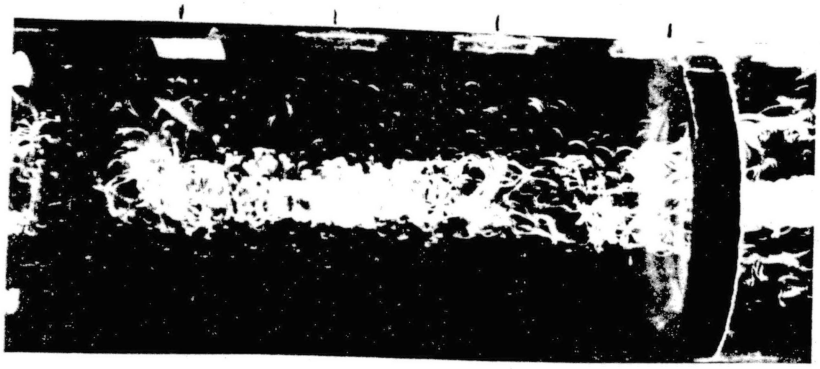

(c) $\phi = 70°$

Figure 19. Flow Visualization Photographs for Flows with Expansion Ratio D/d = 1.5, Expansion Angle $\alpha = 90°$ and Small Blockage

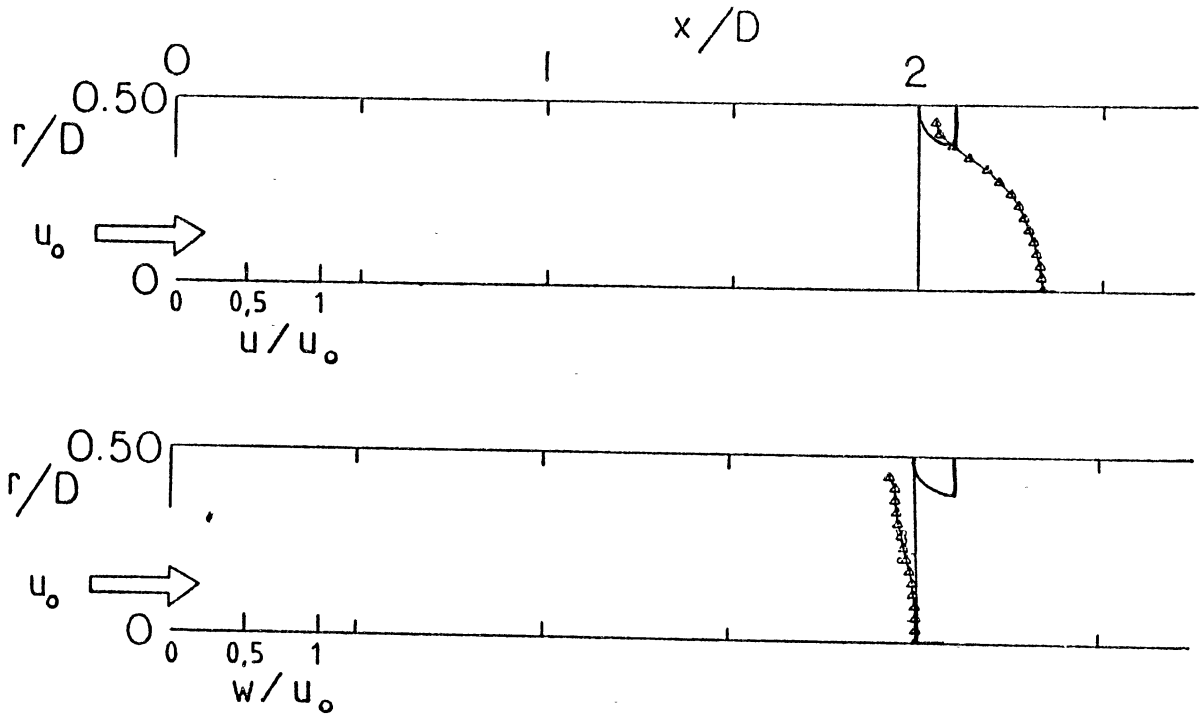

(a) $\phi = 0°$

Figure 20. Velocity Profiles for Flows with Expansion Ratio D/d = 1.5, Expansion Angle $\alpha = 90°$ and Small Blockage

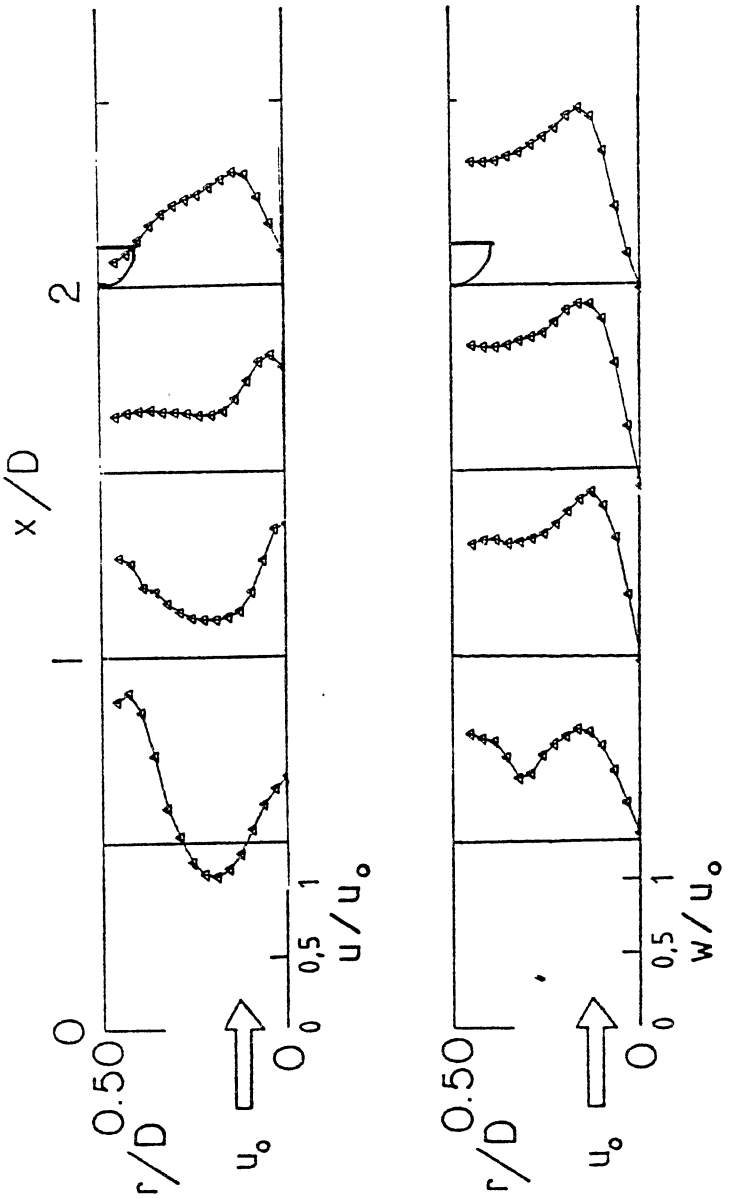

(b) ϕ = 45°

Figure 20. (Continued)

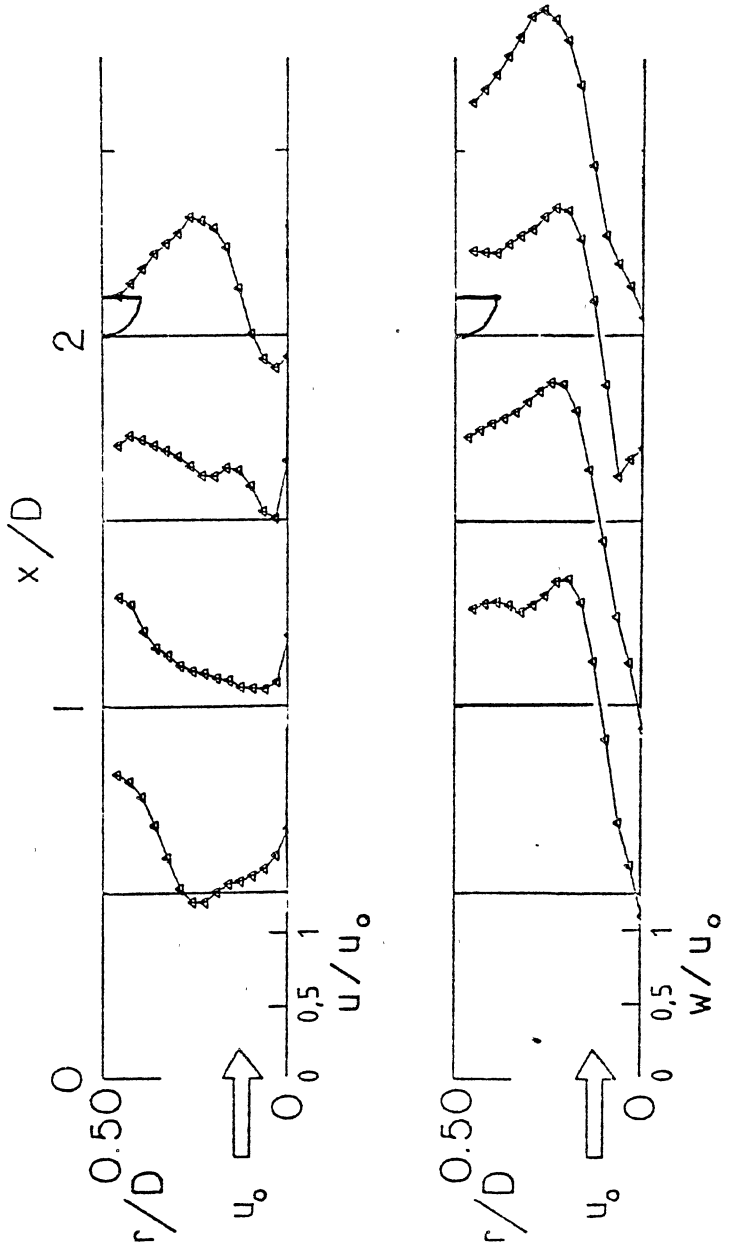

(c) ϕ = 70°

Figure 20. (Continued)

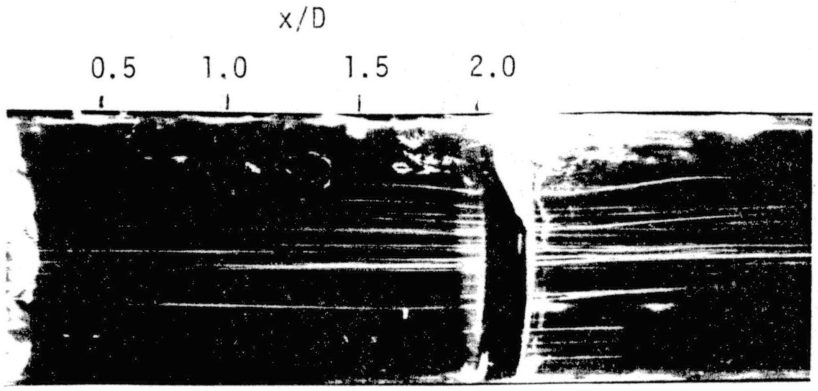

Figure 21. Flow Visualization Photograph for Non-swirling Flow with Expansion Ratio D/d = 1.0 and Small Blockage

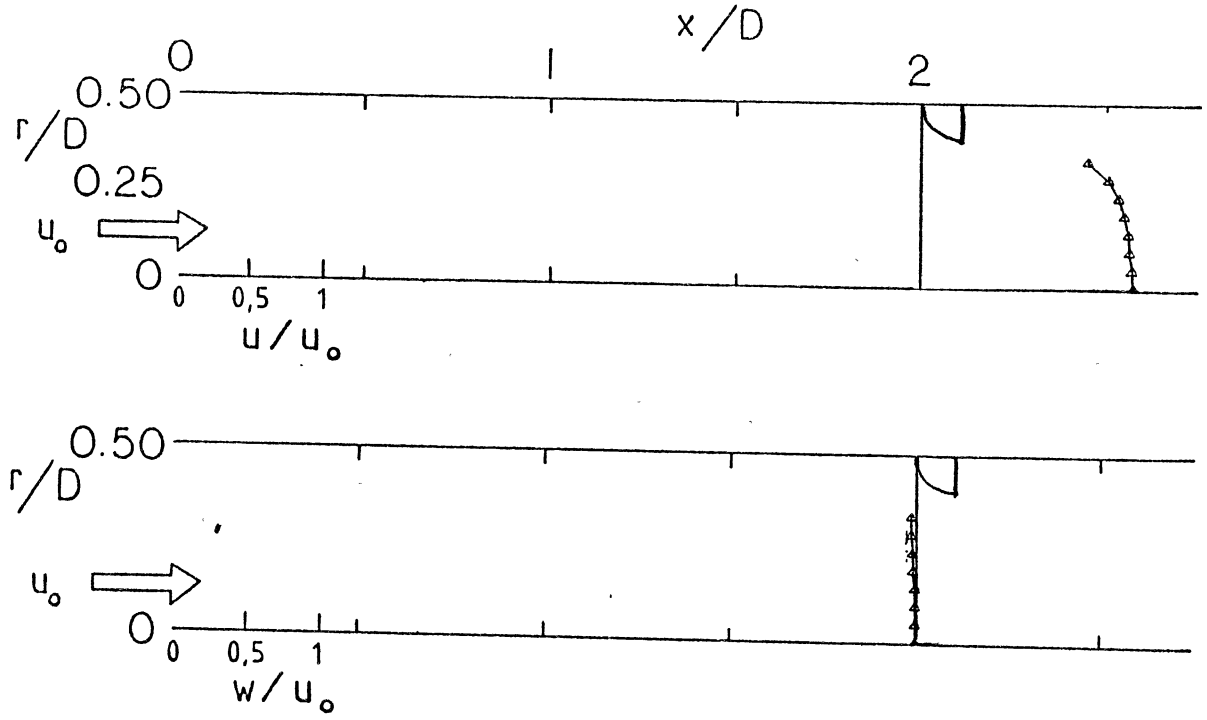

(a) $\phi = 0°$

Figure 22. Velocity Profiles for Flow with Expansion Ratio D/d = 1.0 and Small Blockage

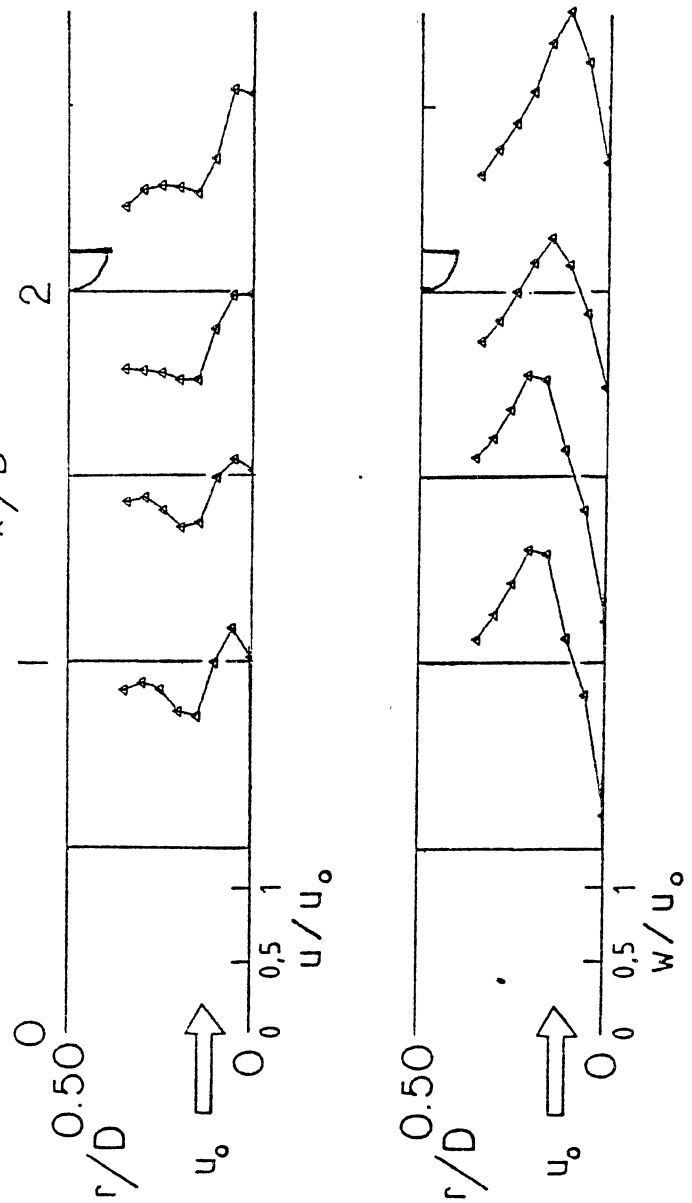

(b) $\phi = 45°$

Figure 22. (Continued)

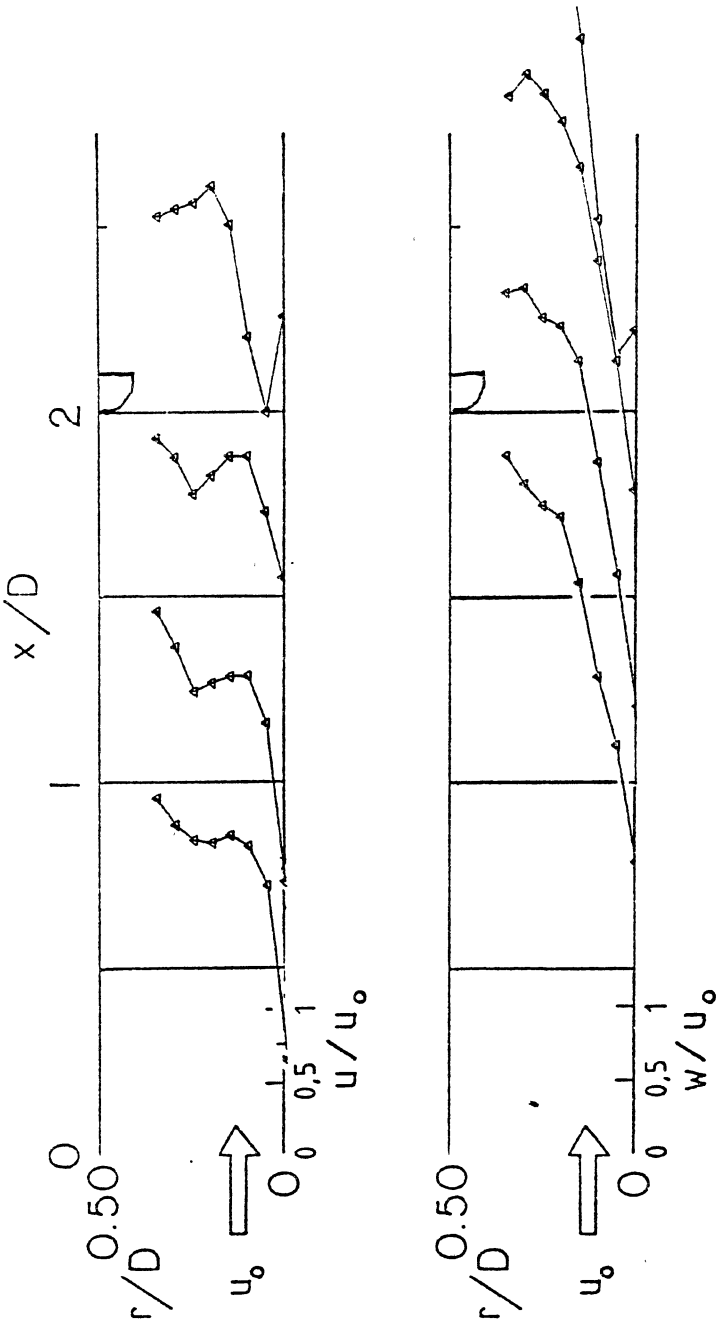

(c) ϕ = 70°

Figure 22. (Continued)

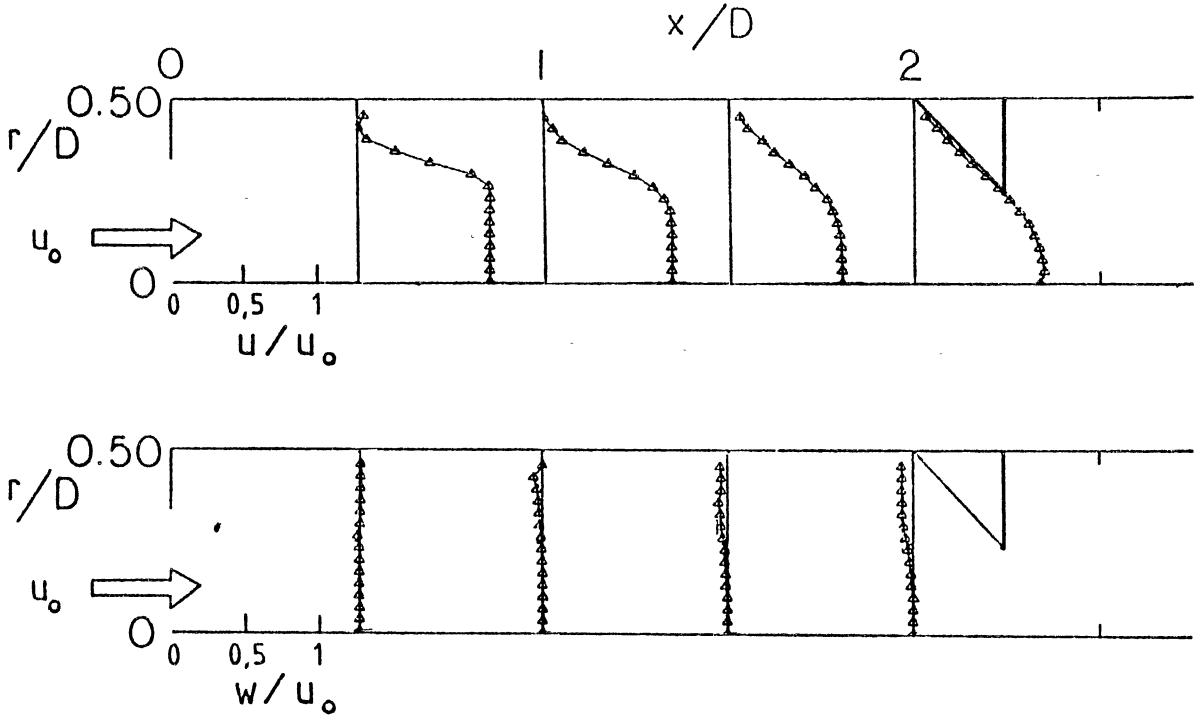

(a) $\phi = 0°$

Figure 23. Velocity Profiles for Flow with Expansion Ratio D/d = 1.5, Expansion Angle $\alpha = 90°$ and Large Blockage

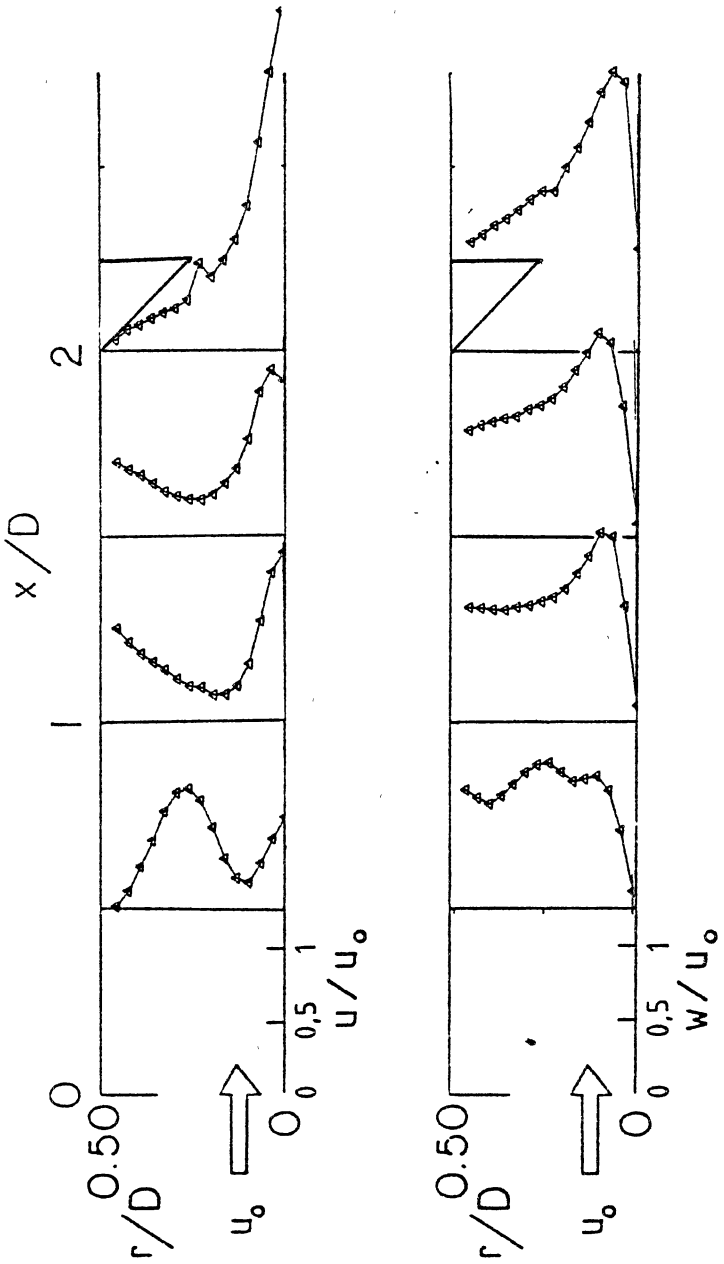

(b) ϕ = 45°

Figure 23. (Continued)

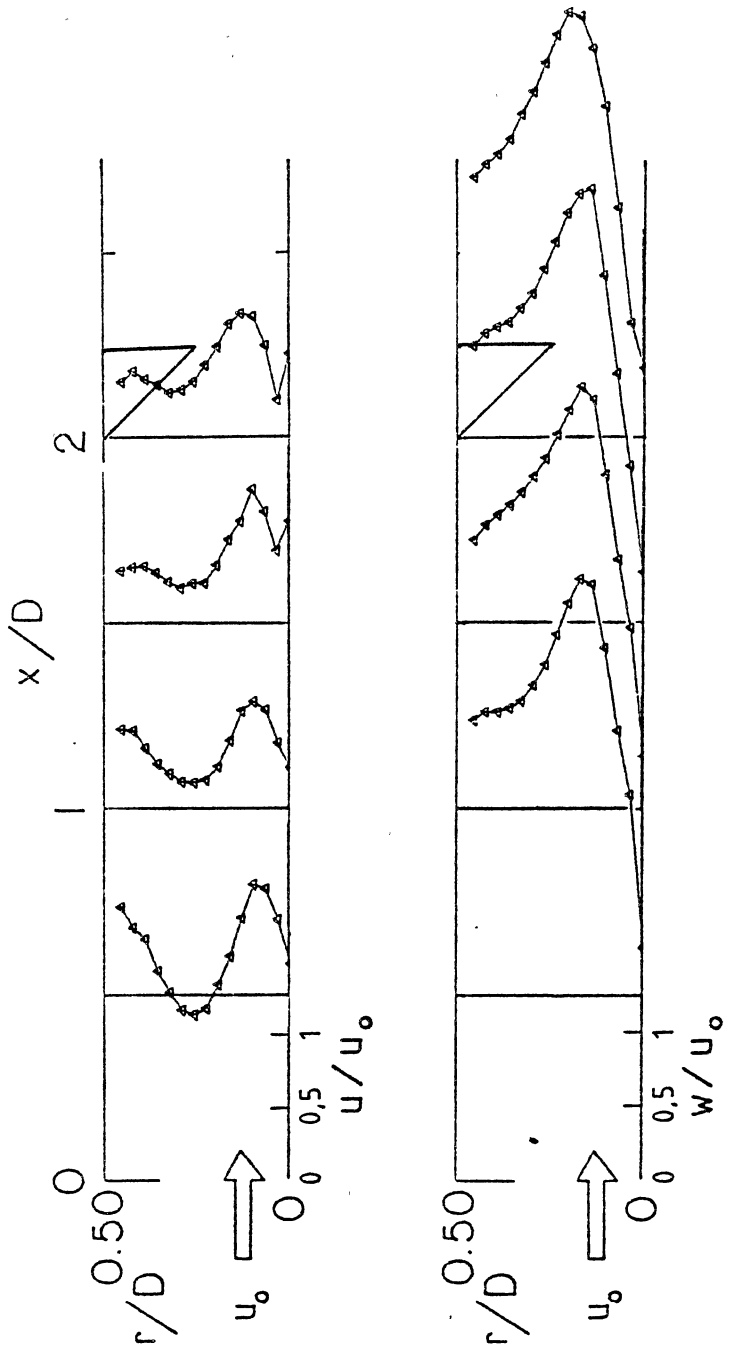

(c) ϕ = 70°

Figure 23. (Continued)

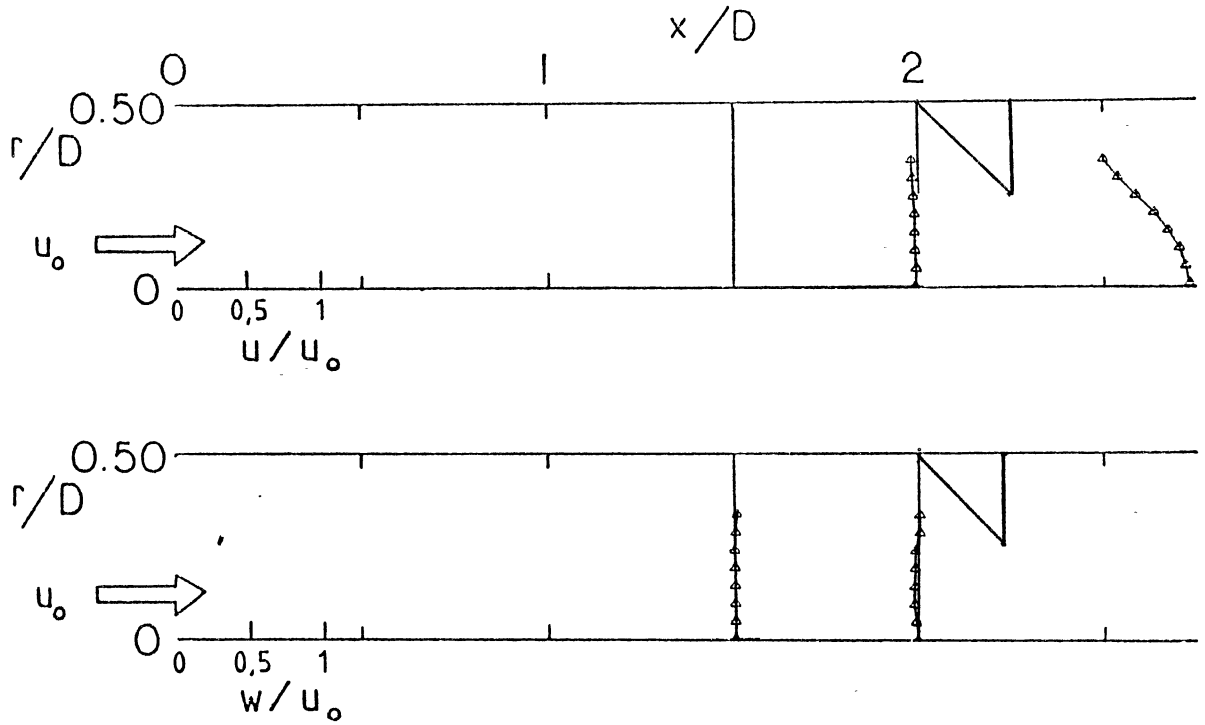

(a) $\phi = 0°$

Figure 24. Velocity Profiles for Flow with Expansion Ratio D/d = 1.0 and Large Blockage

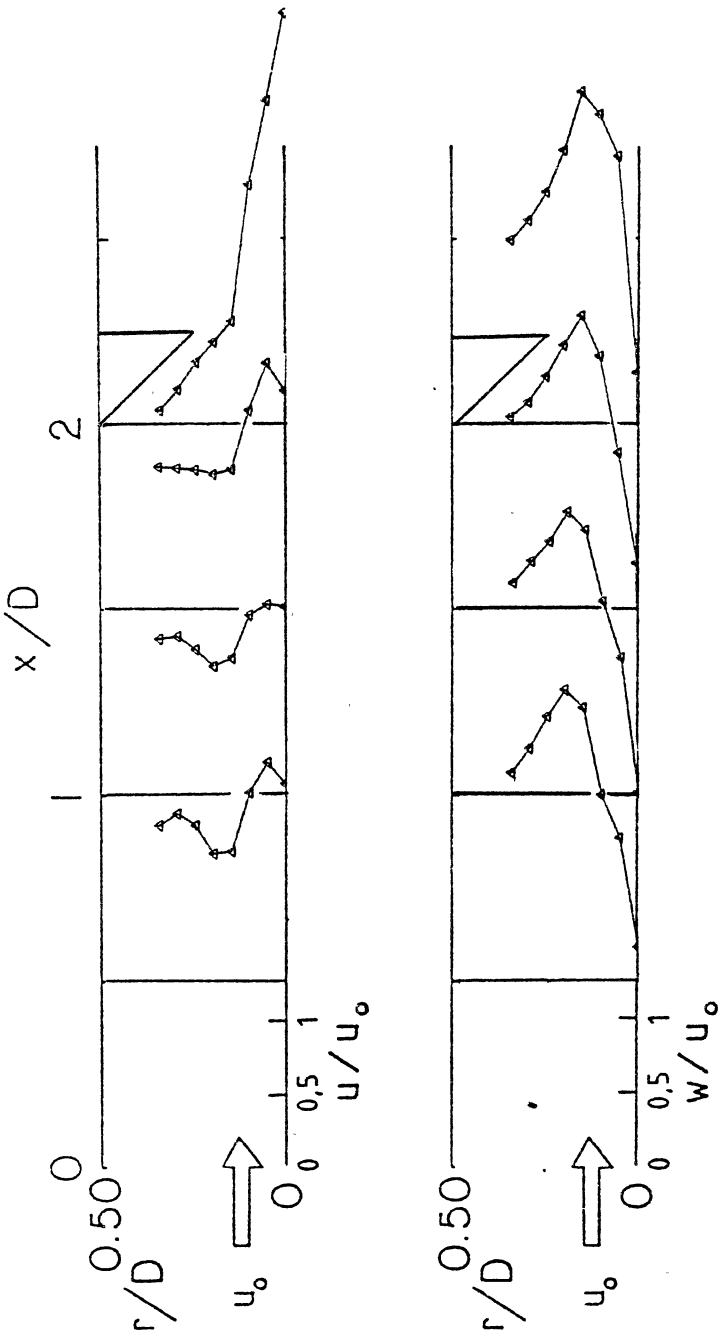

(b) ϕ = 45°

Figure 24. (Continued)

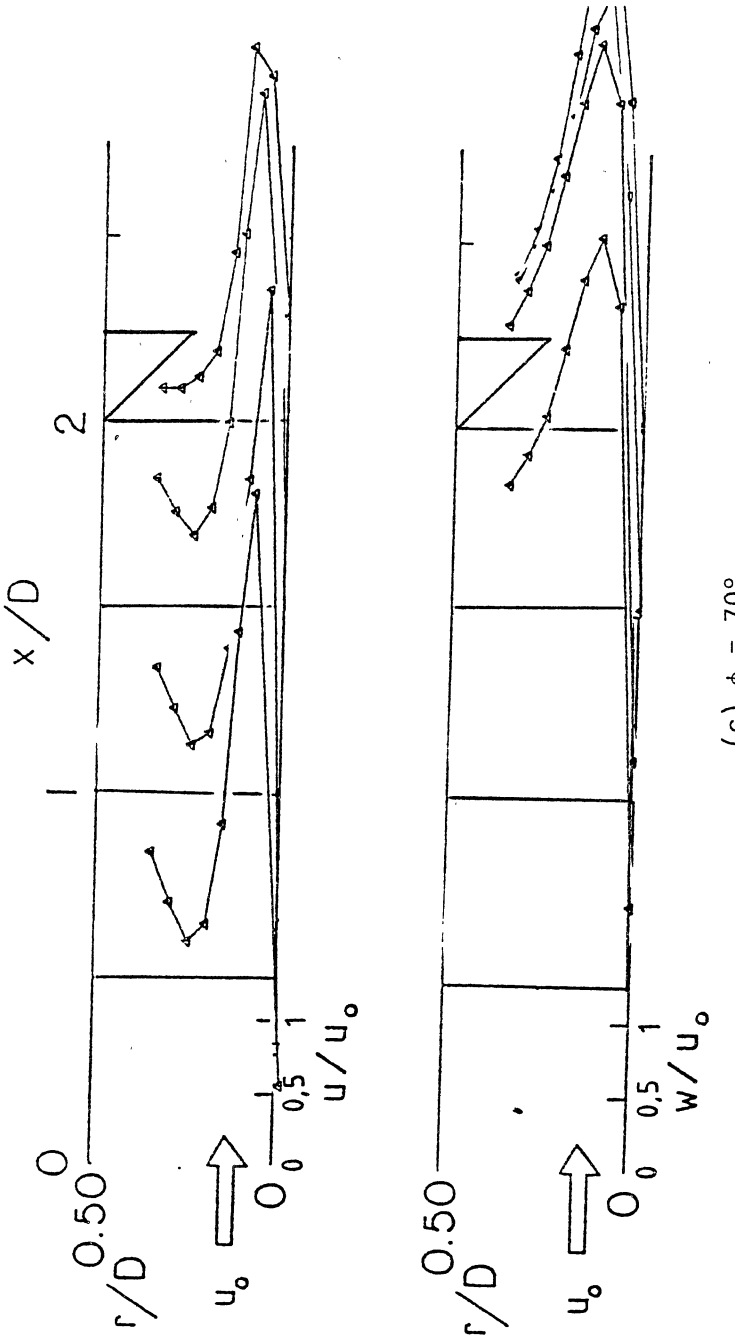

(c) ϕ = 70°

Figure 24. (Continued)

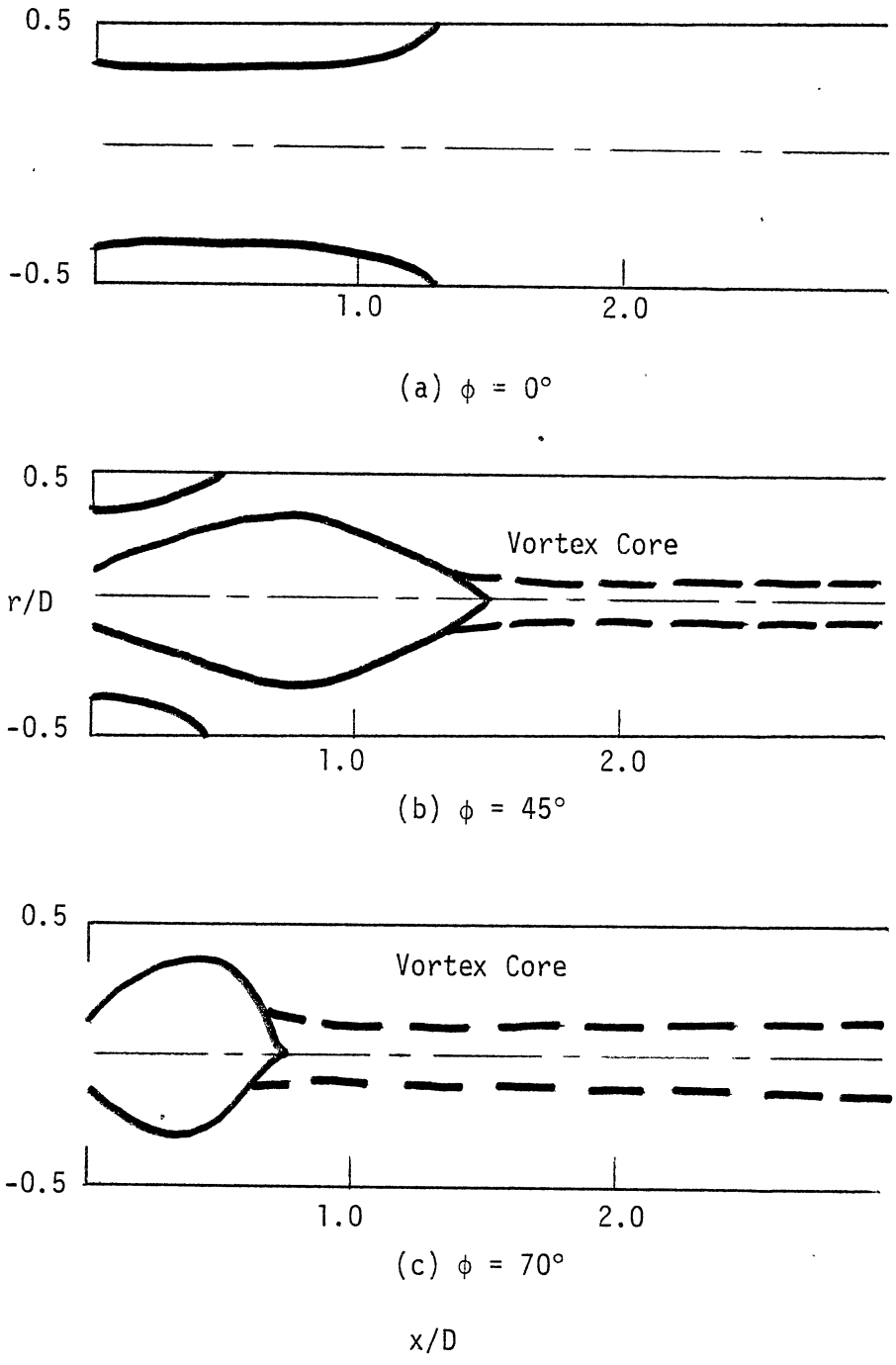

Figure 25. Artistic Impressions of Dividing Streamlines for the Flow of Figure 13 [D/d = 1.5, α = 90°, Open-Ended]

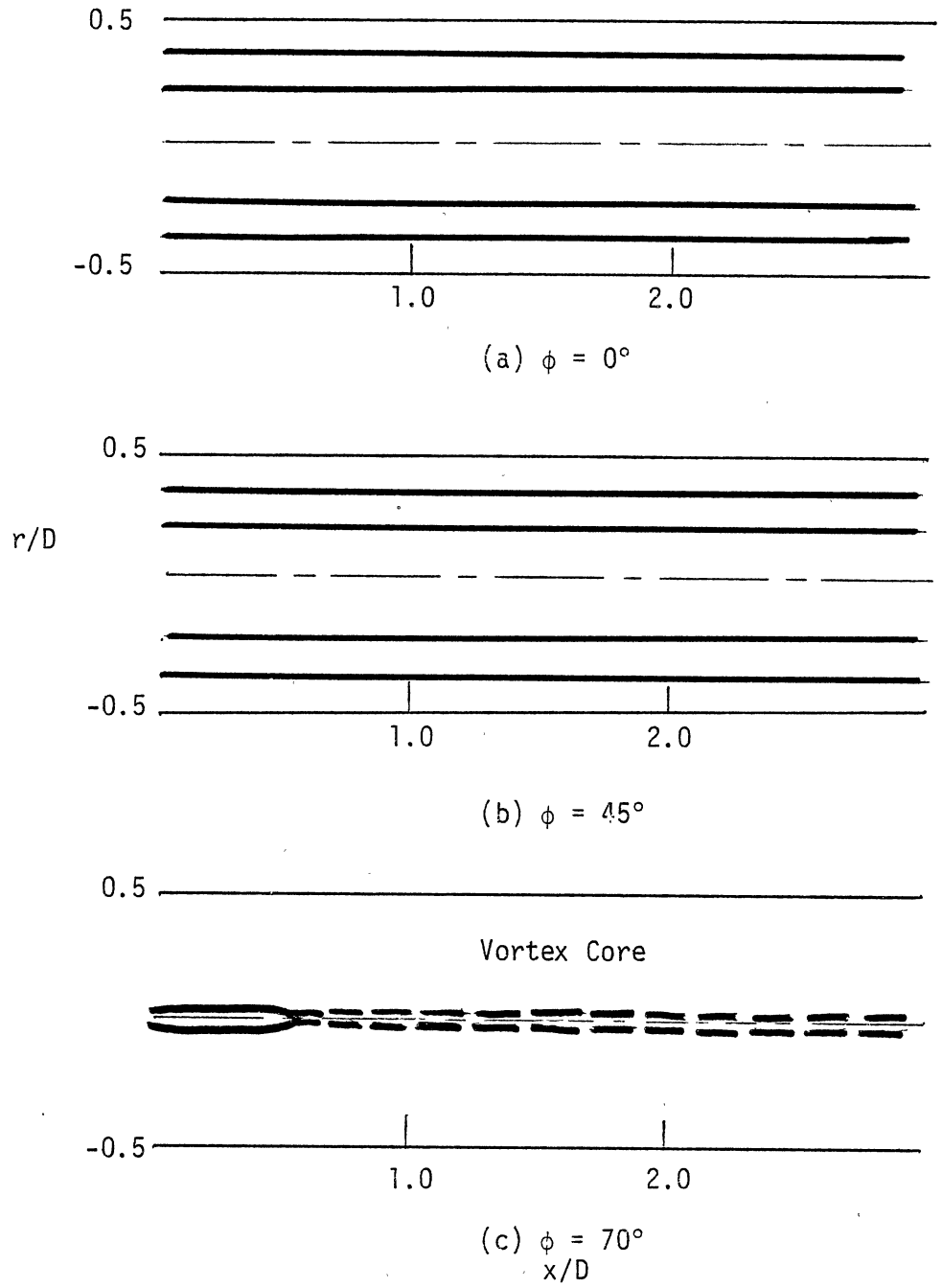

Figure 26. Artistic Impressions of Dividing Streamlines for the Flow of Figure 15 [D/d = 1.0, Open-Ended]

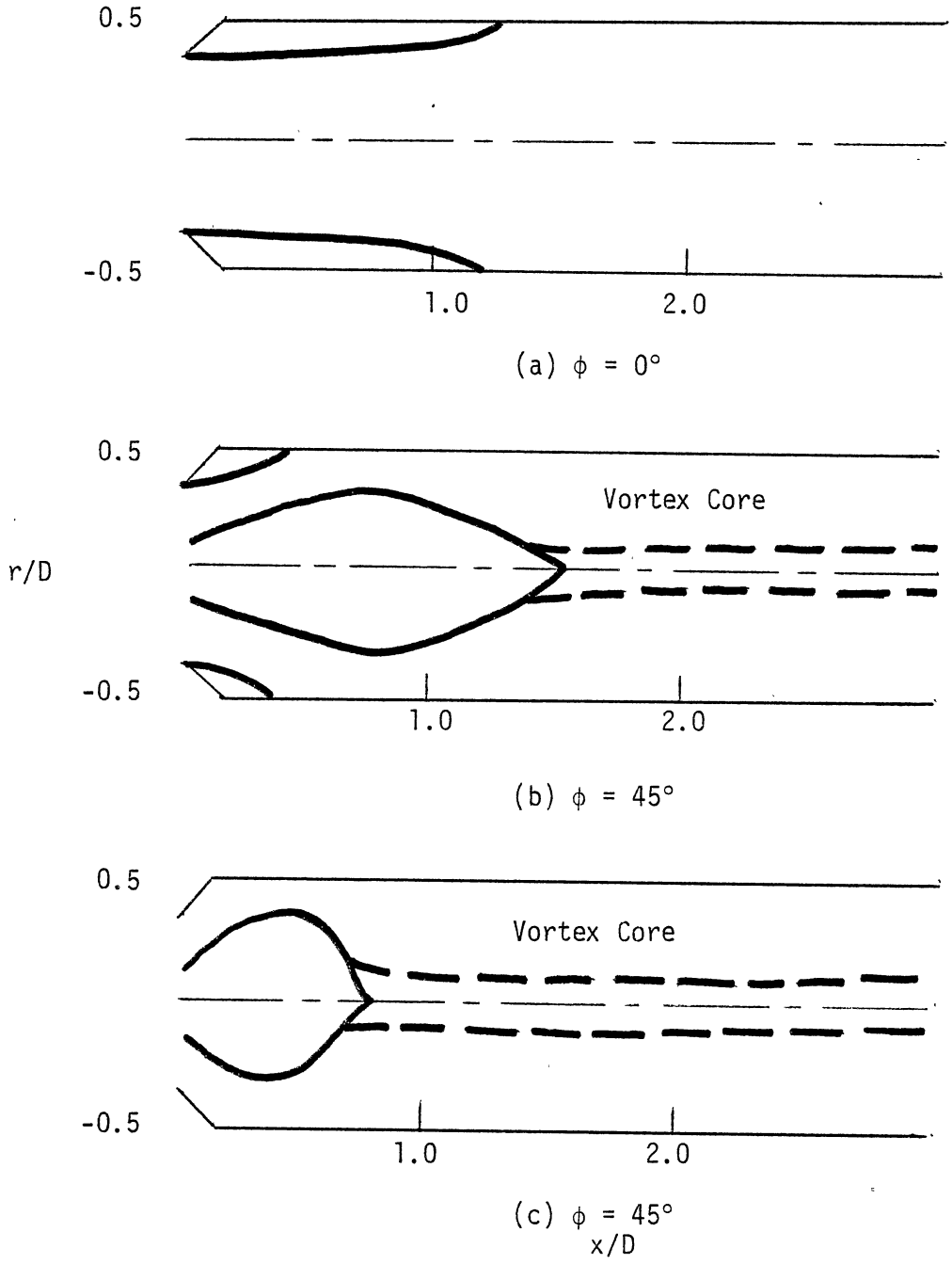

Figure 27. Artistic Impressions of Dividing Streamlines for the Flow of Figure 18 [D/d = 1.5, α = 45°, Open-Ended]

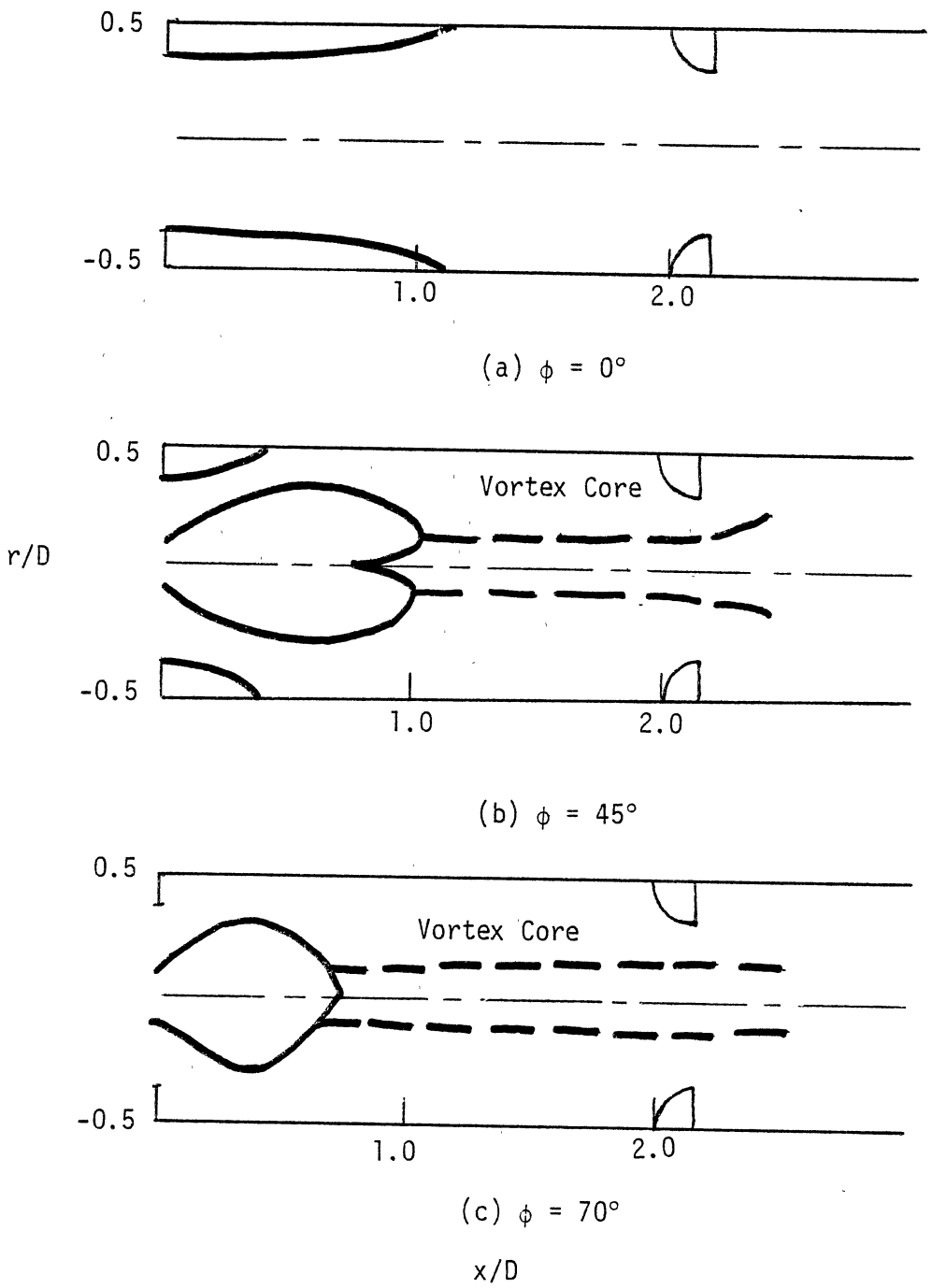

Figure 28. Artistic Impressions of Dividing Streamlines for the Flow of Figure 20 [D/d = 1.5, α = 90°, Small Blockage]

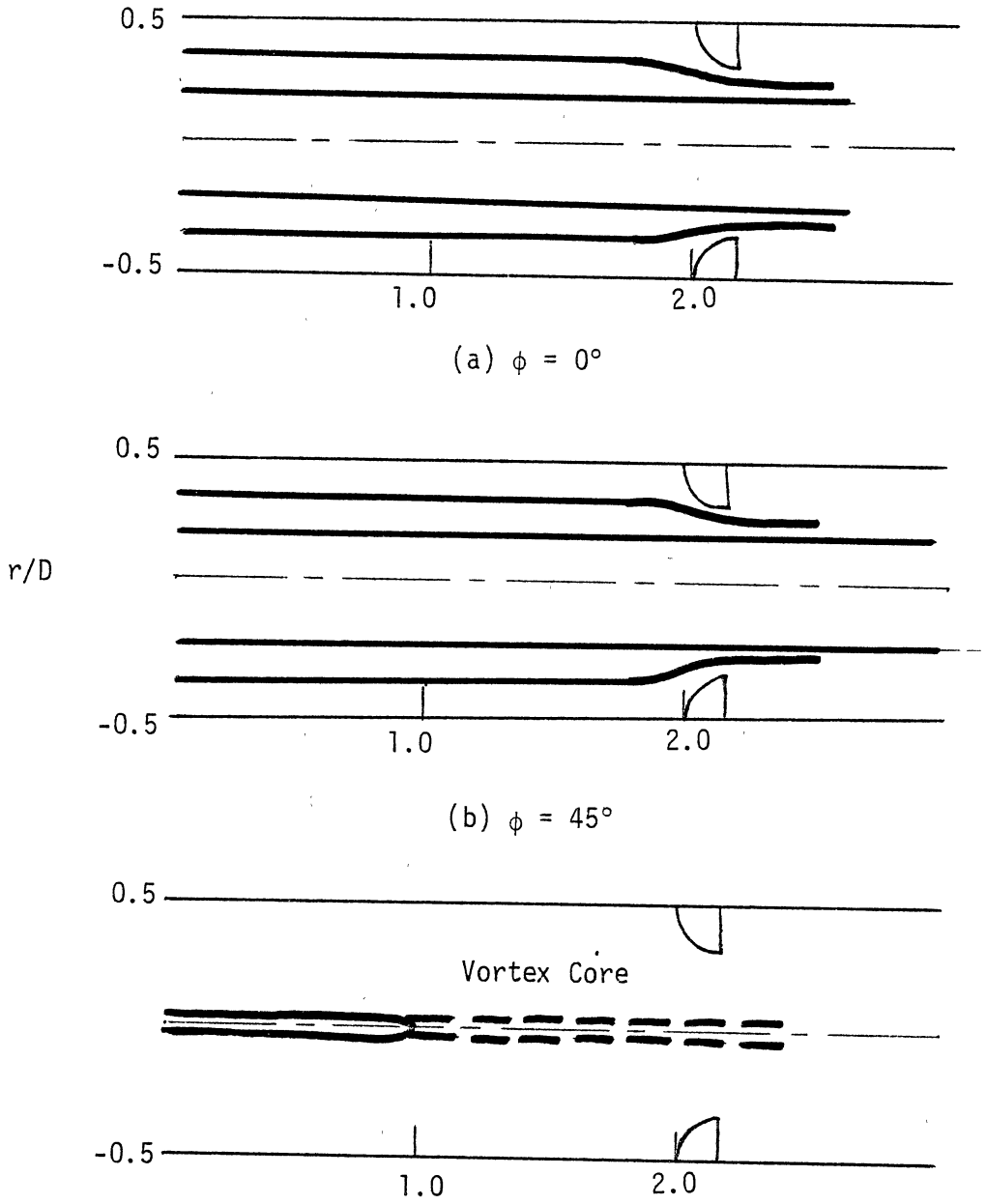

Figure 29. Artistic Impressions of Dividing Streamlines for the Flow of Figure 22 [D/d = 1.0, Small Blockage]

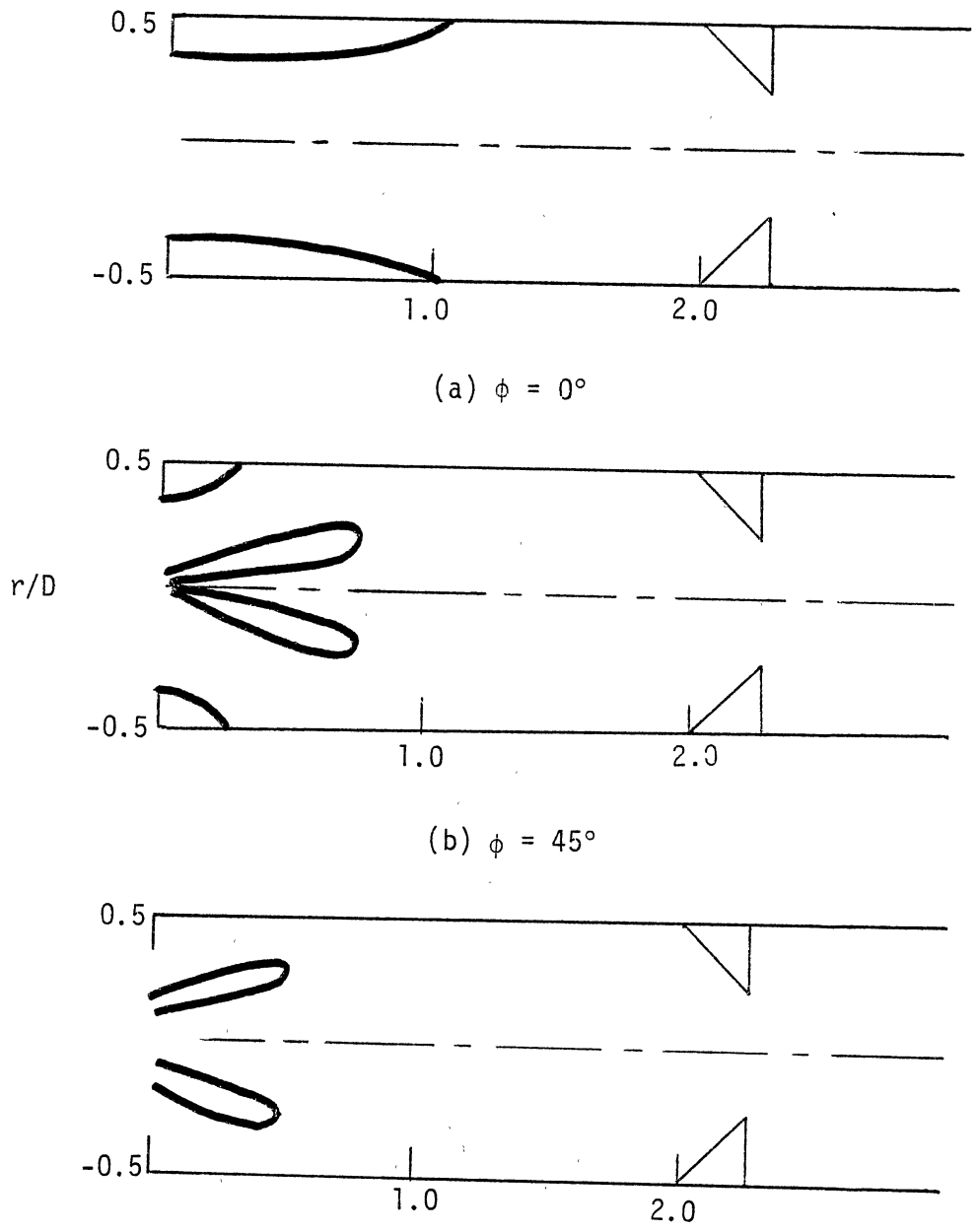

Figure 30. Artistic Impressions of Dividing Streamlines for the Flow of Figure 23 [D/d = 1.5, α = 90°, Large Blockage]

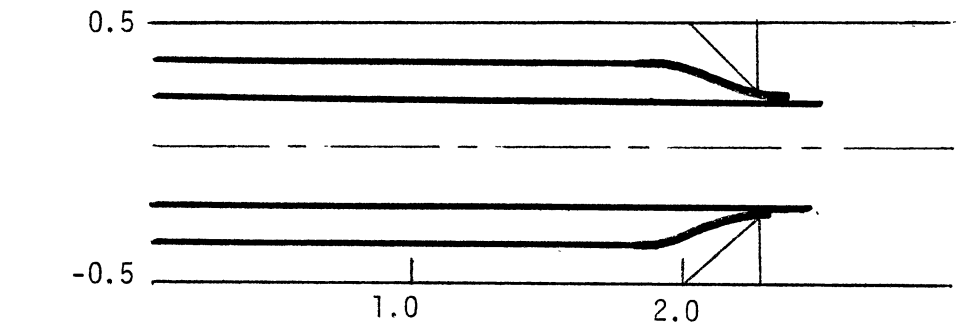

(a) ϕ = 0°

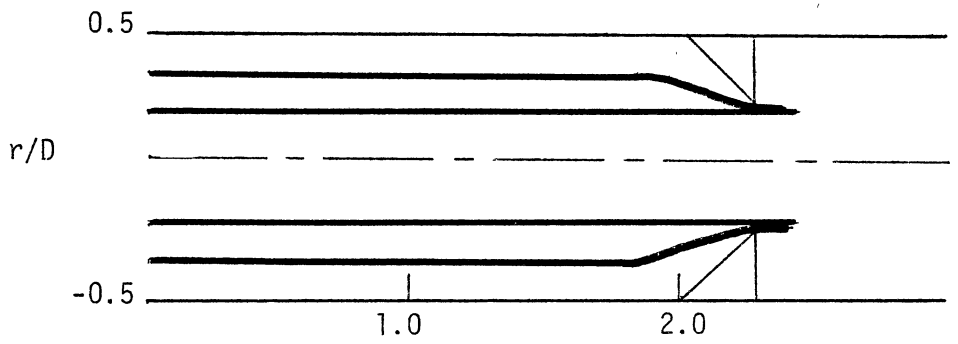

(b) ϕ = 45°

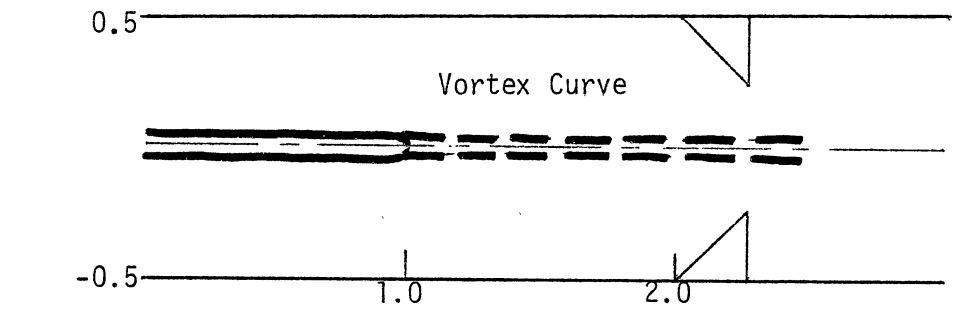

(c) ϕ = 70°

x/D

Figure 31. Artistic Impressions of Dividing Streamlines for the Flow of Figure 24 [D/d = 1.0, Large Blockage]

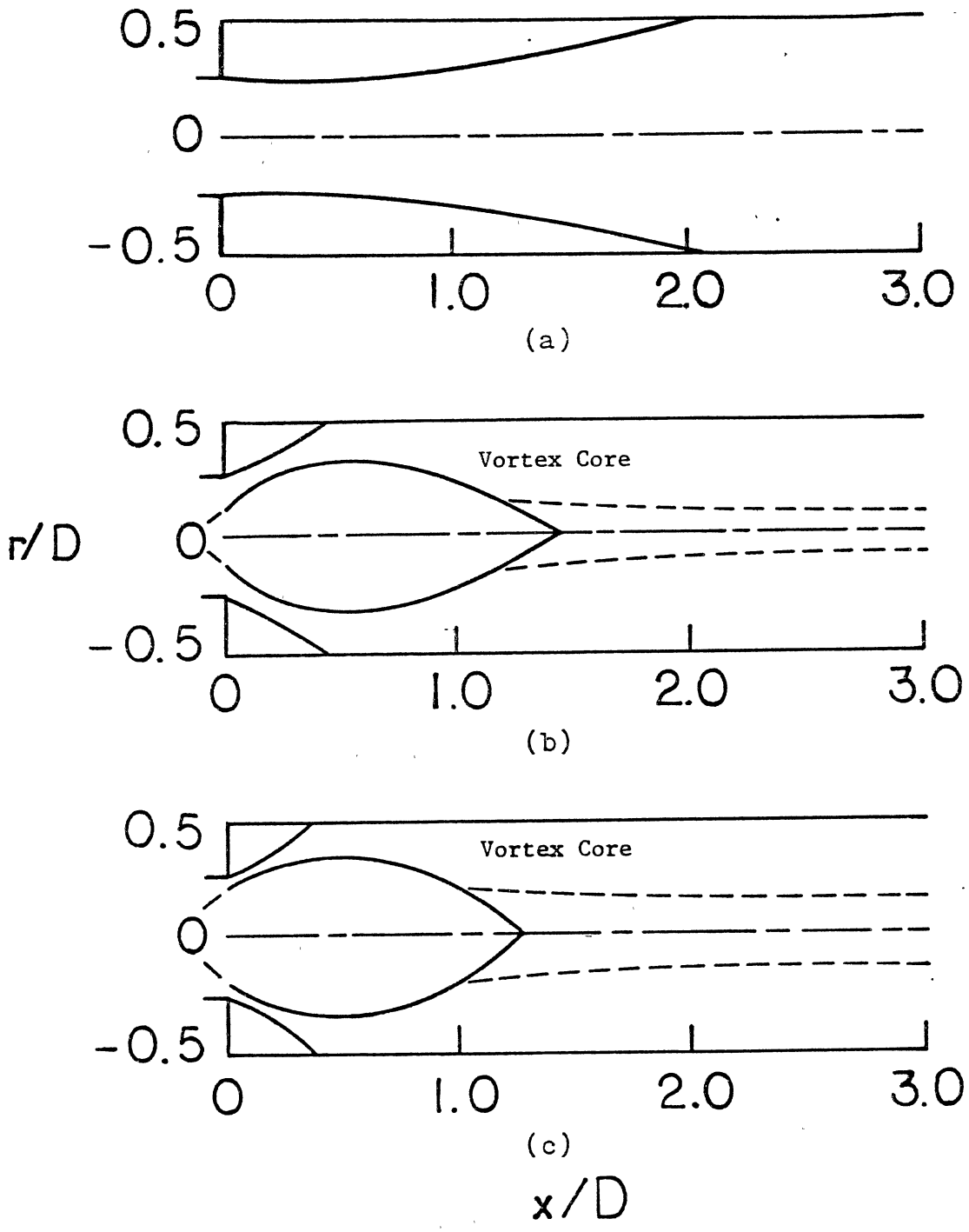

Figure 32. Artistic Impressions of Dividing Streamlines for Open-Ended Flow with Expansion Ratio D/d = 2.0 and Expansion Angle α = 90° (10)

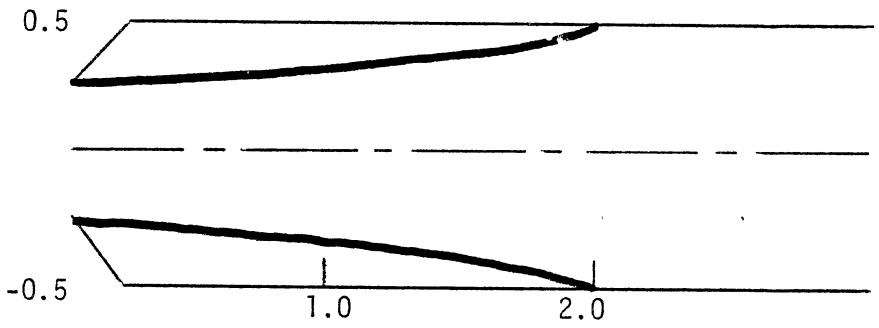

(a) ϕ = 0°

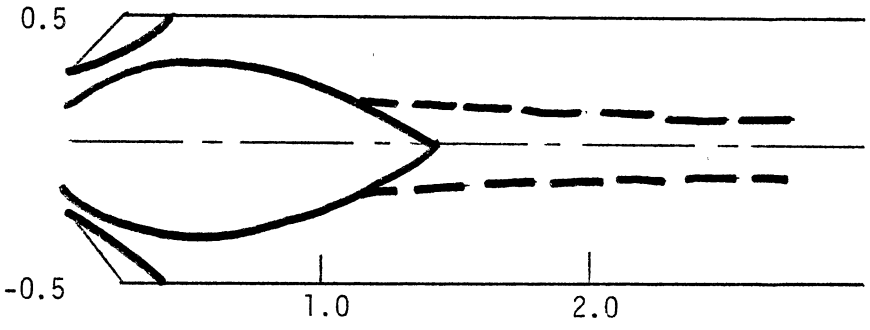

r/D

(b) ϕ = 45°

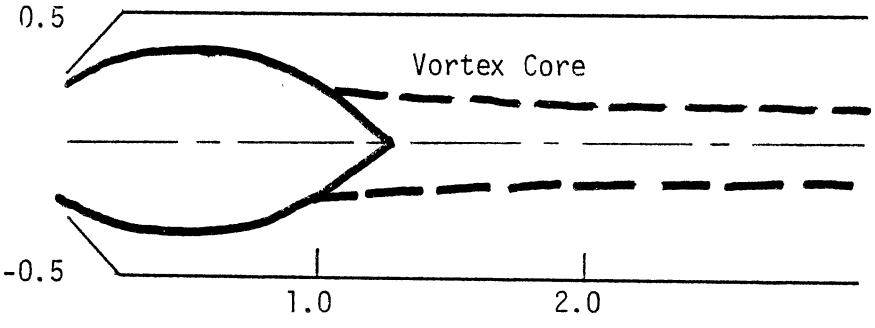

(c) ϕ = 70°

x/D

Figure 33. Artistic Impressions of Dividing Streamlines for Open-Ended Flow with Expansion Ratio D/d = 2.0 and Expansion Angle α = 90° (10)

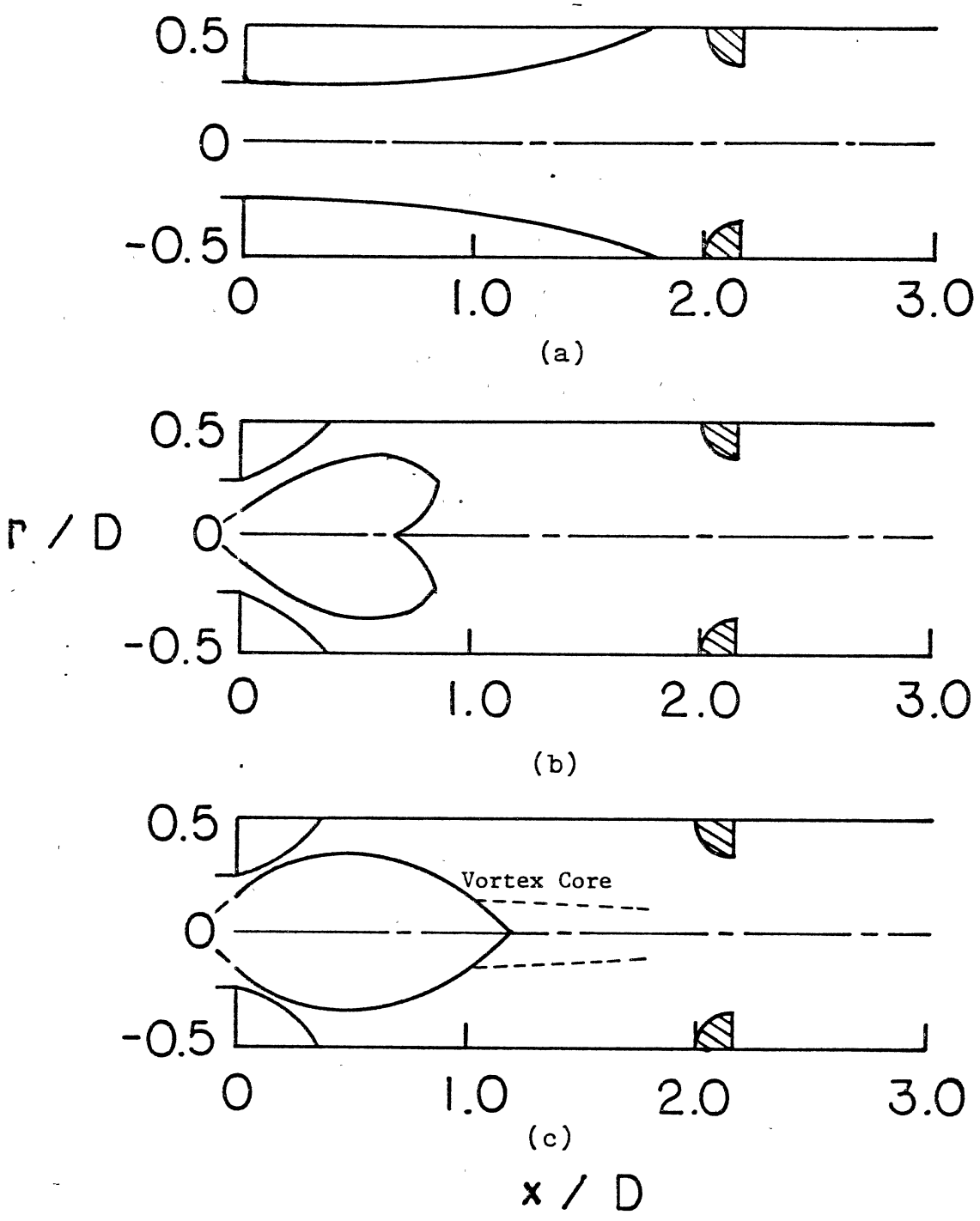

Figure 34. Artistic Impressions of Dividing Streamlines for Flow with Expansion Ratio D/d = 2.0, Expansion Angle α = 90° and Small Blockage (10)

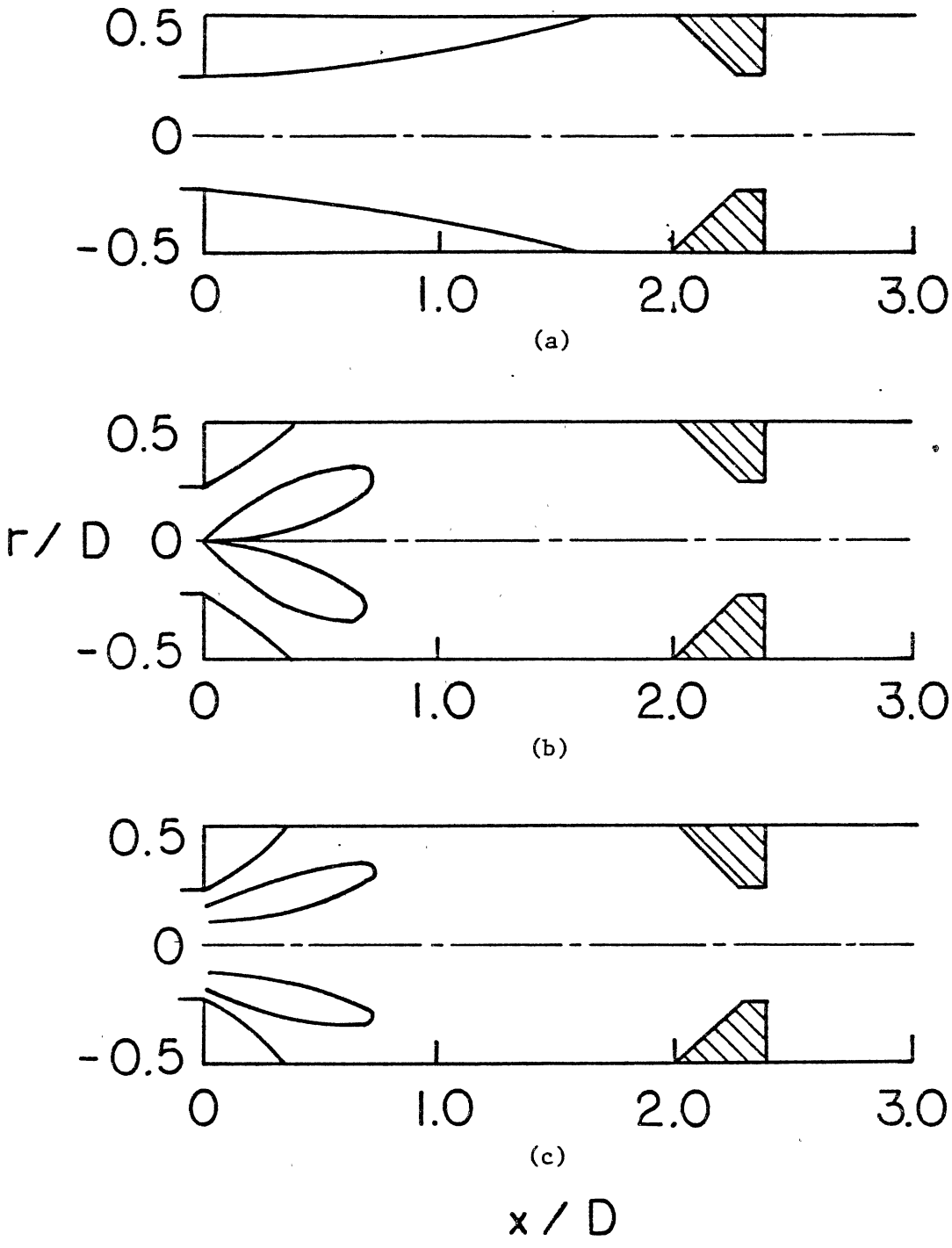

Figure 35. Artistic Impressions of Dividing Streamlines for Flow with Expansion Ratio D/d = 2.0, Expansion Angle α = 90° and Large Blockage (10)

VITA 2

Gregory Lloyd Scharrer

Candidate for the Degree of

Master of Science

Thesis: SWIRL, EXPANSION RATIO AND BLOCKAGE EFFECTS ON CONFINED TURBULENT FLOW

Biographical:

Personal Data: Born in Baltimore, Maryland, June 9, 1960, the son of Mr. and Mrs. Carl J. Scharrer Jr.

Education: Graduated from Severna Park High School, Severna Park, Maryland, in June 1978; received Bachelor of Science in Engineering from Northern Arizona University, May, 1982; completed requirements for the Master of Science Degree at Oklahoma State University in May, 1984.

Professional Experience: Research assistant at Oklahoma State University, School of Mechanical and Aerospace Engineering, 1982-1983.

Honor Societies: Tau Beta Pi, Phi Kappa Phi

Professional Society: AIAA